Chem

CellPress

Review

Supramolecular Chemistry: A Toolkit for Soft Functional Materials and Organic Particles

Aramballi J. Savyasachi,[1,*] Oxana Kotova,[1] Sankarasekaran Shanmugaraju,[1] Samuel J. Bradberry,[1] Gearóid M. Ó'Máille,[1] and Thorfinnur Gunnlaugsson[1,*]

Self-assembly has proven to be a powerful tool for the construction of complex superstructures. The assembly of monomers into supramolecular architectures via non-covalent interactions is chiefly directed by the molecular structures, their functional groups, and environmental conditions. The principal advantage of non-covalent interactions is reversibility, which allows the assembly of monomers into supramolecular structures *in situ* depending on the local conditions. In addition, the supramolecular approach provides a degree of control over self-assembly at the molecular level, thereby influencing the macroscopic level and facilitating tuning of the bulk material properties. This review discusses the meritorious examples of supramolecular materials constructed through the molecular assembly process, guided by the classical principles of supramolecular chemistry. Furthermore, this year (2017) marks the 50th anniversary of supramolecular chemistry in honor of the first example of supramolecular structure reported by Charles J. Pedersen and the achievements in the area of supramolecular chemistry ever since.

INTRODUCTION

Supramolecular chemistry has been described as "chemistry beyond the molecule and" involves the design and construction of complex supermolecules with smaller building blocks held together through various non-covalent interactions.[1] Generally, these interactions are weaker than covalent bonds and include van der Waals forces, dipole-dipole interactions, hydrogen bonding, π-π interactions, metal-ligand interactions, and many more.[1,2] In the field of supramolecular chemistry, self-assembly describes the process whereby relatively simpler/smaller subunits with complementary functionalities interact spontaneously with one another to organize themselves into more complex (supramolecular) structures. Nature provides us with many inspiring examples of such systems, for example, proteins, enzymes, metalloproteins, etc. One of the most common examples is the DNA double helix structure; in which two polymeric entwined strands are held together through π-π stacking and H bonding between its complementary base pairs.[1] This demonstrates the perfect combination of roles between organic, covalent, macromolecular, and supramolecular chemistry, demonstrating that reversibility is necessary for the self-assembly process, allowing supramolecular systems to adapt to local changes.

Supramolecular chemistry provides the framework for the design of molecules with interactive properties. The large variety of potential supramolecular interactions of different specificities available offers endless possibilities for the

The Bigger Picture

Many breakthrough developments in the past few decades have been achieved through multidisciplinary research. Supramolecular chemistry has played an extensive role in bridging chemical, physical, and biological sciences together. These interdisciplinary studies benefit our understanding of individual and hybrid systems. The supramolecular approach has emerged as a toolkit with remarkable capability for the assembly of rationally designed building blocks, which precisely organize in three-dimensional space to form intricate molecular assemblies as well as bulk material with functional properties. Because of such potential, supramolecular chemistry has emerged as a platform for the discovery of new systems and/or novel applications for existing ones. This field also holds great promise for advancement in the discovery of a vast array of systems that can be utilized in material chemistry, nanomaterials, soft materials, light-emitting devices, delivery agents, sensors, etc.

construction of diverse non-covalent supramolecular structures with tunable properties and functionalities. Such systems have found applications in sensors,[3] luminescent materials,[4] gels and materials chemistry,[5,6] light-emitting devices,[7] biological and cell imaging probes,[8,9] among other fields. Given that supramolecular chemistry has expanded and found application in many other areas of study, this multidisciplinary field bridges the chemical, physical, and biological sciences, among others.[10] Recognition of this relatively new field of chemistry was first achieved when the 1987 Nobel Prize in Chemistry was awarded to Lehn, Pedersen, and Cram for the design and development of cryptands, crown ethers, and cavitands, respectively;[11] this year (2017) marks the 50th anniversary of Pedersen's first publication. Because of its endless potential, supramolecular chemistry has since gained immense interest among chemists who wish to understand the intermolecular interactions involved in building supramolecular structures. Over the past few decades, this field has expanded toward the construction of larger and more complex architectures such as macromolecules and multimetallic helicates,[12] rotaxanes,[13] metal-organic frameworks, coordination polymers, clusters, etc.[14] Such studies have guided the design and construction of complex synthetic molecular machines, the discovery of which led to the recent Nobel Prize in Chemistry (2016) being awarded to Sauvage, Stoddart, and Feringa for their pioneering work.[15–23] Many others, such as Leigh, have also made important and pioneering contributions to the development of complex interlocked systems, highlighting the significance of supramolecular interactions in the development of building complex molecular structures.[16,17] Over the years, significant contributions to the field of self-assembly have facilitated our understanding of the principles behind intermolecular interactions and hence guided the development of new targeting and functional materials. The objective of this review is to focus on some of the many discoveries made within the area of supramolecular chemistry in recent times and the utilization of these systems in the construction of novel functional materials. As the selected examples discussed here demonstrate, the properties of the supramolecular materials formed depend on the molecular structures, as well as self-assembly at the molecular level and the environmental conditions. These aspects play a crucial role in the materials' behavior, performance, and application. We anticipate that the examples discussed in this review article will give an overview of the concepts of supramolecular chemistry in building new materials and motivate supramolecular chemists to design new systems with advanced properties. We also hope that this article will motivate other researchers to incorporate the concepts of supramolecular chemistry into existing systems, with perspectives to discover unique materials with hybrid properties, thus further expanding the field into new areas and future-generation technologies.

FUNCTIONAL SUPRAMOLECULAR POLYMERIC MATERIALS

Supramolecular polymers are polymeric arrays of monomeric units held together by reversible and directional non-covalent interactions such as hydrogen bonds, π-π interactions, and metal-ligand binding, etc. The directionality and strength of the interactions are precisely tuned so that the resulting array of molecules behaves as a polymer;[18] the resulting materials therefore maintain their polymeric properties in solution. The first example of linear supramolecular polymers was reported in 1990 by Fouquey et al.,[19] who used the concept of molecular recognition. Over time, many researchers have developed strategies and designed molecules to self-assemble into two-dimensional structures and other nanoscale motifs.[20] Supramolecular polymers are broadly classified according to the mechanism of formation.

[1]School of Chemistry and Trinity Biomedical Sciences Institute, Trinity College Dublin, University of Dublin, Dublin 2, Ireland

*Correspondence: ajsa@tcd.ie (A.J.S.), gunnlaut@tcd.ie (T.G.)

https://doi.org/10.1016/j.chempr.2017.10.006

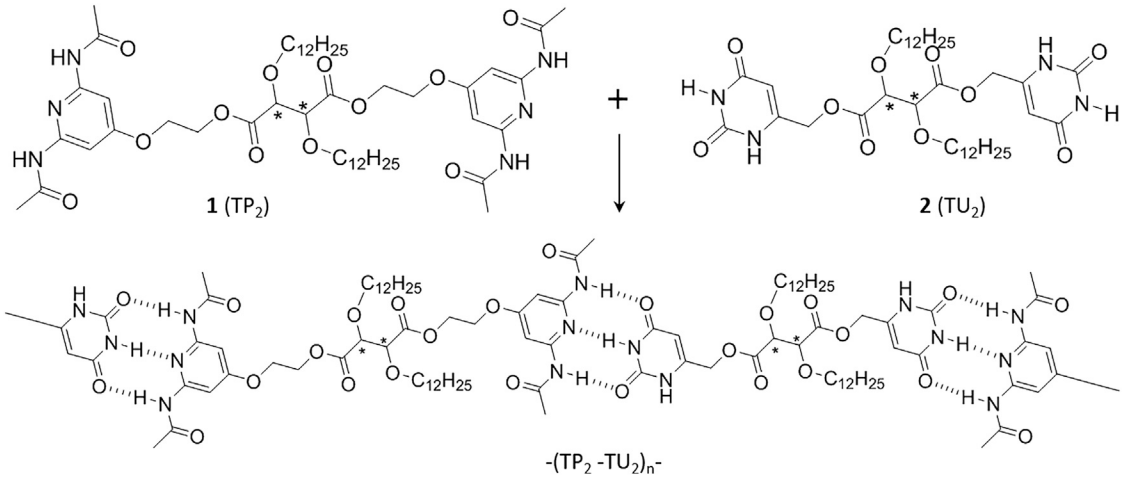

Figure 1. Supramolecular Polymer Formation through H Bonding

Molecular structures of **1** (TP_2) and **2** (TU_2) and its polyassociation to form liquid crystalline materials. Asterisks indicate chiral centers. Reprinted from Gulik-Krzywicki et al.[21] Copyright 1993 National Academy of Sciences.

One classification includes those formed through isodesmic supramolecular polymerization where the monomers undergo stepwise reversible association, which is identical throughout the polymerization process, and hence characterized by having the same association constant in every step of monomer addition. This is usually characterized by high polydispersity and absence of the critical concentration and critical temperature. Another classification includes those formed by cooperative supramolecular polymerization, in which the polymer chain growth occurs in at least two stages. The first stage consists of isoseismic polymerization until the nucleus is formed, with association constant K_n (nucleation stage). After the formation of the nucleus, the elongation stage occurs with the further addition of monomers to the nucleus with an association constant K_e higher than K_n. This is usually characterized by (1) the existence of critical concentration and critical temperature, representing the monomers in equilibrium with supramolecular polymer; and (2) having time lag in the formation of supramolecular polymer; however, this time lag can be reduced by seeding, which includes the addition of preformed nucleus.[18] Cooperative self-assembly is more often related to the formation of crystals and gels. A few classical examples of such supramolecular systems are briefly outlined in the next sections.

H-Bonded Polymeric Materials

Hydrogen-bonded supramolecular polymers are an important class of materials. In such materials, H bonds play the key role in the formation of a structured array of molecules.[1] Proper design of the molecular building blocks to tune the directionality and strength of the interaction between the molecules plays a crucial role in achieving functional supramolecular polymeric materials. Depending on the molecular structure and the functional groups present, molecules self-assemble to form different shapes, sizes, and structures. An early and simple example of such a system exhibiting helical structures was reported by Lehn and co-workers, where they observed the polyassociation of supramolecular liquid crystalline species, **1** (TP_2) and **2** (TU_2) bearing complementary components to form helical structures (Figure 1). The chirality in this system is controlled with different types of tartaric acid (D-, L-, or the meso form) connected to pyridine (P) or uracil (U) derivatives.[21]

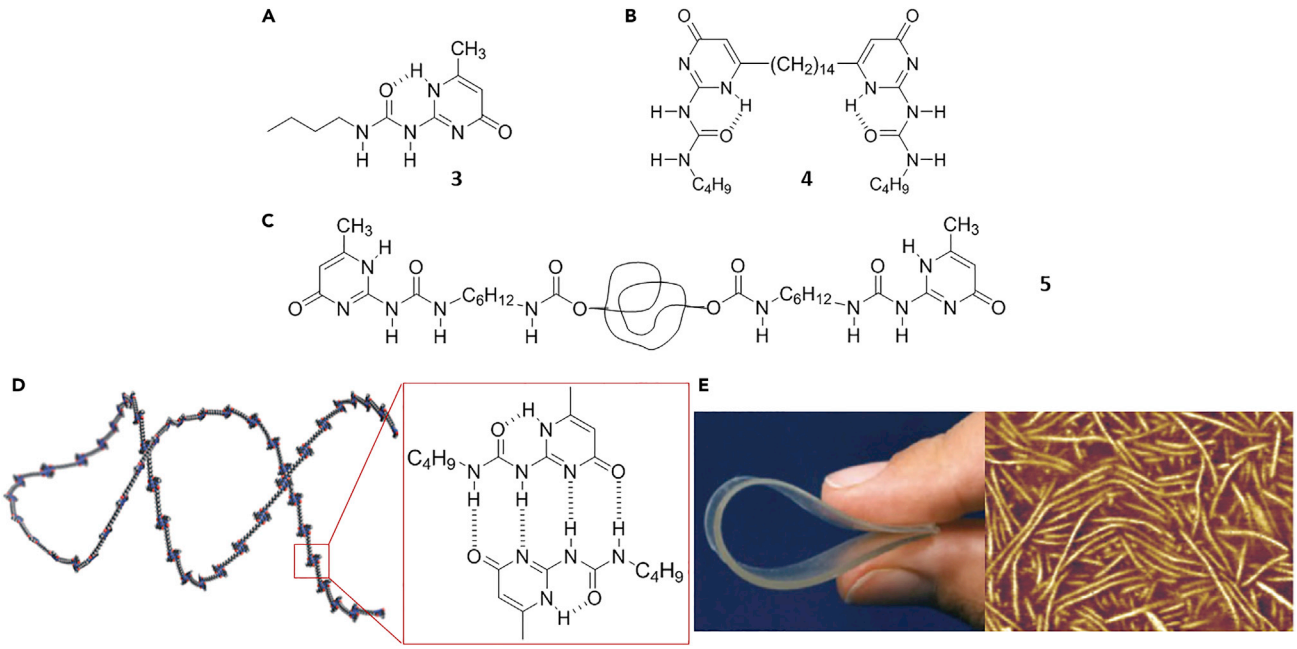

Figure 2. Ureido-Pyrimidone (Upy)-Based Polymeric Material

(A–C) Molecular structure of Upy unit **3** (A), a linear molecule with two Upy moieties at both ends **4** (B), and a Upy moiety attached to the terminal ends of telechelic polymer chain **5** (C). Reprinted with permission from Sijbesma et al.[24] (copyright 2012 American Association for the Advancement of Science) and Folmer et al.[26] (copyright 2000 Wiley-VCH Verlag GmbH, Weinheim, Fed. Rep. of Germany).

(D) Schematic representation of the supramolecular polymer formed through quadruple H bonding between self-complimentary Upy moieties. Reprinted with permission from Aida et al.[25] Copyright 1997 American Association for the Advancement of Science.

(E) Supramolecular polymeric elastic material made from **5** and its atomic force microscopy images showing nanofibers. Reprinted with permission from Folmer et al.[26] Copyright 2000 Wiley-VCH Verlag GmbH, Weinheim, Fed. Rep. of Germany.

Early examples of supramolecular polymers show self-assembly of monomers with various non-covalent interactions.[22] Multiple H-bonded supramolecular polymers were then reported, which showed properties of polymeric materials in solution as well as in bulk. Meijer and co-workers reported supramolecular motifs that were dimerizing through self-complementary quadruple H bonding (dimerization constant, $K_{dim} \sim 10^2$–10^5 M^{-1}).[23] Appropriate modifications to such systems, by reducing the repulsive and increasing the attractive secondary interactions, produced 2-ureido-4-pyrimidone moieties (Upy) **3**, which dimerized strongly ($K_{dim} > 10^6$ M^{-1} in $CHCl_3$, enhanced binding strength) through an array of a self-complementary AADD-DDAA (D = donor and A = acceptor) four H-bonding sequence.[24] These motifs with enhanced binding strength as end groups, in a linear bifunctional molecule linked by long alkyl chains (**4**), form a supramolecular polymer unit, which can achieve longer supramolecular polymer chain lengths. Such systems behave like conventional polymers in solutions as well as exhibit robust mechanical properties in bulk (Figure 2).[24,25] Unidirectionality of these linear bifunctional systems (**4**) prevents crystallization in the bulk, or gel formation, in solution at higher concentrations. This unidirectionality was confirmed when monofunctional compound **3**, which act as a chain stopper, was added to the solutions of **4**. Viscosity of the solution of **2** (in $CHCl_3$) decreased linearly with the increasing amount of **3** (chain stopper). This confirmed the reversible association process and the absence of uncontrolled gel formation. Furthermore, appropriate modifications to **3** and attaching to the terminal groups of a classical telechelic polymer yielded compound **5** as an elastic solid (Figures 2C and 2E).[26]

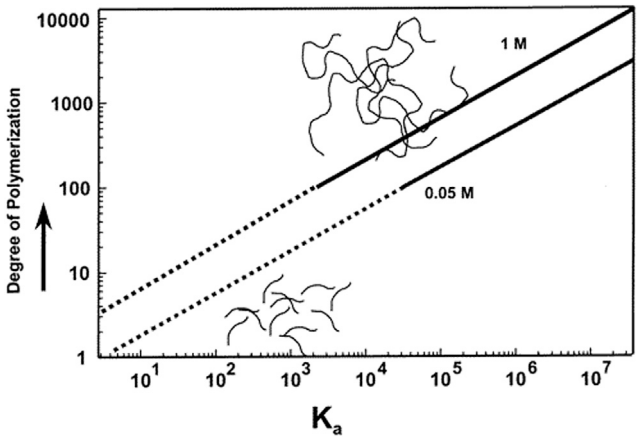

Figure 3. Theoretical Relationship Explaining the Linear Dependence of DP on K_a between End Groups

Reprinted with permission from Brunsveld et al.[27] Copyright 2001 American Chemical Society.

In supramolecular polymeric materials formed by reversible association of bifunctional units, their chain length or degree of polymerization (DP) is directly proportional to the strength of the terminal group interaction. The theoretical treatment explaining the relationship between the DP (chain length), concentration of the solution, and the association constant (K_a) between supramolecular end groups is shown in Figure 3.

Biological Supramolecular Filament and Microcapsules

Stupp and co-workers showed the self-assembly of a biological molecule, a large peptide amphiphile (PA) **6**, which aggregates to form a bioactive filament resembling collagen and hydroxyapatite (HA).[28] The three key structural features introduced in **6** were (1) a long hydrophobic alkyl chain, (2) an amino acid segment (having the tendency to form β sheets), and (3) a polar unit bearing phosphorylated serine residues for interaction with calcium ions to direct the mineralization of HA and cell adhesion by RGD ligand (a collagen-associated protein containing sequence Arg-Gly-Asp). This cone-shaped molecule aggregates because of the hydrophobic effect, wherein the alkyl chains are buried inside the fiber and the β sheets are arranged outside in a twisted helical fashion along with the polar head group (Figure 4).

Mineralization of this filament was achieved by diffusing $CaCl_2$ and Na_2HPO_4 on their surface. Preferential alignment of the crystallographic C axis of HA with the PA fiber axis was observed, which helped the nucleation of HA on the PA filament surface. Furthermore, stacking of the cell-binding RGD ligands in the PA assemblies helped to bind to receptors on the cell surface, which allowed the PA filaments to exhibit a high density of biological signals to receptors spatially over a long distance. The advantage of this kind of material over covalent polymers is that these can be self-assembled by the cell itself (because of the strong interactions between supramolecular assemblies and receptors) in order to fit the local geometry by easily breaking and reforming non-covalent bonds *in situ*.[30] Similar supramolecular filaments, formed by the assemblies of molecules containing a peptide segment conjugated to lipid chains, were found to be very bioactive *in vivo*, for example, in regeneration of bone and cartilage, growth of blood vessels, and more.[31,32]

Similar PAs, when in contact with oppositely charged biopolymers in dilute solutions, self-assemble to form supramolecular polymeric filaments that act as

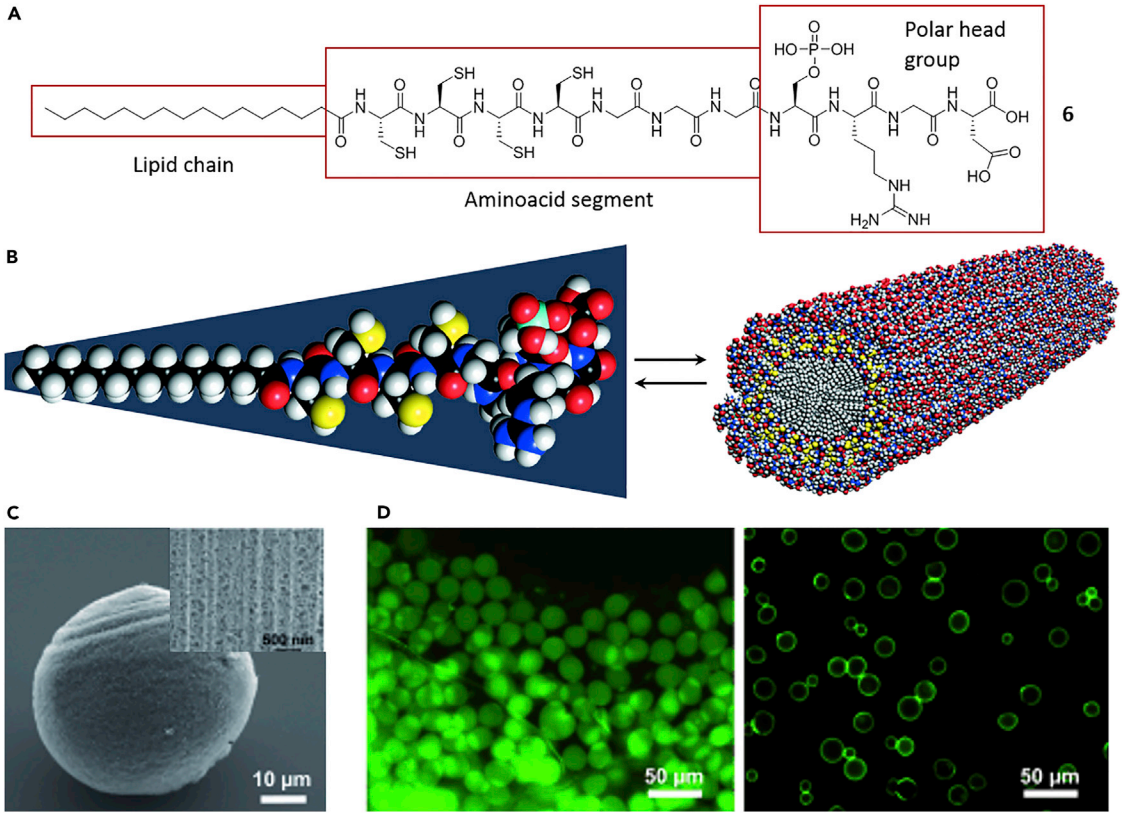

Figure 4. Supramolecular Filament and Microcapsule Formed from Peptide Amphiphiles

(A) Chemical structure of the peptide amphiphile **6**.

(B) Molecular model of **6** showing the conical shape of the molecule and the schematic representation of its self-assembly into cylindrical micelles. Reprinted with permission from Hartgerink et al.[28] Copyright 2001 American Association for the Advancement of Science.

(C and D) SEM image of a microcapsule made from PA-biopolymer combination (C) and fluorescence microscopy images of microcapsules with encapsulated fluorescent-tagged proteins and containing fluorescent-labeled PA in their shells (D). Reprinted with permission from Rożkiewicz et al.[29] Copyright 2011 Wiley-VCH Verlag GmbH & Co. KGaA, Weinheim.

membranes at the interface of the solutions. The microstructure of the resulting material consists of highly ordered nanofiber bundles.[33] Optimization of this process to the micrometer scale with the use of materials with similar properties has paved the way for demonstrating the synthesis of cell-like microcapsules. These microcapsules were used for encapsulation and release of fluorescent-tagged proteins (Figures 4C and 4D).[29]

Light-Emitting Supramolecular Co-polymers

The addition of functional groups to these materials results in the formation of supramolecular co-polymers with hybrid functional properties. This approach was illustrated by Schenning and co-workers in the design of a light-emitting supramolecular co-polymer that optimizes energy transfer in materials to perform as organic light-emitting diodes (OLEDs).[34] The material was designed with three π-conjugated oligomers, oligofluorene (OF, blue, **7**), oligo(phenylene vinylene) (OPV, green, **8**), and perylene bisimide (Pery, red-emitting, **9**) chromophores functionalized with two self-complementary quadruple hydrogen-bonding Upy moieties as end groups. These then self-assemble to form supramolecular polymers both in solution and in bulk (Figures 5A and 5B). Upon excitation of the oligofluorene moiety of the polymer chain with light, energy transfers to the other chromophores, resulting in emission

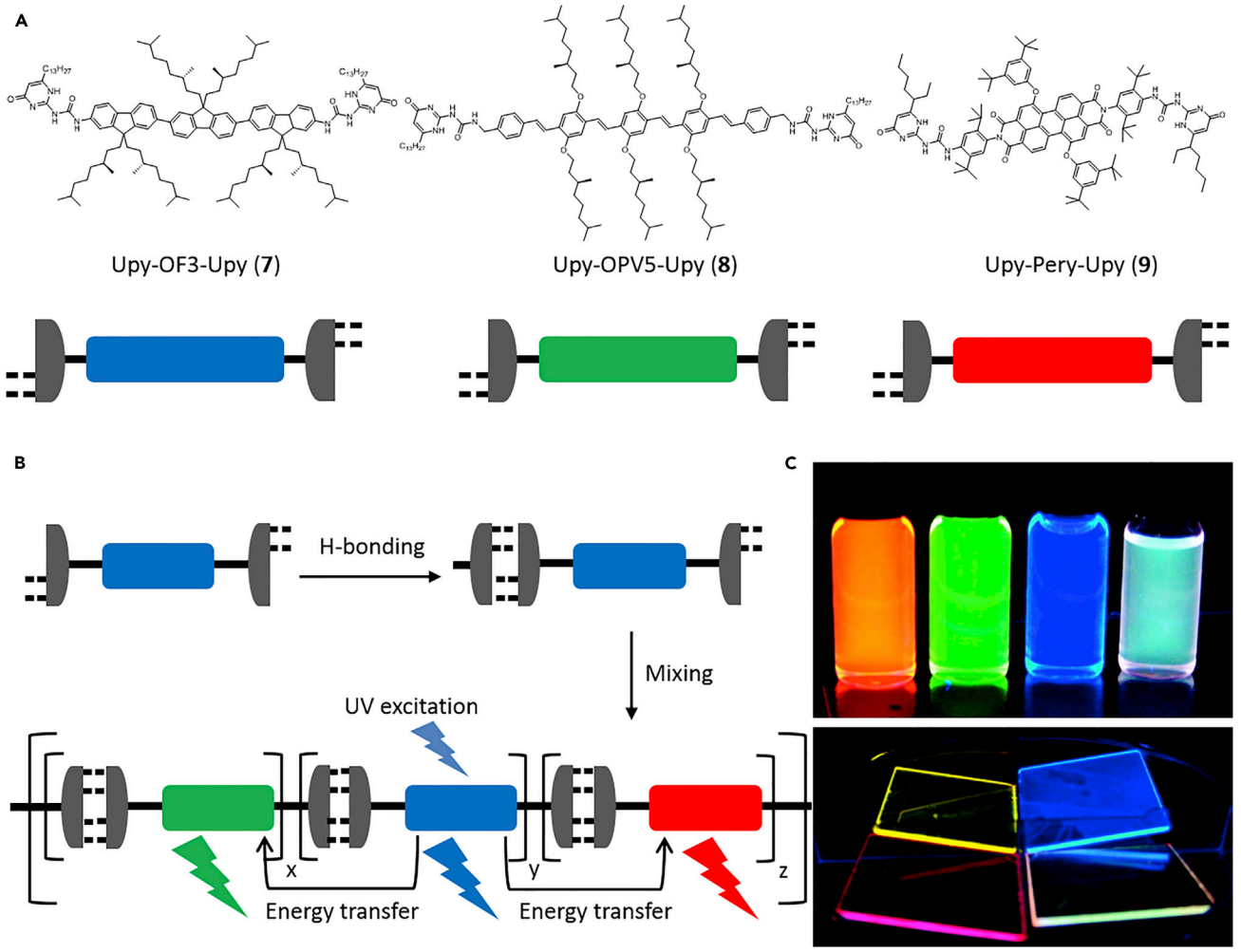

Figure 5. Supramolecular Co-polymers as Materials for OLEDs

(A) Chemical structure of chromophores with di-functionalized Upy moieties as end group (**7**–**9**) and their schematic representation.

(B) Schematic representation of H-bonded supramolecular polymers illustrates the concept used to achieve white-light emission.

(C) Solutions of pure supramolecular polymers **7**–**9**, their mixture in $CHCl_3$, and their thin films show emission under UV irradiation (λ_{ex} = 365 nm).

Adapted or reprinted with permission from Abbel et al.[34] Copyright 2009 American Chemical Society.

from all three components. Appropriate mixing of these components resulted in the combination of emission from all three chromophores, yielding a white light-emitting material (Figure 5C).

Furthermore, Meijer and co-workers modified the OPVs by using appropriate chiral groups at the periphery and introducing alkyl chains and an ureidotriazine moiety on both ends to obtain *S*-oligo(*p*-phenylene vinylene)s (SOPVs) **10**, which dimerize through H bonding between the ureidotriazine end groups to form π-conjugated dimers. In apolar solvents, these dimers undergo a self-assembly process by hierarchical organization and subsequently form reversible helical columnar supramolecular structures (Figure 6).[35,36] In constructions of polymer chains from the dimerized product, π-π stacking plays a key role in the self-assembly of the dimers, and the chiral groups in the periphery take control of the supramolecular chirality, resulting in helical structures.[37] An interesting feature of these polymeric materials is the ability to control their length and properties by varying parameters such as solvent polarity

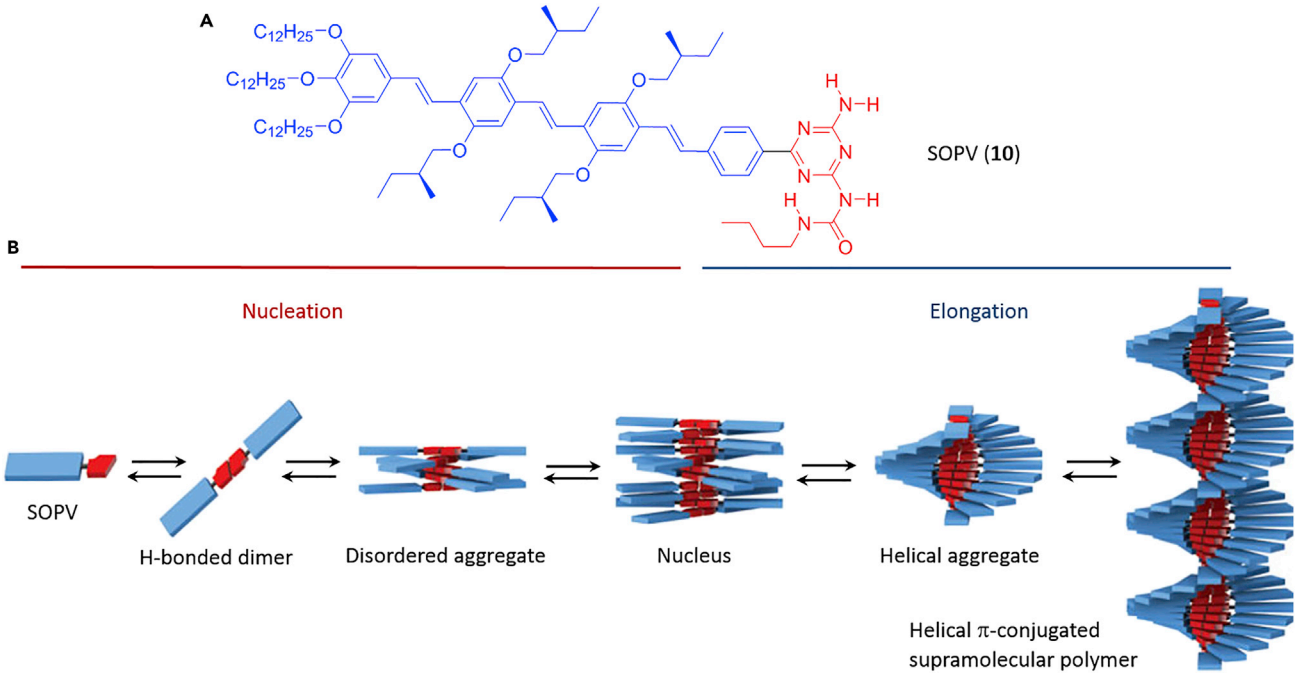

Figure 6. One-Dimensional Supramolecular Polymers Formed through H Bonding and Helical Stacking

Molecular structure of SOPV (**10**) (A) and schematic representation of the hierarchical aggregation pathways, initiated by a quadruple H-bonded dimer to form an elongated supramolecular polymer (B). Adapted or reprinted with permission from Korevaar et al.[35] Copyright 2012 Nature Publishing Group.

and temperature. Formation of these helical architectures was analyzed by UV-visible absorption, fluorescence, and circular dichroism spectroscopy as well as microscopic techniques.

BENZENE-1,3,5-TRICARBOXAMIDE (BTA)-BASED HYDROGEN-BONDED SUPRAMOLECULAR POLYMERS AND GELS

As discussed earlier, all supramolecular materials with tunable properties emerge from the self-assembly process under thermodynamic conditions. It is important to understand how small changes in the molecular structure of the building blocks affect the aggregation properties and yield different classes of materials such as one-dimensional supramolecular polymers, gels (hydro-, organo-, or metallo-), liquid crystals, porous materials, magnetic resonance imaging (MRI) contrast agents, etc. A large number of building blocks are available; however, many of them require multistep synthesis or show limited aggregation properties. In the past few decades, the benzene-1,3,5-tricarboxamide structure, also known as the BTA motif, has attracted considerable interest as a building block for the construction of such materials because of the tendency of three amide groups to form intermolecular H-bonding interactions.[38] BTA is a very good example of a class of compound that yields different classes of materials when different substituents are placed on its side chain. Such properties have enabled BTA-based systems to form nanostructured architectures with various applications, some of which are addressed below. The amide groups on the benzene ring can be attached either via the carbonyl group, giving C=O centered BTAs, or attached via nitrogen, giving N-centered BTAs (Figure 7). When all the substituent R groups are same, the molecule becomes C_3 symmetric.[38] In this review, we focus on C=O centered, symmetric molecules.

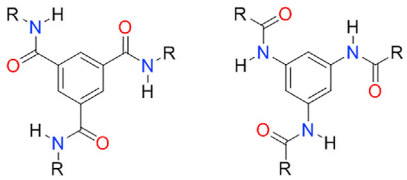

Figure 7. General Structure for C=O- and N-Centered BTA Molecules

Self-Assembly of BTA Scaffolds Yielding Different Materials

The nature of the side chains (R) plays an important role in the behavior of the BTA molecules. BTA derivatives bearing polar water-soluble groups (**11**) can form hydrogels,[39] non-polar substituents on the BTA (**12**) can result in the formation of organogelators,[40] and groups with coordinating moieties (**13**) yield metallogels (Figure 8A).[41] Substituents with bulky groups (**14**) often self-assemble in a distorted manner, and the resulting columnar self-assembled structure has voids, making a porous organic material (Figure 8B).[42] Many BTA molecules with long alkyl chains (**15–16**) are known for their liquid crystalline properties (Figure 8C).[43] Recently, BTA with an azobenzene moiety (**17**) was used in making microcapsules, with cucurbit[8]uril as host in the presence of ditopic methyl viologen monomer, by making ternary host-guest interactions (Figure 8D).[44] BTAs appended with water-soluble MRI active Gd(III) complexes at the periphery (**18**) were explored as MRI contrast agents (Figure 8E).[45] Furthermore, they are well known for self-assembling in unidirectional supramolecular polymers and other nanostructured materials, which are discussed in the coming sections. In addition to this, Gunnlaugsson and co-workers reported bowl-shaped structures from N–CH_3 substituted BTA molecules.[46]

Because of their facile synthesis and the facility to append a variety of different substituents to the side chain of the BTA scaffold, a wide range of BTA homologs are available.[38] Arising from this, BTA scaffolds have emerged as useful systems to study and understand the structural variation and the role of solvent on the self-assembly mechanisms of supramolecular polymers. Over the years, such studies have proven to be very helpful in designing molecules that self-assemble into well-defined nanostructures with high stability and great applicability.[18]

BTA-Based Hydrogen-Bonded Supramolecular Polymers

One of the simplest examples of such BTA molecules self-assembling as one-dimensional supramolecular polymers was reported by Banerjee and co-workers. There, the C=O centered BTA molecules were equipped with enantiomeric pairs of chiral amino acids, **19R**, **19S**, and **20**, self-assembling through triple H bonding and forming intertwining triple helical cylindrical nanofibers (Figure 9A).[47]

Single-crystal X-ray analysis confirms that the molecule **19R** has crystallographic three-fold symmetry within a hexagonal unit cell, facilitating columnar packing parallel to the crystallographic c axis (Figure 9B). These exhibit the handedness of the triple helical nanofibers, and they can also be tuned by reversing the chiral nature of the molecular building blocks. This triple helical structure is formed through intermolecular hydrogen bonds with an overall right-handed twist and other non-covalent interactions including π-π stacking interactions between the central aromatic moieties (Figure 9B). This type of self-assembly can be analyzed by microscopic imaging techniques such as transmission electron microscopy (TEM). The formation of the opposite chiral construction from these enantiomeric pairs of discotic molecules

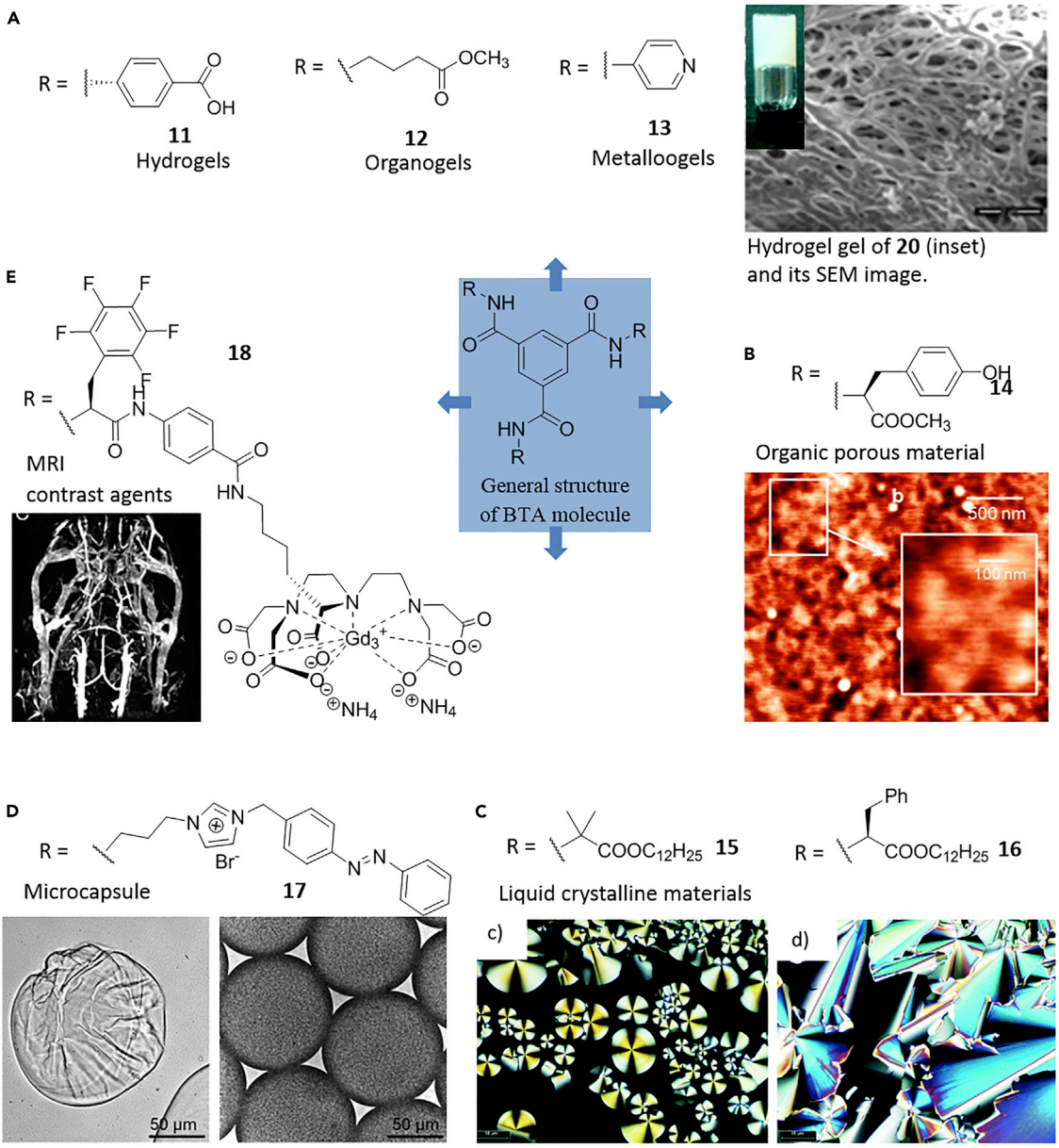

Figure 8. Generalized View of a BTA Molecule with Different Substituents Found in Applications in Different Fields of Research

(A) BTA-based hydro-, organo-, and metallogelators. Scale bar, 2 μm. Reproduced from Howe et al.,[39] Paikar et al.,[40] and Zhong et al.[41] with permission from the Royal Society of Chemistry.

(B) BTA-based organic porous material. Reprinted with permission from Jana et al.[42] Copyright 2014 American Chemical Society.

(C) BTA-based liquid crystalline materials. Reproduced from Desmarchelier et al.[43] with permission from the Royal Society of Chemistry.

(D) Microcapsules formed with a BTA molecule bearing a methyl viologen moiety via heteroternary host-guest complex. Reproduced from Groombridge et al.,[44] published by the Royal Society of Chemistry.

(E) MRI-active BTA molecules. Reprinted with permission from Besenius et al.[45] Copyright 2012 John Wiley & Sons, Ltd.

revealed that control over chirality was possible with different substituents, as observed in TEM microscopic images (Figure 9C).

Meijer and co-workers used simple BTA molecules with achiral and chiral aliphatic side chains to study self-assembly by different spectroscopic techniques in solution and methylcyclohexane (MCH) as solvent. Circular dichroism (CD) spectroscopy

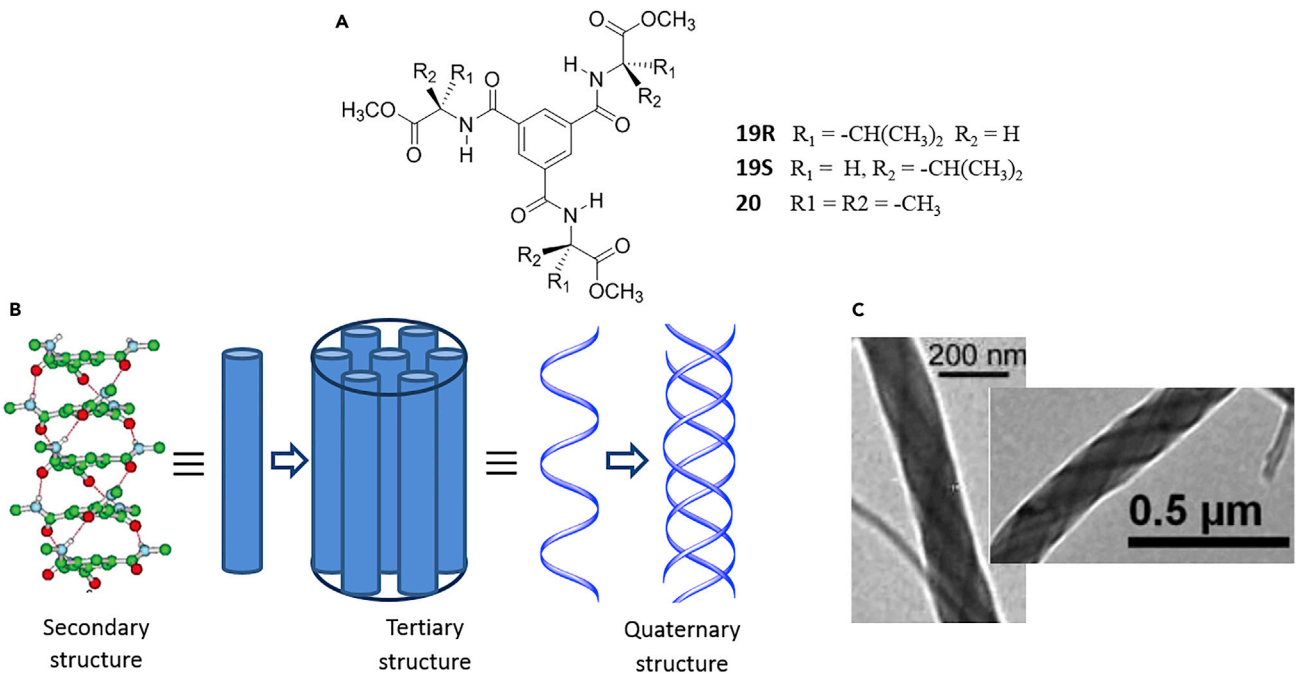

Figure 9. One-Dimensional Supramolecular Polymers Formed from Chiral BTA Molecules
(A and B) Molecular structures of **19R**, **19S**, and **20** (A) and the schematic representation of their self-assembly forming fibers (B). (C) TEM images of **19R** and **19S**. Reproduced from Bose et al.[47] with permission from the Royal Society of Chemistry.

studies of BTA systems with simple alkyl chains containing a chiral center (**21**) showed a strong Cotton effect centered around 220 nm in dilute solution, confirming the helical nature of the BTA aggregate.[48] No Cotton effect was observed for **22** and **23** under similar conditions. Further studies revealed that the chiral groups in the side chains direct the self-assembly toward one type of helical conformation over the other.

Further CD experiments carried out on mixed systems of **21** and **23** in heptane display the "sergeants-and-soldiers" principle. A composition of 4% of **21** (by concentration) directs the whole supramolecular chain formed with **23** in the same handedness as found for columns exclusively consisting of **21** by amplification of the chirality (Figure 10).[49] Many other BTA molecules with chiral aliphatic side chains showed similar behavior.[48] In these systems, it was also observed that addition of competitive solvents such as acetonitrile to the solutions of BTA helical aggregates results in the dissolution of the supramolecular polymers formed by reversible intermolecular H-bonding interactions.

BTA-Based Supramolecular Polymers in Aqueous Media

Meijer, Palmans, and co-workers reported water-soluble BTA molecules (**24**–**26**) bearing amphiphilic side chains. The alkyl chains shielded the H-bonding central BTA core, and hydrophilic ethylene glycol motifs helped with water solubility (Figure 11A).[50] The chiral center in **25** helped to give information on the helical arrangement of the supramolecular polymers. Cryo-TEM analysis carried out on aqueous solutions of **24** and **25** showed the formation of long thin fibers of micrometer length and approximately 5 nm in diameter (Figure 11B). In comparison, **24** showed a slightly larger diameter along with subtle and periodic variation in diameter and contrast, which are not observed in **25**. Such structures are often seen in helical fibers

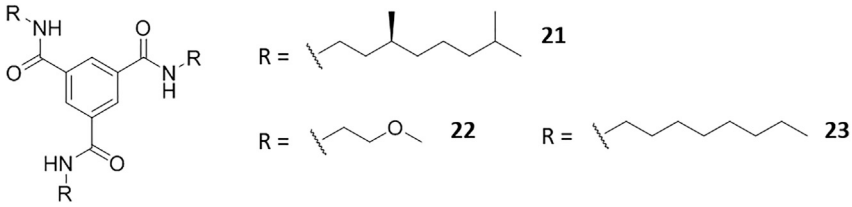

Figure 10. Chemical Structures of BTAs with Different Side Chains
Reprinted with permission from Smulders et al.[49] Copyright 2008 American Chemical Society.

(Figure 11B). From CD experiments, **25** in H_2O showed the Cotton effect at 220 nm ($\Delta\varepsilon$ = 40 M^{-1} cm^{-1}), similar to its helical columnar aggregates in organic solvents (Figure 11C).

These results suggest that minimal difference in the hydrophobic chains has a significant effect on the columnar packing of monomers. The UV absorption of **24** observed over time showed a red shift of the absorption maximum at 192 nm, suggesting the formation of initially helical stacks that eventually convert to one-dimensional linear structures, as seen in TEM. Such changes are not observed for **25**, which suggests the stereogenic methyl group in the side chain drives the molecule toward columnar packing. However, **26** did not show any changes in its UV absorption spectrum, as was observed for **24** and **25** in H_2O, signifying the inability of **26** to form intermolecular H bonds because of the lack of an NH group necessary for H bonding. This indicates the importance of H bonding for the formation and stabilization of aggregates. Very recently, Meijer and Palmans and co-workers reported similar BTAs with amphiphilic side chains, demonstrating the importance of balance between hydrophobicity and hydrophilicity required to form ordered and stable supramolecular polymers in water.[51]

Using the principle of hydrophobic shielding of the H-bonding BTA core, Palmans and Meijer reported more water-soluble compounds with peripheral hydrophilic gadolinium chelates (**18** and **27**) (Figure 12).[52] The peripheral paramagnetic Gd(III) ion chelates were introduced with the aim of increasing the ionic character of the molecule, forming supramolecular polymers that could result in a new class of MRI contrast agents. The balance between attractive forces (π-π stacking, dipole interactions, and solvophobic effects) and repulsive forces in **27** enable the formation of stable and non-interacting columnar assemblies of several length scales (25–75 nm, depending on the concentration) with controlled shape, size, and stability. This approach paves the way for solving the challenges faced in the formation of functional supramolecular polymers in water.

BTA-Based Hydrogen-Bonded Gels

Originally, the discovery of gels was serendipitous, and they were often observed during recrystallization processes. Gels are usually composed of a very high volume of liquid, typically >99% w/v. The gel network can be formed by chemically cross-linking polymer chains via covalent bonds in polymers, such as in hydrogels. In high-molecular-weight biopolymer molecules such as collagen and pectin, networks can be formed by entangled molecular chains. In general, the gel can be considered as comprising a solid matrix that immobilizes a liquid component by surface-tension effects. From the early 1990s, research groups began strategically designing low-molecular-weight molecules for gelation. In the case of supramolecular gels, low-molecular-weight gelators (LMWGs) self-assemble to form gels (as examples below demonstrate).

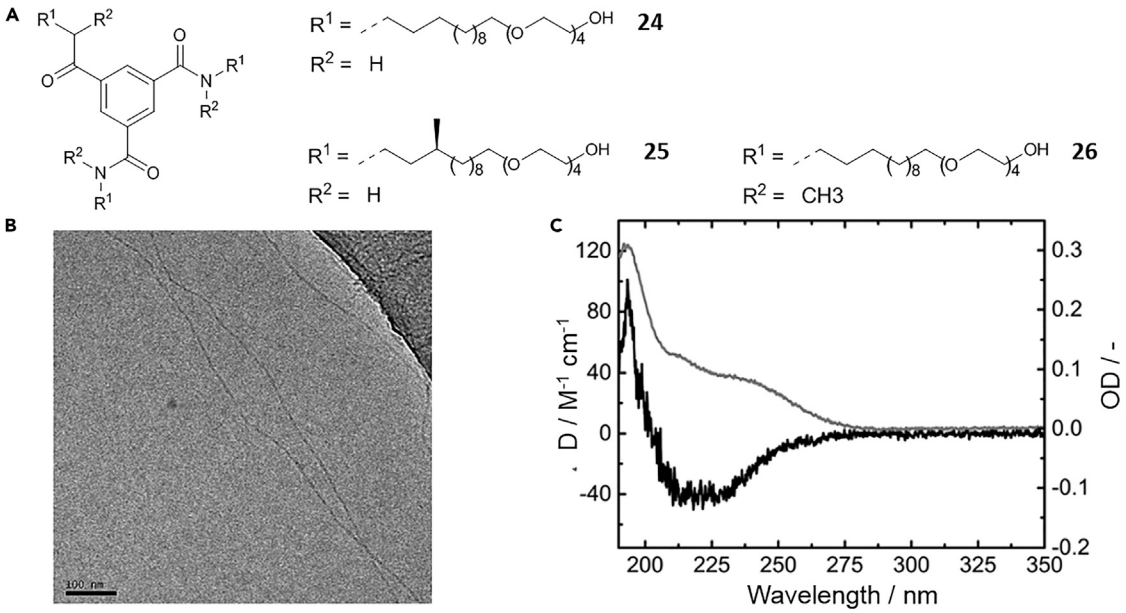

Figure 11. BTA Derivatives with Hydrophobic Ethylene Glycol Motifs

(A) Chemical structures of BTA with amphiphilic side chains.

(B and C) TEM of **24** showing fibrillar aggregates (B) and UV-visible absorption (gray) and CD (black) of **25** (C). Reproduced from Leenders et al.,[50] published by the Royal Society of Chemistry.

As discussed above, the supramolecular polymers are one-dimensional fibrils of approximately the same width, which usually exist in dilute concentrations. Upon increasing the concentration, these fibrils can undergo bundling to form fibers. These fibers then grow into three dimensions, forming an infinite cross-linked and entangled fibrous network. This network encapsulates and immobilizes the solvent in its matrix, thus forming a gel. However, some of the supramolecular polymer fibers fails to undergo entanglement. In this case, the solution remains as viscous medium with only fibers in it and no cross-linking network to immobilize solvent molecules. An advantage of supramolecular gels over others types is their inherent reversibility, which is important in applications such as delivery systems.[53] Gels in which weak forces hold fibers recover faster to their original state after breaking, exhibiting thixotropic behavior. Such materials are often suitable for printing, injection molding, and other processing methods.[54] Gels are broadly classified depending on their composition. For example, gels formed in water and organic solvent are termed hydrogels and organogels, respectively. When the liquid component is replaced by gas, then it is termed as aerogel. Incorporating metal ions through coordination interactions with the LMWG results in metallogels.[55]

In supramolecular gels, the self-assembly of LMWGs occurs through non-covalent interactions such as H bonding, solvophobic effects, metal-ligand interactions, ion pair coupling, etc. During the gelation process, the molecules are dissolved in a certain solvent and then induced to self-assemble, which renders them less soluble. Self-assembly can be induced by a heat-cool cycle, changes in pH, or charge, addition of metal salts, and by mixing of more than one material, etc. Because highly directional non-covalent interactions are essential, the design of the molecule is important, and the balance of solubility has to be taken into account. In addition, a number of strategies have to be included, emphasizing known gelators.[5] From the past decade, metal complexes were also investigated as supramolecular

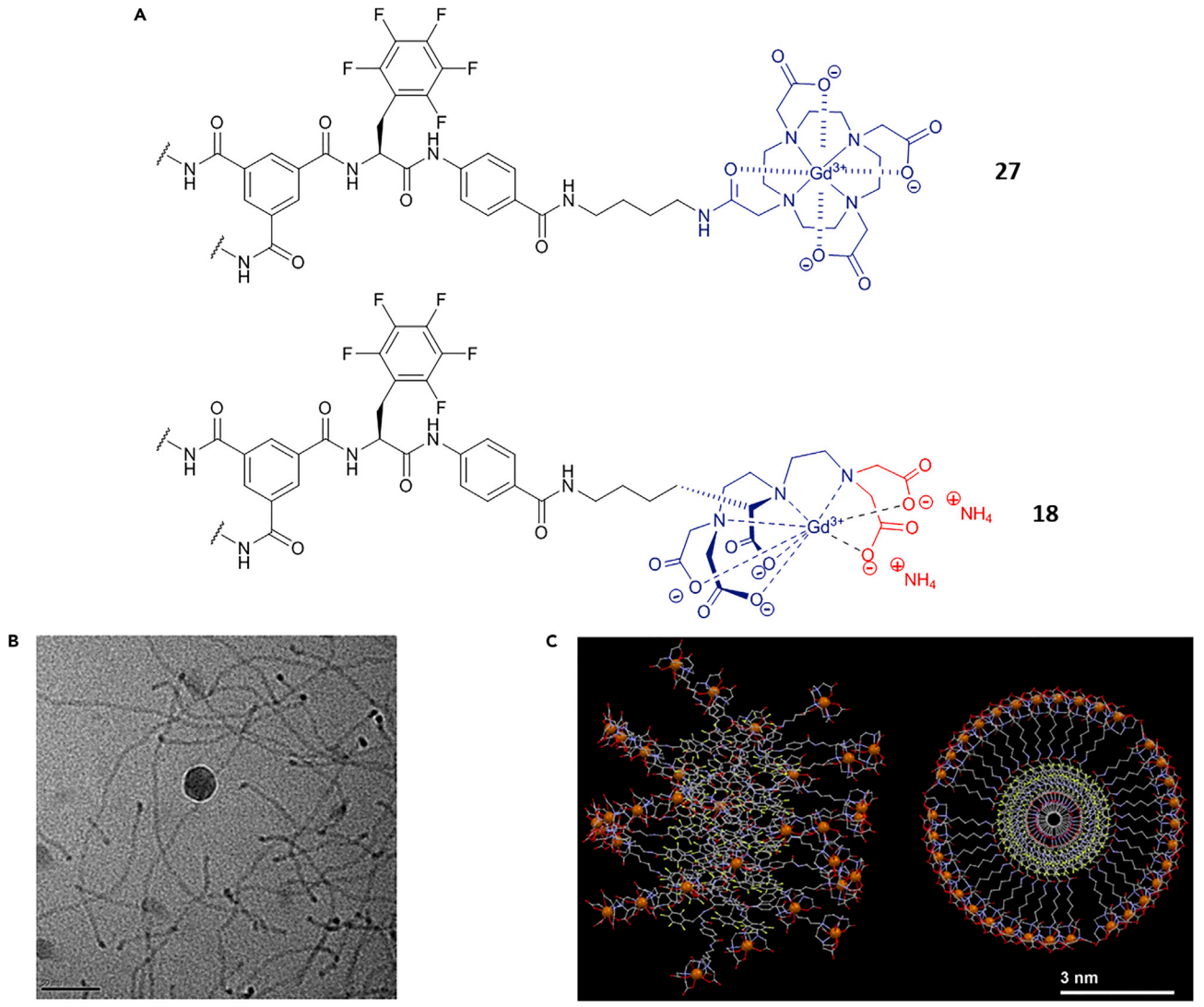

Figure 12. BTA Molecules Bearing Gd-Based MRI Contrast Agents

(A) Chemical structures of BTAs with peripheral hydrophilic metal complexes.

(B and C) TEM micrograph of self-assembled monomers of **27** in citrate buffer (100 mM, pH 6; scale bar, 50 nm) (B) and schematic representation of stack of **18** (left, side view; right, top view) (C). Reprinted from Besenius et al.[52]

metallogelators because of their better control over the self-assembly process and the fact that additional properties and function can be achieved by metal-ion coordination.[55,56]

As discussed above, BTA derivatives self-assemble by cooperative three-fold helical hydrogen bonding. Many versatile derivatives of BTA have been synthesized by incorporating different functional groups—such as alkyl, aryl, pyridyl, bipyridyl, poly (ethylene glycol), amino acids, dipeptide and oligopeptide, oligo(*p*-phenylene-vinylene), porphyrinyl, etc.—for the formation of supramolecular polymers.[38] Recently, Haldar and co-workers used BTA derivatives with simple side chains containing β-alanine **28** and γ-aminobutyric acid **29** to investigate the effect of side chain-side chain interactions in the assembly process.[40] Compound **29** was found to form thermoreversible opaque gels in aromatic hydrocarbon solvents such as

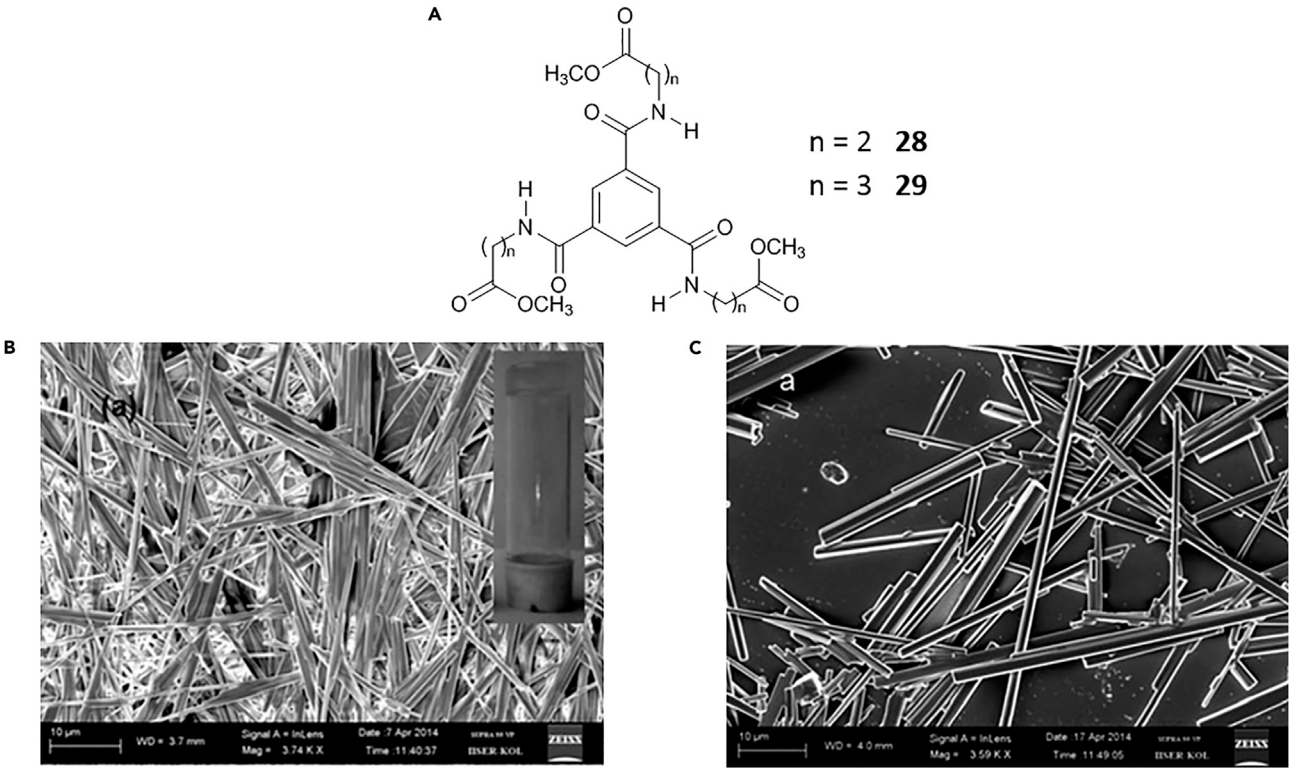

Figure 13. BTA Derivatives Showing the Role of Side-Chain-Side-Chain Interactions in the Assembly Process

(A) Molecular structures of BTA with alkyl side chains **28** and **29**.

(B and C) SEM of xerogel of **29** from toluene (B) and dropcast solution of **28** from 1,2-dichlorobenzene shows crystalline morphology (C). Reproduced from Paikar et al.[40] with permission from the Royal Society of Chemistry.

toluene, *o*-xylene, *m*-xylene, *p*-xylene, although, under similar conditions, **28** did not show any aggregation and failed to form a gel. Scanning electron microscopy (SEM) images of the xerogels of **29** of organic solvents showed unbranched fibers with an entangled network (Figure 13B). To examine the morphological difference between non-gelator **28** and gelator **29**, solutions of both molecules in 1,2-dichlorobenzene were dropcast and analyzed by SEM, where **28** showed unbranched polydispersed rigid crystalline morphology, whereas gelator **29** showed a long fibrous entangled network similar to its xerogel, which can grow in a three-dimensional network encapsulating the solvent molecules leading to gelation. Very recently, Gunnlaugsson and co-workers reported similar BTA compounds with varied side-chain length and functionality.[57] The carboxylic acid derivatives showed a tendency to form gels, and the ester derivatives formed crystalline phases with thermotropic phase transition properties.

X-ray crystallographic analysis showed that both **28** and **29** form individual columnar structures via three-fold H bonding. Detailed analysis shows that the secondary structure of **29** further self-assembled through multiple additional hydrophobic interactions through intermolecular and intercolumnar interactions between side chains (between the γ-aminobutyric acid β-methylenes and between the ester methyl groups), which gives additional support for the formation of the supramolecular networks. Ligand **28** formed self-assembled bundle-like structures, indicating the effect of side-chain interactions on the formation of quaternary structures.

The previously discussed BTAs self-assembled in cooperative fashion to form supramolecular polymers in organic solvents. For several other systems, H-bond-driven self-assembly in water has been reported,[28] but only a few examples of BTA derivatives forming supramolecular polymers in water have been reported.

Helical Arrangement of Achiral Gelators

Recently, Wang, Liu, and co-workers reported a non-chiral BTA connected to ethyl cinnamate (BTAC) **30** possessing increased π surface area that self-assembled to form gel (*c* = 15 mg/mL) in a 60% mixture of dimethylformamide (DMF) and H_2O.[58] Despite its achiral nature, the molecule was found to simultaneously form left- (*M*) and right (*P*)-handed twists in unequal number. When there were more *M* twists than *P* twists, CD spectra showed a negative Cotton effect; this was reversed when the *P* twists were higher in number, suggesting uneven symmetry breaking and resulting in bulk macroscopic chirality of the gels. The SEM images also showed an uneven number of *P* and *M* twists in the same sample.

At an early stage of gelation, some of the BTAC molecules (**30**) reorganize themselves, facilitating the formation of one-dimensional helical aggregates with predominantly either *P* or *M* conformation. Further aggregation then follows the original chiral conformation as a result of steric hindrance caused by crowded molecular packing. Thus formed helical nanostructures undergo hierarchical self-assembly, forming larger twisted ribbons with an unequal number of *P* and *M* conformations (Figure 14A).

Control over the handedness of the twists and macroscopic chirality of **30** gel is gained by addition of a chiral dopant, 1-cyclohexyl ethylamine, **31** (R/S). Gels formed from a mixture of **30**/**31R** (1:3 molar ratio), showed only *M* twists in the SEM image (Figure 14B) and a strong CD signal with an exciton-type Cotton effect at 409 nm and a cross-over at 330 nm. Contrary to the above, the **30**/**31S** gel showed only *P* twists and a mirror image of the CD response. Interestingly, even after removal of the chiral additive **31** (R/S) by vacuum drying, the macroscopic chirality of the system was retained. This was possibly because of a small amount of **31** (R/S) reacting with **30** through an amide-ester exchange reaction, forming **32**, which later directs the helical self-assembly formation in the absence of **31**. Similar results were obtained when other chiral amines were used in place of **31**. However, macroscopic chirality was not observed when additives possessing two chiral centers were used. Thus, addition of external chiral entities allows gaining control over the chirality of the system. Such principles help to develop the systems with highly ordered arrangement of assemblies at the molecular level. Similarly, supramolecular chirality was observed to form other non-chiral systems through the assembly of achiral monomers at the air water/interface.[59]

In addition, many other BTA derivatives with increased π surface area can be formed by introducing different moieties such as bipyridine, naphthalene diimide, etc.[60] Self-assembled structures of these BTAs exhibit interesting properties such as functional supramolecular polymers, columnar liquid crystalline mesophases, remnant polarization in bulk phases,[61] etc. Similar to BTAs, other systems exhibiting self-assembly that result in the formation of nanostructures and functional materials are discussed in the following sections.

Self-Assembly of 1,3,5-Cyclohexyltrisamide-Based Scaffolds

Another class of C_3 symmetric ligands well known to form one-dimensional columnar structures are the 1,3,5-cyclohexyltrisamide-based scaffolds. Feringa, Van Esch, and co-workers, formed efficient hydrogelators by using 1,3,5-cyclohexyltrisamide-based

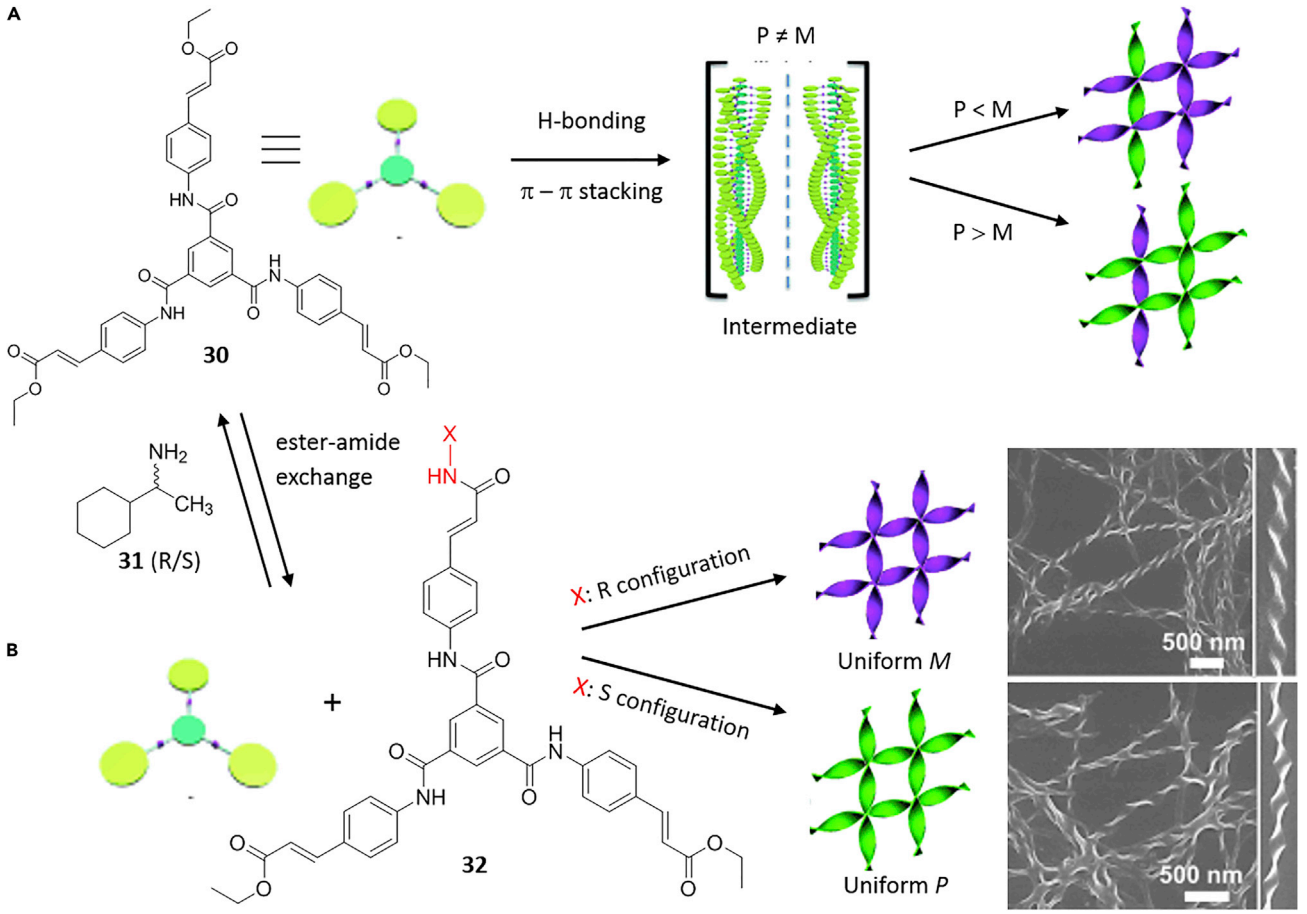

Figure 14. BTA Molecules Forming Left- and Right-Handed Twists

(A) Chemical structure of **30** and schematic representation of gel formation with both *P* and *M* twists.

(B) Gel formation of **30** in the presence of **31** (**R** or **S**) by controlling chirality.

Reprinted with permission from Shen et al.[58] Copyright 2014 Wiley-VCH Verlag GmbH & Co. KGaA, Weinheim.

scaffolds conjugated to amino acids, which are further connected to various side chains.[62] The examples discussed in this section demonstrate how modification of the side chain influences the self-assembly behavior. These molecules were designed according to a modular architecture approach (Figure 15A), which helps to obtain hydrogels with properties that can be controlled at the molecular level. In 1,3,5-cyclohexane-trisamide, three H-bonding amide groups align perpendicularly to the mean plane of the molecule and parallel to each other. This supports self-complementary uniaxial intermolecular interactions, which help unidirectional self-assembly, subsequently leading to gelation.[62] Among the molecules prepared according to the modular architecture shown in Figure 15A, molecules **33**–**35** with hydrophobic substituents (R) and hydrophilic side chains (X), formed a gel in aqueous solution. Compounds **36**–**37**, lacking hydrophobic substituents, failed to gel under similar conditions, thus highlighting the importance of hydrophobic groups in the gelation process in aqueous media.

Later Van Esch and co-workers showed that compound **38** exhibits orthogonal self-assembly behavior in water. In the presence of surfactants, **38** undergoes a concurrent self-assembly process, where the formation of a fibrillar network with encapsulated micelles was observed, showing the two independent supramolecular

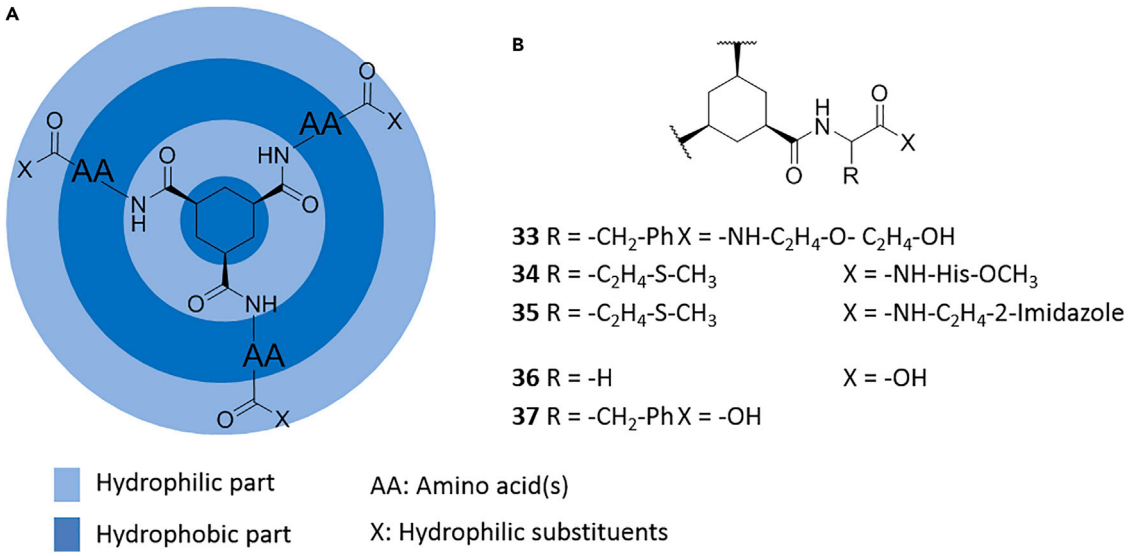

Figure 15. 1,3,5-Cyclohexyltrisamide-Based Hydrogelators

(A) Schematic representation of modular architectures of gelators.

(B) Molecular structures of **33**–**37**.

Reprinted with permission from van Bommel et al.[63] Copyright 2004 Wiley-VCH Verlag GmbH & Co. KGaA, Weinheim.

structures coexisting in the same systems.[64] In another observation, compounds **39** and **40** (and other modified gelators) showed gelation in the presence of spherical micelle-forming surfactants, such as alkyl trimethylammonium bromide (C_nTAB, n = 12, 14, 16), cetyltrimethylammonium tosylate (CTAT) or SDS and even in presence of zwitterionic lipids such as dipalmitoylphosphatidylcholine (DPPC), dimyristoylphosphatidylcholine (DMPC), and dioleoylphosphocholine (DOPC) that form bilayer vesicles showing interpenetrating networks (Figure 16).[65] Hence, orthogonal self-assembly of hydrogelators and surfactants was proven to be a valid strategy toward self-assembled interpenetrating networks and nanoarchitectures, as well as various organizations of micelles or vesicles coexisting with fibrous networks. This indicated dependence of the gelation ability of the molecules on the strength of the intermolecular interactions, which varies according to the structural parameters of the molecules.

As discussed above, like 1,3,5-substituted cyclohexyl scaffolds, BTAs form hydrogen-bonded self-assembled columns.[66] The ability of both of these C_3 symmetric molecules to form one-dimensional structures is examined with simple alkyl-derived LMWGs and thickeners on the basis of the cyclohexane and BTA core. Hence, in order to have a better understanding of the intermolecular interactions (which is a driving force for the self-assembly of these two scaffolds), de Loos et al. analyzed and compared molecules **41** and **42**, as well as **43** and **44**, with the same substituents (Figures 17A and 17B).[67]

BTA molecules **41** and **42** were found to show poor aggregation without showing any signs of gelation, indicating the poor influence of H-bonding units, which might be due to sterically demanding R groups. However, the cyclohexyl-cored compounds **43** and **44** exhibited aggregation properties, forming gels. From the crystal structure of the cyclohexane-cored compound **45**, the orientation of the amide groups was found to be perpendicular to the plane of the core and parallel to each other, this enabling stronger one-dimensional H bonding and increased

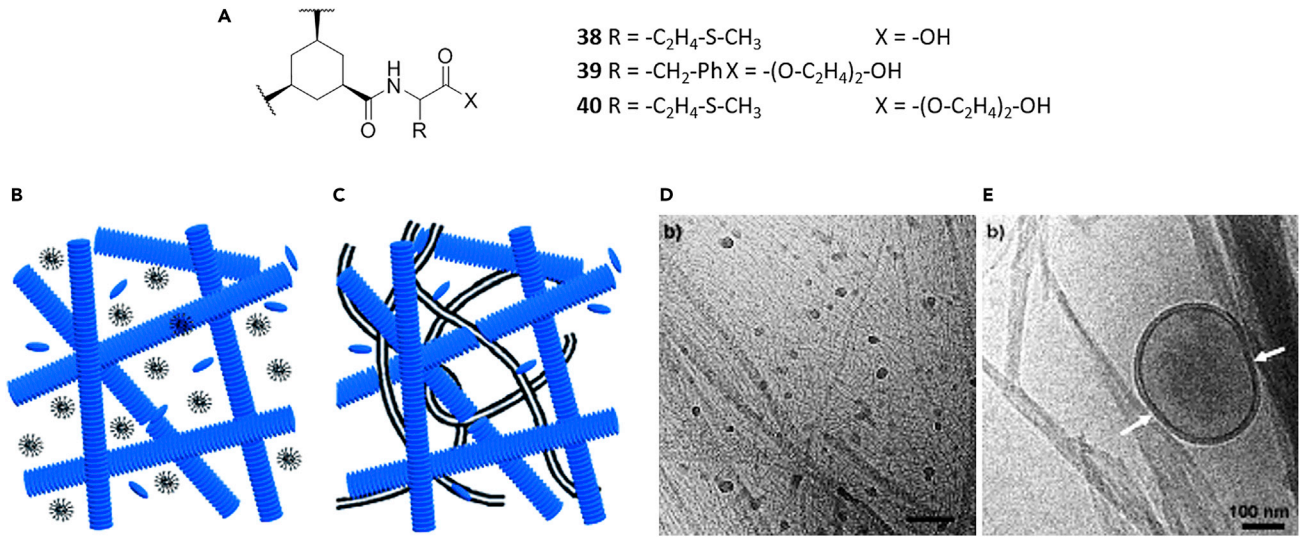

Figure 16. 1,3,5-Cyclohexyltrisamide-Based Hydrogelators Exhibiting Orthogonal Self-Assembly

(A) Molecular structures of **38**–**40**.

(B and C) Schematic representation of the orthogonal self-assembly strategy using C_3 symmetric molecules (B) and surfactants forming more complex and compartmentalized structures (C).

(D and E) TEM images of the fibrous network of **39** (2 mM) in the presence of CTAT (100 mM, as cylindrical micelles; scale bar, 100 nm) (D) and unilamellar dioctadecyldimethylammonium bromide vesicles and fibers of **40** (E). Arrows indicate the shape of the vesicle.

Reprinted with permission from Brizard et al.[65] Copyright 2008 Wiley-VCH Verlag GmbH & Co. KGaA, Weinheim.

gelation ability.[63] In the benzene core compounds, the H-bonding units preferred to be in-plane of the core because of delocalization, as observed in the crystal structure of **46** (Figure 17C).[66] The type and number of H-bonding units and substituents (R groups) also have a significant influence on the aggregation of molecules.[43,51,67] From these results, the cyclohexyl scaffolds were found to be better at forming one-dimensional structures and forming gels than BTA scaffolds.

It is well known that the properties of the bulk material depend on the self-assembly rate of the building blocks or monomers. Smith, Van Esch, and other groups reported the *in situ* formation of a supramolecular gelator by using two-component systems, which later self-assemble through non-covalent interactions to form a gel. Examples of such two-component gel systems are discussed in further sections. Ulijn and co-workers reported the effect of the rate of enzyme-catalyzed *in situ* gelator formation on the morphology of gels; upon simply increasing the enzyme concentration and therefore gelator generation, they achieved control over the formation of nanometer to micrometer fibers, which consequently resulted in a gel with higher thermal stability.[68]

Catalytic Control over the Gel Properties

Van Esch and co-workers showed that catalytical control of *in situ* formation of the cyclohexane-core-based gelator (which ultimately self-assembles to form gels) allowed for indirect control of the morphology and properties of the gel.[69,70] On mixing clear aqueous solutions of **47** and **48** at pH 5.0 (in 0.1 M phosphate buffer), the acidic conditions catalyzed the *in situ* formation of compound **49**, which underwent immediate self-assembly to form an opaque/turbid gel in the same medium (Figures 18A and 18B). Furthermore, similar results were obtained on mixing **47** with **48** at pH 7.0 in the presence of aniline (as a result of an aniline-catalyzed reaction), which resulted in compound **49**, and subsequently formation of a gel. The gels obtained

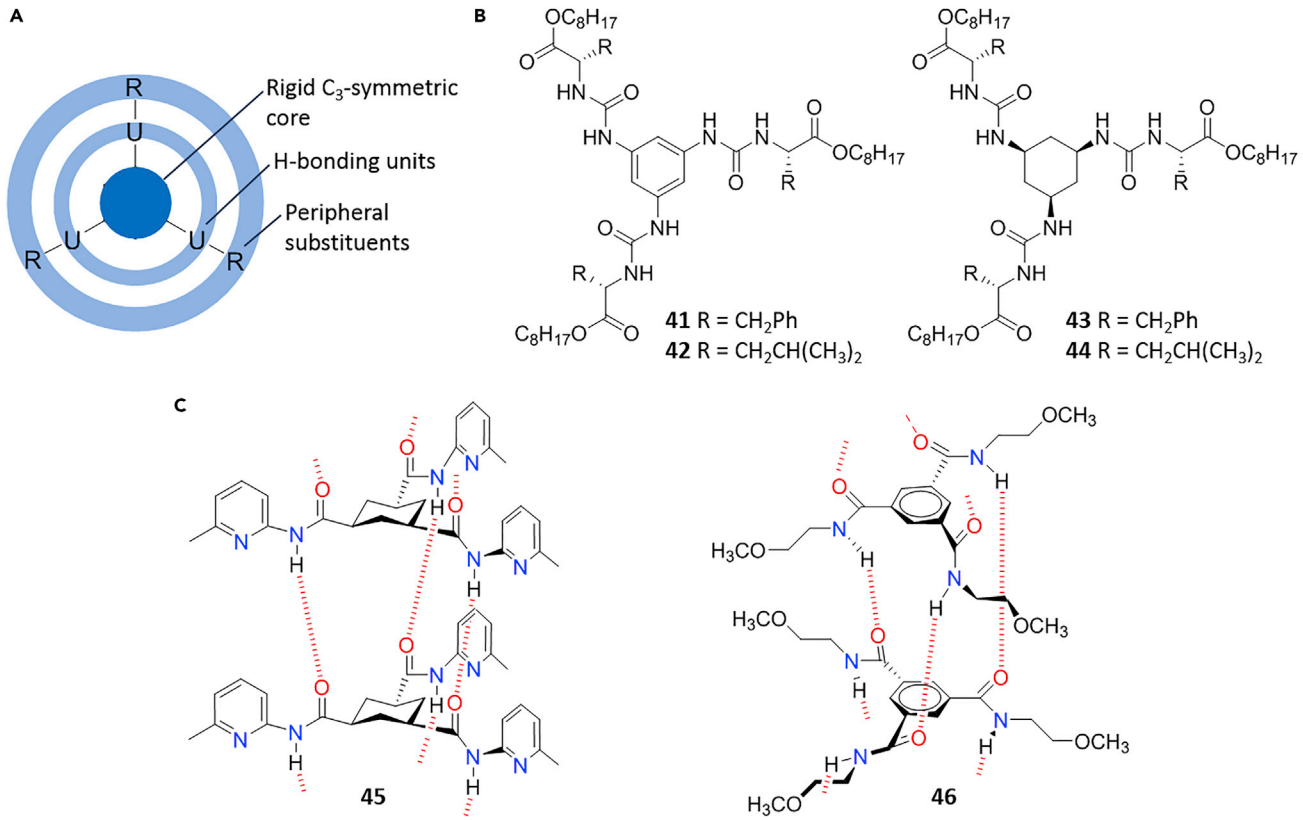

Figure 17. Alkyl-Derived LMWG and Thickeners Based on Cyclohexane and BTA Core

(A and B) Schematic design of the C_3 symmetric compound (A) and the molecular structure of the tris-urea-based compounds **41–44** (B). Reprinted from de Loos et al.[67]

(C) Representation of translational H-bonded stack of cyclohexane tricarboxamides (**45**) and triple helical H-bonded benzene tricarboxamide derivative (**46**) (from crystal structures). Reproduced from Fan et al.[62] and Lightfoot et al.[66] with permission from the Royal Society of Chemistry.

were pH responsive with thermal stabilities up to 120°C. However, in the absence of a catalyst at pH 7.0, only turbid solutions were observed with no gel formation. The final turbidity was lowest for the acid-catalyzed sample and highest for the uncatalyzed sample, indicating a clear influence of catalysis on the formation of the gelator (Figure 18B). SEM analysis of these samples revealed that the morphology of both catalyzed samples showed a highly branched entangled fibrous network, but only thick and less branched fibers were seen in the uncatalyzed sample (Figures 18C and 18D). Moreover, the catalyzed samples had greater mechanical stability, as determined by rheology, where the storage modulus (G′) increased by an order of magnitude to 50 kPa and 55 kPa for the acid- and aniline-catalyzed samples, respectively. This clearly indicates the influence of the catalyst on the *in situ* formation of the gelator, which subsequently influences the gelation process.

Self-assembly of smaller building blocks leading to soft materials such as gels and their applications is discussed in further sections.

SUPRAMOLECULAR GELS FROM OTHER LMWGS AND THEIR APPLICATIONS

In the previous sections, BTA derivatives, which form gels, were discussed. Gels are an important class of soft materials. They are formed from a broader range of building blocks and have found application in many areas: food, cosmetics, pharmaceuticals,

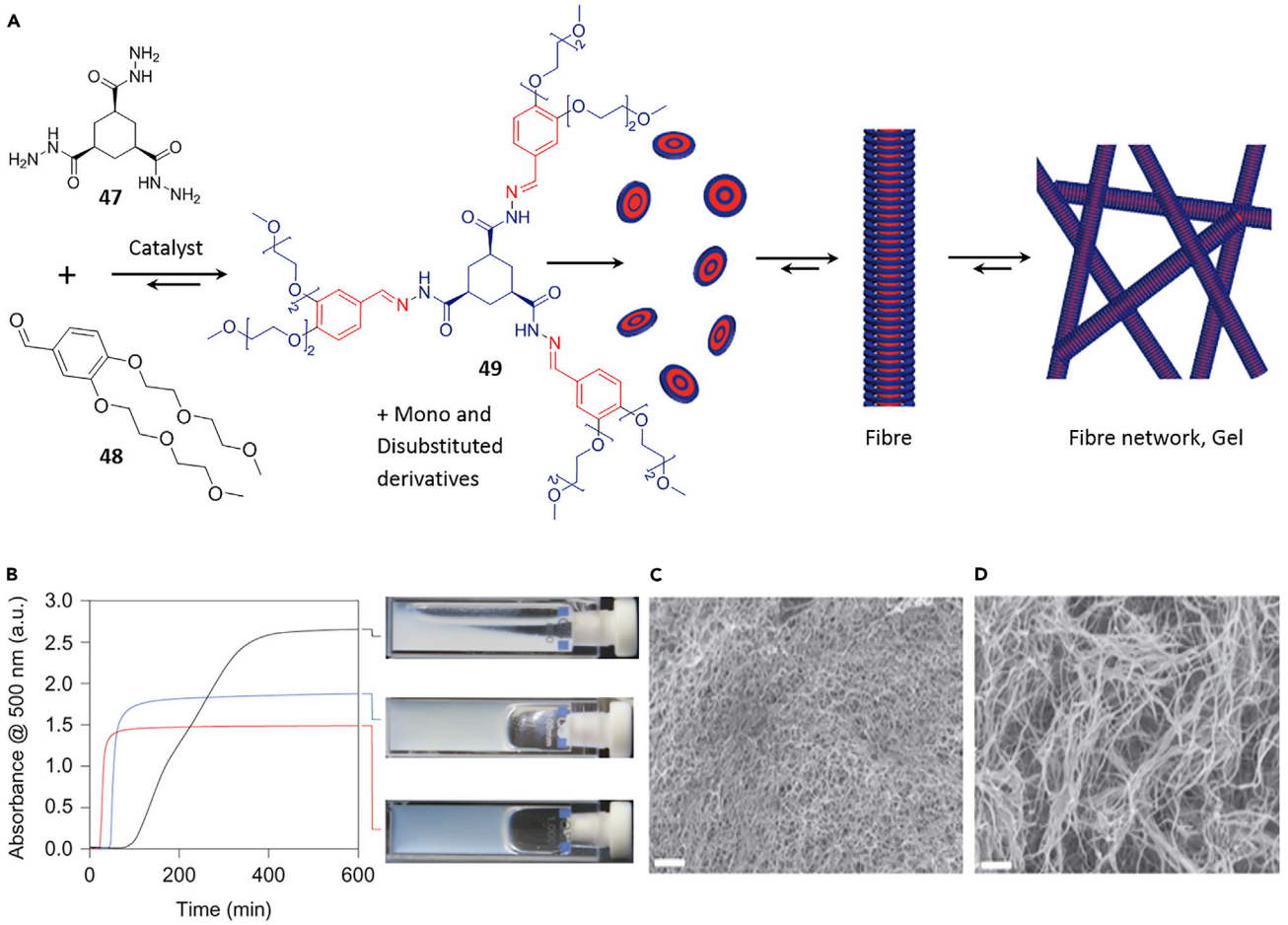

Figure 18. Catalytically Controlling the *In Situ* Formation of Hydrogelator

(A) Catalytic *in situ* formation of tris hydrazine hydrogelator (**48**, blue, hydrophilic; red, hydrophobic functional groups), which eventually self-assembles to fibers, leading to gelation.

(B) Turbidity measurements of **49** gel show absorbance at 500 nm as a measure of structure formation (red, pH 5.0; blue, 10 mM aniline at pH 7.0; black, pH 7.0 [**47**] = 8 mM; 0.1 M phosphate buffer). Thus, the acid-catalyzed **49** gel is more transparent.

(C and D) SEM images of aniline-catalyzed gel **49** show dense branched fibers (C), and images of the uncatalyzed gel show thick, less branched fibers (D). Scale bars, 500 nm.

Reprinted with permission from Boekhoven et al.[69] Copyright 2013 Nature Publishing Group.

petroleum, and many more.[71] In this section, recent examples of supramolecular gels as smart materials are discussed, highlighting their modern applications.

Generally, single-component systems self-assemble to form gels. Using more than one component, however, gives further opportunity to tune the properties of the gels.[5] Hirst and Smith highlighted this aspect in their review with examples of two-component systems exhibiting control over the self-assembly process.[72] In true two-component systems, the gel is formed only upon addition of a second component to the first one. In this case, usually self-assembly is controlled by manipulating the single molecular recognition events. In some cases, the second component significantly modifies the behavior of the known gels by allowing self-assembly of simpler building blocks to form complex functional materials at the macroscopic level.

Multicomponent Gel Systems

Smith and co-workers have studied further multicomponent systems by using dendritic L-lysine-based peptide with carboxylic acids groups (**50**) and different aliphatic

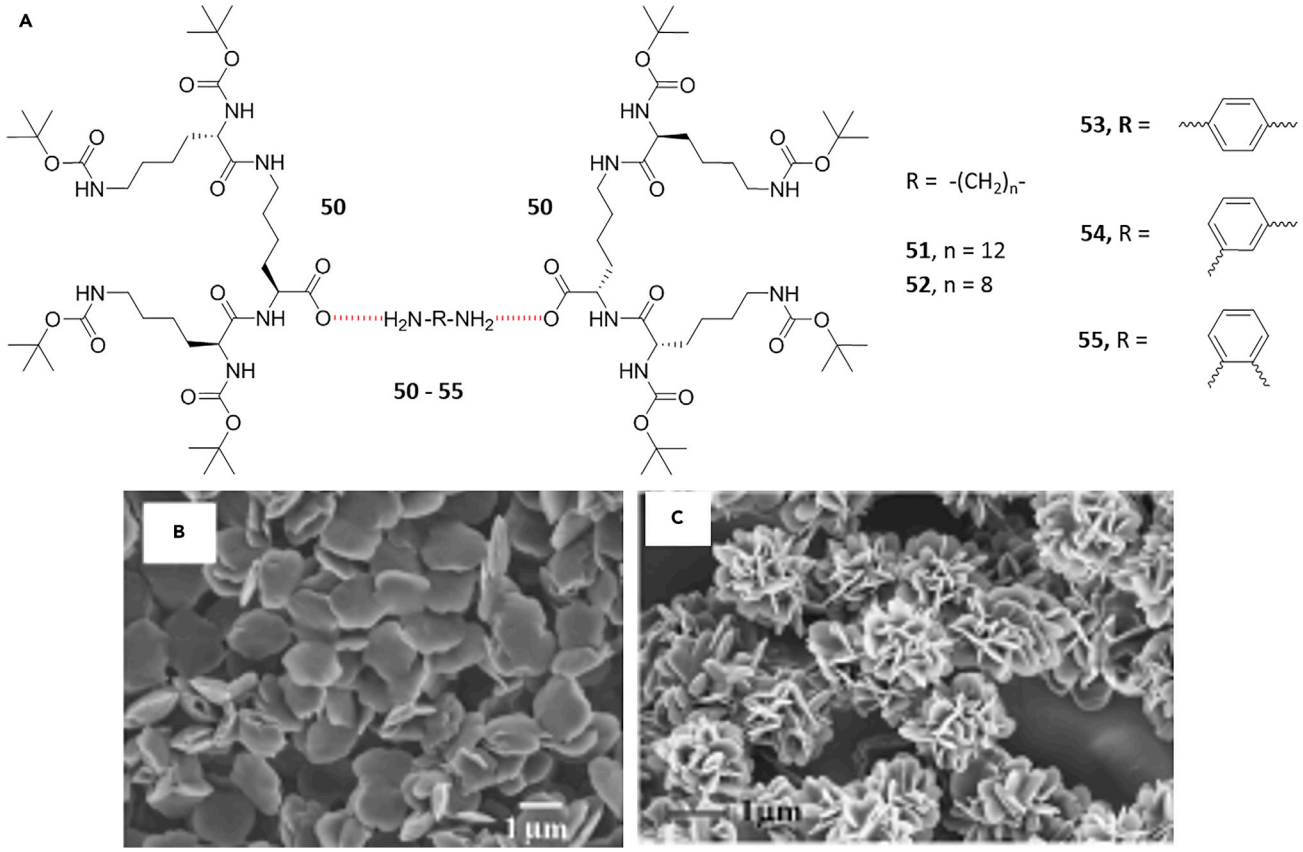

Figure 19. Dendritic L-Lysine-Based Molecules and Their Gels

(A) Structures of dendron **50** and diamines **51**–**55**.

(B and C) SEM images of the platelets formed from the **50:51** mixture (1:4.5 molar ratio) (B) and rosettes formed from the **50:52** mixture (1:5 molar ratio) (C). Reprinted with permission from Hirst et al.[74,75] Copyright 2005 and 2009 Wiley-VCH Verlag GmbH & Co. KGaA, Weinheim.

and aromatic diamines (**51**–**55**) self-assembling via H bonding in toluene (Figure 19A).[73] They showed that increasing the length of the aliphatic diamine chain (**51**–**52** and C8–C12) leads to a dramatic increase in the thermal stability of gels (4°C–105°C). The role of **51**–**52** in tuning the transcription of chirality from the molecular level to the macroscopic level was highlighted. Furthermore, varying the molar ratio of **50** to **51**–**52** resulted in significant differences in the thermal stability and morphology of the assembles species.[74] For the **50:51** system (1:4.5 molar ratio), the morphology changed from nanofibers to platelets (Figure 19B). Whereas, for the **50:52** (1:5 molar ratio) system (**52** with a shorter chain length), interesting morphologies such as nanoscale "rosettes" were observed (Figure 19C).

The effect of aromatic diamines **53**–**55** indicates the importance of molecular geometry in intermolecular interactions for the formation of gels.[75] Mixing **50** with **53**, **54**, or **55** in toluene results in different behavior; **50:53** formed gels, **50:54** formed irreproducible partial gels, whereas **50:55** did not form a gel. In the **50:53** gel, a 1:1 molar ratio was found in the gel network by nuclear magnetic resonance (NMR), and this ratio remained the same even when 3 equiv of **53** was added to the system, with the excess remaining in solution. Interestingly, mixing **50** with **53**, **54**, and **55** in (1:1:1:1) together in toluene resulted in gel formation. From NMR studies of the solution component, the majority of **53** was involved in gelation with significantly less of compounds **54** and **55**, highlighting the importance of molecular geometry in the

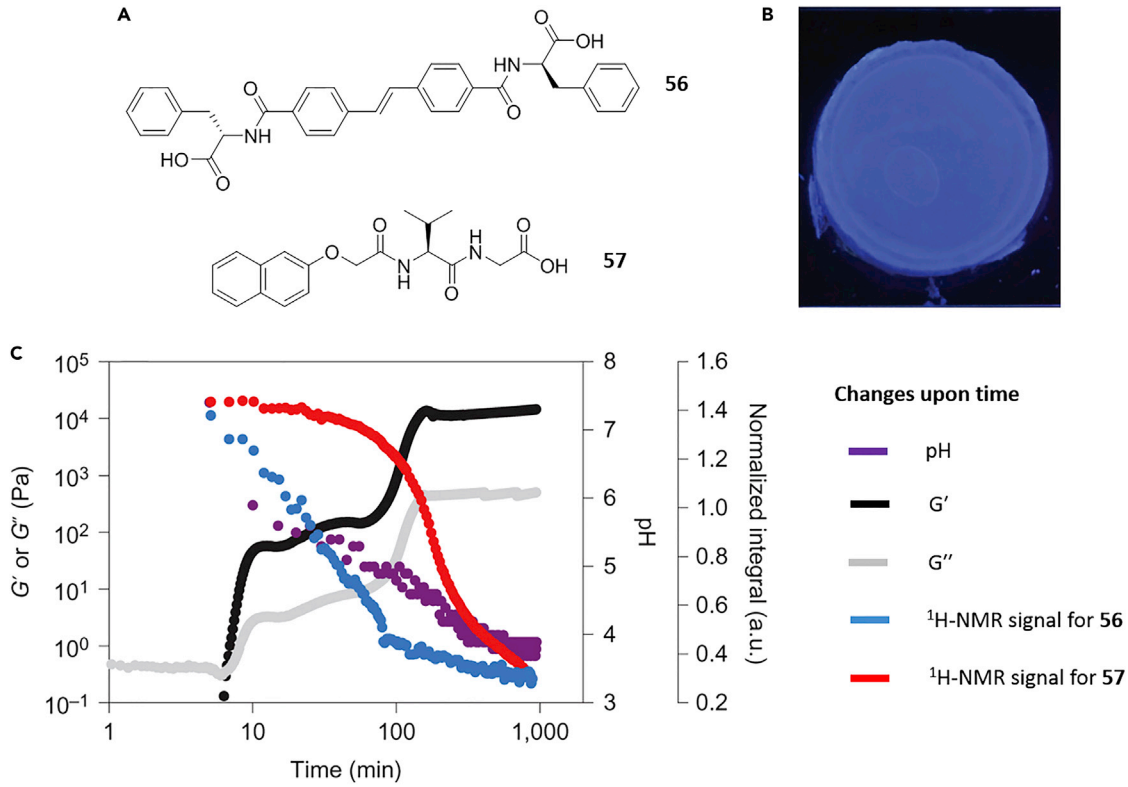

Figure 20. Multicomponent Gel from Stilbene-Based Molecules

(A and B) Chemical structures of **56** and **57** (A) and a **56/57** mixed gel under 365 nm UV light (B).

(C) Multi-scale diagram showing the evolution of pH (purple), G′ (black), G″ (gray), and H NMR integrals with time for a mixture of **56** (blue) and **57** (red). Reprinted with permission from Draper et al.[78] Copyright 2015 Nature Publishing Group.

gelation process (Figure 19A). Many other examples of similar multicomponent systems showing control over gelation and gel morphology through component selection exist,[76] opening up the opportunity for further development of smart soft materials.

Multicomponent Self-Sorted Gel Systems

Recently, Adams and co-workers reported a two-component gel system with self-sorted networks by using two pH responsive gelators, which form two independent fibrous networks upon slow decrease of pH.[77] As the pH decreases, the gelator with the highest pK_a assembles first and buffers the system. Later, the second gelator assembles when the pH corresponds to its pK_a. This kind of approach most often results in a self-sorted network in which each set of fibers is made exclusively of one gelator. Later, Adams and co-workers also used two gelators **56** and **57**, where **56** is both pH and light sensitive, for the development of a spatially resolved multicomponent system.[78]

The *trans*-isomer of stilbene-based gelator **56** (c = 5 mg/mL) formed a hydrogel by controlled decrease of pH from 10 to 4. The pH was changed uniformly throughout the sample by hydrolyzing glucono-δ-lactone (GdL) to gluconic acid.[78] Gelator **56** has a pK_a of 5.8 and forms gel when the pH is below this (Figure 20B). However, the *cis*-isomer of **56** did not form a gel under similar conditions, resulting only in precipitate, proving this isomer to be an inefficient gelator. When **56** gel was irradiated with a 365 nm light-emitting diode (LED) and a mask, selective spatial conversion of

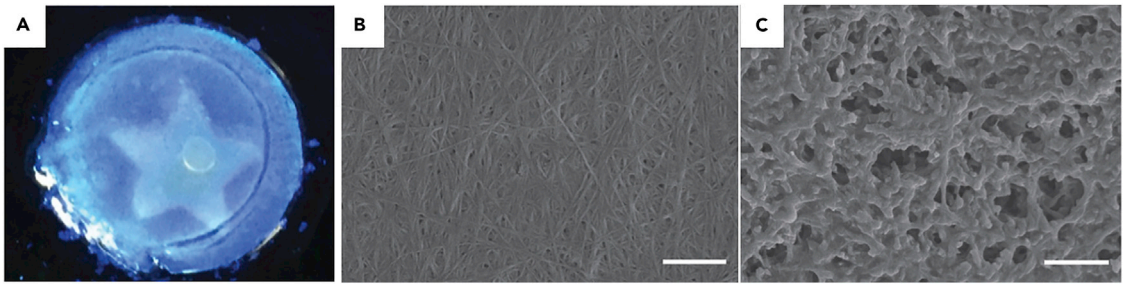

Figure 21. Spatially Resolved Mixed Gels

(A) The **56/57** mixed gel irradiated with 365 nm UV light and a star-shaped mask.

(B and C) SEM images of the **56/57** mixed gel: samples were taken from the edge (non-irradiated region) (B) and from the center (irradiated region) (C). Scale bars, 1 μm.

Reprinted with permission from Draper et al.[78] Copyright 2015 Nature Publishing Group.

the gel to liquid was achieved, similar to other light-triggered gelators. Morphology of the gel before irradiation consisted of the fibers formed by self-assembly of **56**. After irradiation, the morphology of the sample was similar to that observed from *cis*-**56**. On mixing **56** with a second gelator **57**, a solution with pH 10 was prepared (c = 5 mg/mL each). The gel formed from **57** alone was not affected by 365 nm LED irradiation. Gels were formed from a mixed solution of **56** and **57** with GdL, which allowed slow pH change, facilitating monitoring of the gelation process. The gelation process was followed by ^{1}H NMR spectroscopy as the molecules self-assembled into fibers. The plot of integral size for **56** and **57** is shown in Figure 20C.

Evolution of the ^{1}H NMR spectra as the pH decreases clearly indicates a sequential assembly process, whereby **56** disappears before **57** because of its apparent higher pK_a (Figure 20C, blue and red). Rheological measurements performed in parallel showed an increase of both storage modulus (G′) and loss modulus (G″) after 8 min and a second increase after 20 min, indicating the gelation of **56**, which is common for this kind of gelator when GdL is used (Figure 20C, black and gray). As the pH drops to 5, **57** also starts to disappear in the ^{1}H NMR spectra. A significant increase in G′ and G″ was observed, corresponding to gelation of **57** alone. This confirms that the self-assembly of **56** and **57** is a sequential process along the multi-length scale. The final **56** and **57** gels formed from self-sorting mixtures were translucent and homogeneous with no phase separation (Figure 20B). The identification of the self-sorted network was complicated by the similar morphology displayed by both components.

On irradiating the **56** or **57** gel with a 365 nm LED, it retained structural integrity, but a decrease in gel strength was observed. When the irradiation was continued, rheological data showed a gradual decrease in G′ and G″, which stabilized after 2 hr, and values lower than for the irradiated **56** or **57** gel. However, these data were in close agreement with those for the **57** gel alone. Furthermore, under irradiation of the **56** or **57** gel, fibers formed from only **56** were selectively removed as it was isomerized, and the **57** network remained undisturbed. Furthermore, under this methodology, spatial patterning of the **56** or **57** gel was achieved by selective irradiation using a star-shaped mask (Figure 21A). From SEM, the areas that were not irradiated were not affected and still composed of fibers of the **56/57** gel. The exposed part, however, showed a dense network with some aggregates, similar to *cis*-**56**, indicating the disruption of only **56** fibers in the irradiated region (Figures 21B and 21C). This kind of methodology opens up the opportunity for development of spatially resolved gels and of spatially controlling the properties of these gels.

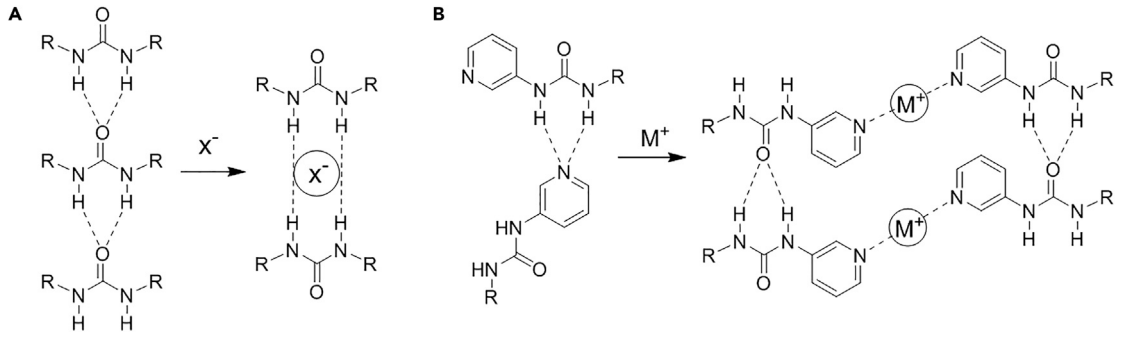

Figure 22. Schematic Representation of α-Tape H Bonding between Bis(urea)-Derived LMWGs

(A) Schematic representation of the interaction of anion (X^-) in α-tape H bonding between the urea motif of bis(urea) LMWGs reducing the gel strength. Reproduced from Lloyd et al.[79] with permission from the Royal Society of Chemistry.

(B) Metal ion (M^+) interacting with pyridyl nitrogens, forcing the urea motifs to form α-tape H bonding and metal coordination. Adapted from Piepenbrock et al.[80] with permission from the Royal Society of Chemistry.

From the examples discussed above, the need to control the properties of gels is highlighted. This can be achieved by understanding how to control intermolecular interactions. However, it is still difficult to predict the effect of supramolecular interactions at molecular level on the bulk material properties.

Steed and co-workers used metal-ligand interactions and anion binding in order to gain control over the assembly process and monitor the strength of the resulting bulk material. In some cases, an anion was used to tune the strength of the gel, wherein the anion reduces gel strength by interacting with the α-tape H bond between bis-urea gelators (Figure 22A).[79] Addition of metal salts (e.g., Cu(II) and Ag(I)) to pyridyl urea gelators, **58** and **59**, results in gels formation, wherein metal-pyridine interactions reduce the urea-pyridyl interactions, forcing the urea groups to form H bonds leading to fiber formation (Figure 22B).[80] Such manipulations allow control over the bulk material properties.

Multicomponent Halogen-Bonded Gel Systems

Recently, Steed, Resnati, and co-workers used halogen bonding as a new tool for intermolecular interaction in the development of two-component supramolecular gels in polar media.[81] Bis(pyridyl urea) derivatives **58** and **59** form gel in the presence of a halogen-bond donor **60** through halogen bonding. Halogen-bond donor **61** also forms a gel when treated with **62**, $(C_4H_9)_4N^+\ I^-$ (**63**), or **58** (Figure 23).

The mixture of **58** and **60** formed an opaque gel (1% w/v, 1:1 molar ratio) in CH_3OH or in an aqueous mixture with CH_3OH, CH_3CN, or DMSO (4:1 v/v) upon fast cooling of a hot solution (60°C) in a dry-ice bath. However, slow cooling of the same mixture to room temperature resulted in co-crystallization of **58:60** (1:1). From SEM analysis, two-dimensional hexagonal platelet morphology was observed for **58** crystal alone, which changed to one-dimensional needle-like structures upon forming the **58:60** co-crystal (Figures 24A and 24B). Single-crystal X-ray crystallography of **58:60** co-crystals showed the urea moieties forming double, anti-parallel α-tape H bonding (Figure 24B). The additive **60** formed halogen bonds with **58**, acting as a bridge in connecting the two urea tapes, supporting the formation of two-dimensional sheet structures. The X-ray powder diffraction pattern of the xerogel of the fast-cooled **58** or **60** gel matched the single-crystal structure of the **58:60** co-crystal, thus suggesting that the gel structure was similar to the crystals and supporting the involvement of halogen bonding in gelation.

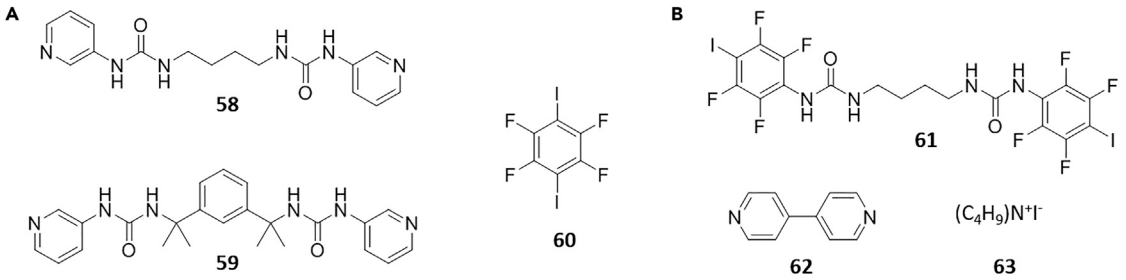

Figure 23. Chemical Structures of Halogen-Bond-Forming bis(urea) LMWGs Forming Two-Component Co-gels and Co-crystals
Halogen-bonding acceptors (**58** and **59**, A) and and halogen-bonding donor (**61**, B). Reprinted with permission from Meazza et al.[81] Copyright 2013 Nature Publishing Group.

Although **59** was not able to form a strong α-tape H-bonding network because of its sterically hindered nature, it formed a fairly strong **59-60** mixed gel (1% w/v, 1:1 molar ratio) in CH_3OH/H_2O (4:1 v/v) on fast cooling. Similar to the previous case, a **59:60** (1:1) co-crystal was obtained upon slow cooling of the solution, but in this case, **60** showed two different environments (Figure 25A). One molecule of **60** formed halogen-bonding bridges between a pair of **59**, but the second **60** was not involved in halogen bonding—it formed only weak H···F and I···I interactions. Arising from this, one of the pyridyl nitrogens H bonded with solvent H_2O, and the urea moieties did not form an α-tape H-bonding network, explaining the weak nature of the **59/60** gel.

In the case of the halogen-bonding donor bis(urea) derivative **61**, gels of **61/62** and **61/63** mixtures were formed (Figures 25B and 25C). The **61/62** co-gel obtained was less crystalline (it showed smaller fibers) and was considerably more stable when formed without fast cooling (Figure 25D). Similarly, mixtures of halogen-bond acceptor **58** and halogen-bond donor **61** formed a **58/61** (1% total concentration) mixed gel through complementary halogen-bonding interactions, in $DMSO/H_2O$ (3:1), upon warming and cooling. This is explained further by the involvement of halogen bonding in gelation.

From these examples, halogen bonding proved to be a new and versatile approach for inducing fiber formation and hence has resulted in the development of two-component gels in polar media. The advantages of halogen bonds over H bonds are that (1) they tend to be more directional, (2) the interaction strength can be tuned depending on the polarizability of the donor halogen atom, (3) the hydrophobic nature of halogen bonds allows them to be used in aqueous conditions, and (4) they can be integrated into the gelator structure or can be introduced by addition of a second component. Such benefits increase the number of options in the toolkit for controlling supramolecular gel formation and manipulating bulk material properties.[82]

Supramolecular Gels as Crystallizing Media

The supramolecular gels reported from the past decade have found applications in various fields such as tissue engineering, drug delivery, templating medium, molecular electronics, sensing, environmental remediation etc.[83,84] In addition to these, supramolecular gels have found their latest application as functional smart materials for crystallizing pharmaceutical compounds. In recent times, supramolecular gels are a better medium for growing crystals with improved physical characteristics (larger size, optical quality, and fewer defects) and facile recovery of crystals. The

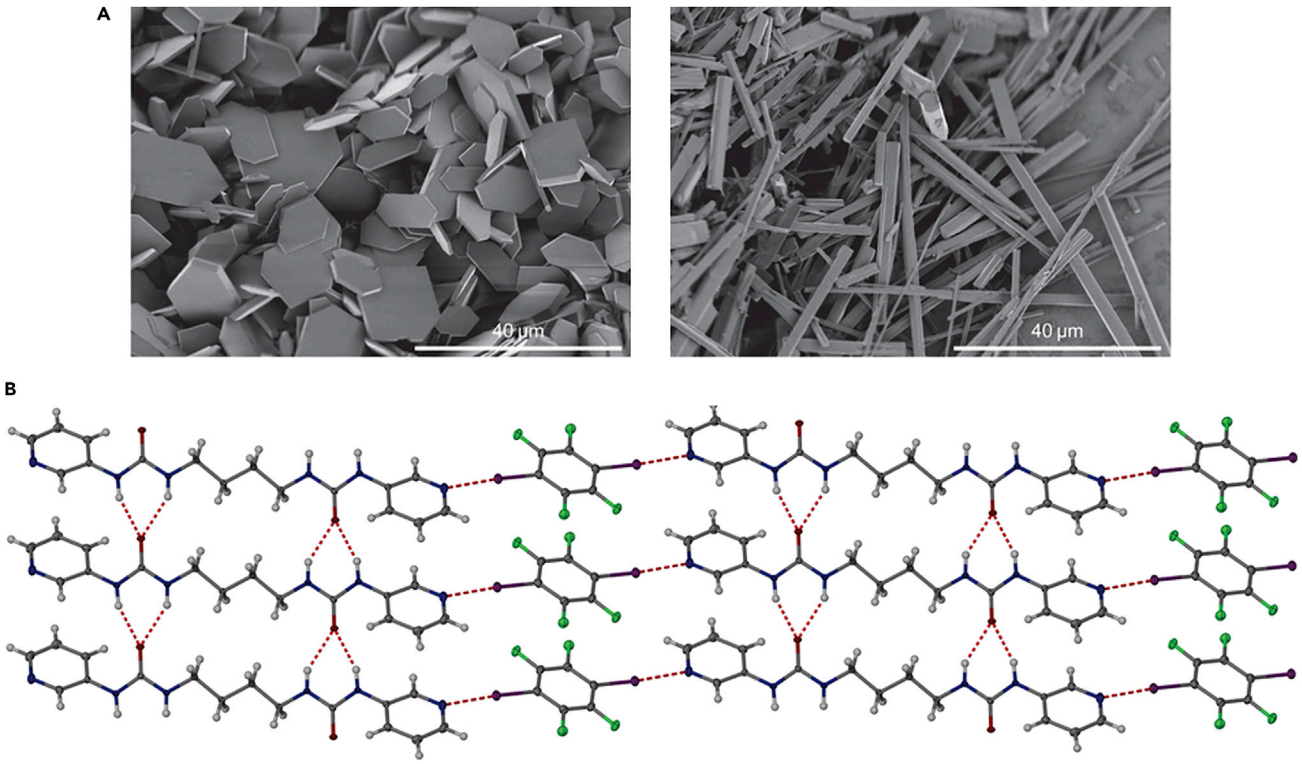

Figure 24. Bis-urea LMWG Forming Two-Component Co-gels

SEM images of crystal **58** and 1:1 co-crystal **58:60** (A) and X-ray crystal structure of co-crystal **58:60** showing α-tape H bonding between urea moieties and halogen bonding between **58** and **60** (B). Reprinted with permission from Meazza et al.[81] Copyright 2013 Nature Publishing Group.

crystals grown from gel media were of better quality, which was attributed to suppressed convectional currents and nucleation supported by the viscous gel media. Conventional hydrogels suffer from the limitations of using only water as solvent, and crystal recovery involves hydrolysis or heating, which damages the crystals. Steed and co-workers used a supramolecular gel based on bis(urea) gelators for the growth of molecular crystals of organic and pharmaceutical compounds.[85] Compound **64** was chosen because it forms gels in various organic and aqueous media, and a Cu(II)-based metallogel from **59** has also been explored. Dissolving bis(urea) gelator **64** and anticonvulsant carbamazepine **65** (1% w/v each) in toluene by heating and cooling resulted in gel formation, followed by formation of crystals of **65** after around 8–12 hr (Figure 26). The presence of the crystals of **65** had no effect on the mechanical properties (storage and loss moduli) of the **64** gel. An increase in yield stress was observed, which was a result of the physical support of the gel by solid **65** crystals, contrary to the effect of anion binding by bis(urea) gels. Addition of excess tetrabutylammonium (TBA) acetate resulted in the dissolution of gels and **65** crystals were recovered without any degradation. This example highlights the use of supramolecular gels as a new medium to grow crystals, allowing access to a wide range of solvent systems. Their reversibility helps in facile release of crystals grown in the gel media.

Very recently, Steed and co-workers developed bis(urea) gelator **66** with a functional group configuration specifically similar to the highly polymorphic drug ROY (**67**).[86] On cooling the hot solution of **66** (1% wt/v) and **67** (100 mg/mL) in toluene, a gel was formed containing red crystals of **67**. The surface of the fiber consisted of an

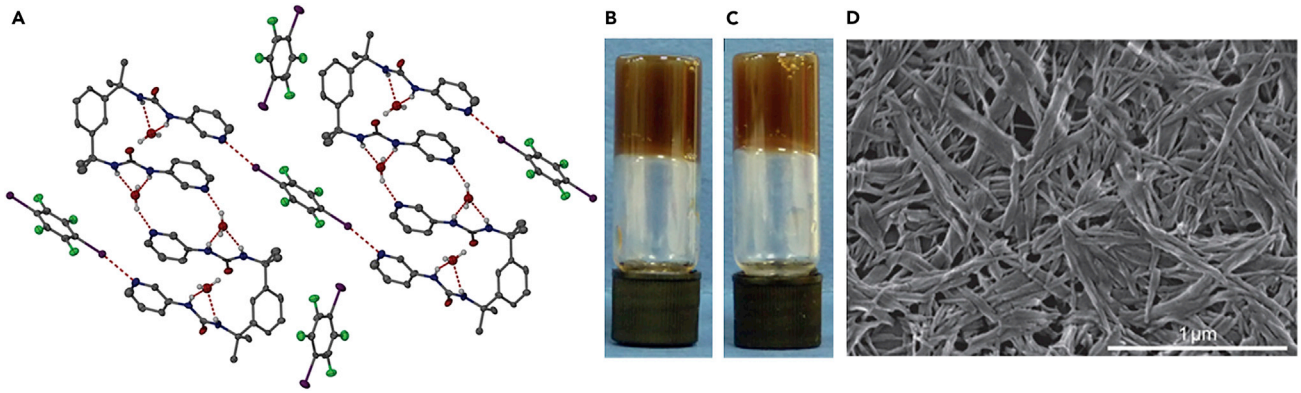

Figure 25. Bis-urea LMWG Forming Two-Component Co-Gels

Crystal structure of co-crystal **59:60** (A), pictures of **61/62** (B) and **61/63** gels (C) (1% each) in DMSO/H_2O (3:1), and SEM image of **61/62** gel (D). Reprinted with permission from Meazza et al.[81] Copyright 2013 Nature Publishing Group.

ordered arrangement of *o*-nitroaniline-derived functional groups of **66**, which chemically mimic the *o*-nitroaniline substituent in **67**, allowing epitaxial crystal growth. This results in the formation of a metastable red form of **67** in a specific manner, instead of its usual thermodynamically stable yellow polymorph (Figure 27).

Similarly, in another case using calixarene diammonium salt and bis-crown ether, Kaufmann et al. reported a two-component supramolecular co-gel in which the hydrophobic cavities on the gel surface act as anchor sites to allow the hydrophobic drug molecule to nucleate and result in the growth of crystals.[87] This new approach uses gelators with a design that enables crystal growth in its fibers, paving the way for the application of supramolecular gels in crystallizing polymorphic pharmaceutical agents in a controlled manner, thus inducing nucleation in compounds that have proven difficult to crystallize. Similarly, Gunnlaugsson and co-workers reported pyridyl urea-based gelators forming organogels with antimicrobial properties through the formation of H bonding between NH urea protons and pyridyl N atoms.[88]

As discussed previously, self-assembly of molecules can be used as an effective pathway for the development of supramolecular architectures. Gunnlaugsson and co-workers have established expertise for the development of novel luminescent Ln(III) probes[89] and multimetallic luminescent Ln(III) self-assemblies[12] for the development of soft materials such as gels, because there is a need for such molecular materials in hydrometallurgy, cosmetics, food processing, lubrications, drug delivery, protein crystallizations, etc.[85] Metal-directed synthesis is recognized as being a key approach to the formation of such assemblies.[90]

BTA-Based Metallogels

Gunnlaugsson and co-workers detailed the first example of a terpyridine-based tripodal molecule (**68**) exhibiting gelation properties in the presence of Eu(III) ions (Figure 28A).[91] They achieved this by using the C_3 symmetrical (BTA) core (known for its formation of triple-stranded hydrogen bonding) connected to three 2,2′,6′,2″- terpyridyl (tpy) moieties, which are expected to coordinate the Ln(III) and function as a sensitizing antenna for the population of the $^5D_0$ excited state of Eu(III).

Spectrophotometric studies conducted in solution of ligand **68** with Eu(III) ions indicated the formation of a (**Eu:68**) complex with a 1:1 stoichiometry. Energy transfer

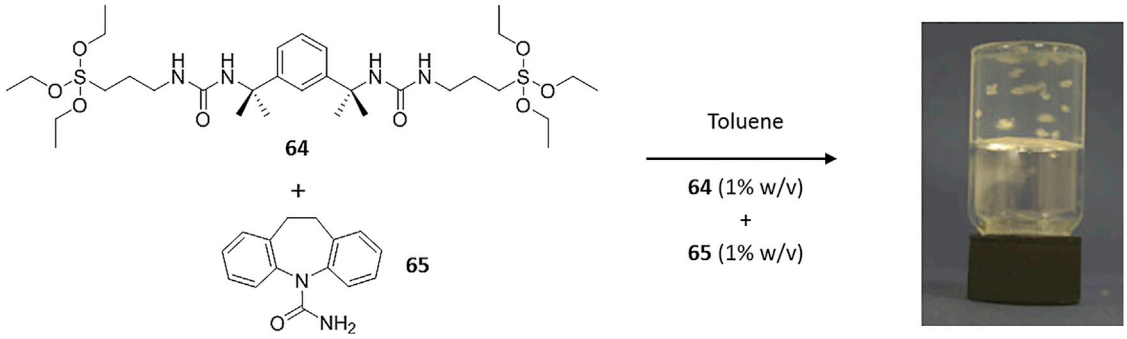

Figure 26. Chemical Structure of Bis(urea) Gelator 64 and Carbamazepine 65 and a Picture of Gel 64 with Crystals of 76
Reprinted with permission from Foster et al.[85] Copyright 2010 Nature Publishing Group.

from ligand **68** to the $^5D_0$ excited state of Eu(III) ions gave rise to the characteristic Eu(III) emission. Nonlinear regression analysis of the experimental data confirmed the formation of 1:1 and 3:2 (**M:68**) species. These results clearly demonstrate that the equilibrium process **Eu + 68** ↔ **Eu:68** can be shifted toward higher stoichiometry and the formation of higher-order self-assemblies. Both **68** and **$EuCl_3$-68** gels were formed in a H_2O/MeOH mixture. The mechanism of $EuCl_3$ gel formation is the collective result of the three-fold intermolecular hydrogen bonding, possibly with additional π-π stacking between the tpy moieties (Figure 28B) along with binding of the two-dimensional polymers with Eu(III) ions to form three-dimensional structures. All the gels formed were luminescent with characteristic Eu(III) emission. SEM analyses of the dried samples showed fibrous microstructures consisting of long intertwining bundles (Figure 29A). **$EuCl_3$-68** gave rise to the formation of more ordered gels (Figure 29B) showing "rope-type" assembly of strands.

Supramolecular Gel as Medium for Nanowire Growth

Continuing this work, Gunnlaugsson, Boland, and co-workers reported an interesting phenomenon of the growth of crystalline salt wires on the surface of the above-described gel matrix upon drying.[92] Using the supramolecular gel based on compound **68**, which forms two-dimensional supramolecular polymers, made it possible to grow nanowires of common halide salts (NaCl, KCl, and KI), from supramolecular gel dropcast onto a silica surface. The same types of wires were also obtained with the **$EuCl_3$-68** gels. SEM images of the dried gels in ambient conditions followed by vacuum drying showed signs of thin wires growing from the surface of the dried gel with a diameter of 130–200 nm (Figure 30).

Further investigations revealed evidence for a base growth mechanism where crystal growth appears to draw some of the gel strands up from the substrate (Figure 30C), strongly suggesting that nanowire growth results from diffusion and crystallization of ions at the lower face of a small seed crystal formed within the gel surface. This is similar to the base growth mechanism suggested for porous membrane wire growth.[92] Closer examination of the nanowires via the TEM diffraction pattern revealed their cubic, single-crystal morphology. Energy-dispersive X-ray (EDX) spectroscopy confirmed the expected 1:1 stoichiometry of sodium chloride, and the diffraction pattern indicated a cubic single-crystal structure. This phenomenon was also found to follow with different salts such as potassium iodide and potassium chloride, displaying the compatibility of these gels with a range of common salts. The approach described here shows the applicability of supramolecular gels toward the development of single-crystal nanowires of unprecedented dimensions and

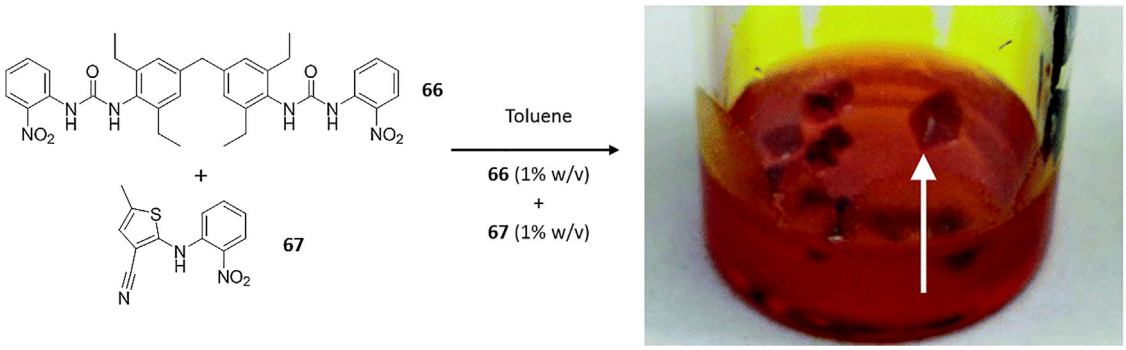

Figure 27. Chemical Structure of Bis(urea) Gelator 66 and ROY 67 and a Picture of Gel 66 with Crystals of 67 (R form)
The arrow indicates the crystal in the gel medium. Reproduced from Foster et al.,[86] published by the Royal Society of Chemistry.

provides an opportunity to test the properties of these important nanoscale material systems.

Lanthanide Based Healable Luminescent Metallogel

Recently, Gunnlaugsson and co-workers reported Ln(III)-based (Ln = Eu and Tb) luminescent metallogels with self-healing properties prepared from cross-linking gels of 1:3 and 1:2 (**Ln:69**) stoichiometries through their terminal carboxylic groups.[93] Initially, in order to obtain gels, the 1:3 (**Ln:69**) metal complex (**Ln(69)$_3$**) was prepared by microwave irradiation. Upon addition of $Ln(CH_3COO)_3$ to **Ln(69)$_3$**, a soft gel-like precipitate was observed at various (**Ln(69)$_3$:Ln(CH$_3$COO)$_3$**) stoichiometries after further microwave irradiation at 75°C, which, later upon centrifugation, resulted in the formation of robust gels. The most appropriate ratio between **Ln(69)$_3$** and $Ln(CH_3COO)_3$ was found to be 1:0.5 for both Eu(III) and Tb(III) gels for the formation of the most stable gel (Figure 31A). Both of the gels obtained were opaque and were highly luminescent under UV-light irradiation; they displayed green and red emission for Tb(III) and Eu(III), respectively (Figures 31B and 31C). The microstructural analysis of both gels showed similar morphologies. Transferring and

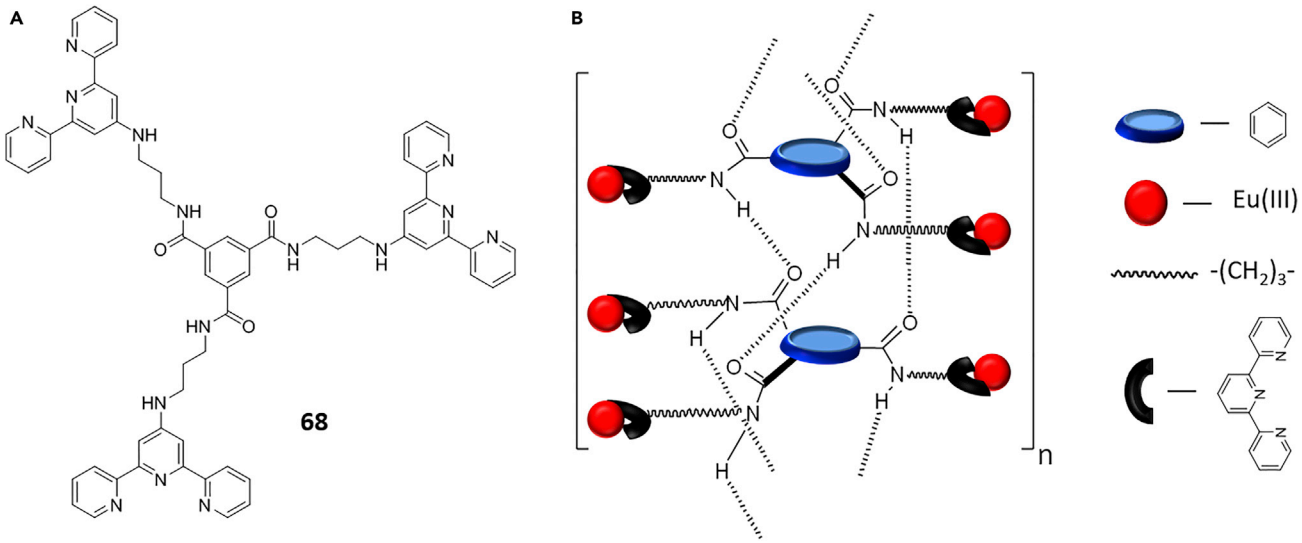

Figure 28. Self-Assembly of a tpy-Based Tripodal Molecule
Molecular structure of the tripodal tpy-based ligand **68** (A) and schematic representation of the three-fold hydrogen bonding in helices of **68** showing the europium binding sites on the outside of the helix (B). Reprinted with permission from Kotova et al.[91] Copyright 2012 Wiley-VCH Verlag GmbH & Co. KGaA, Weinheim.

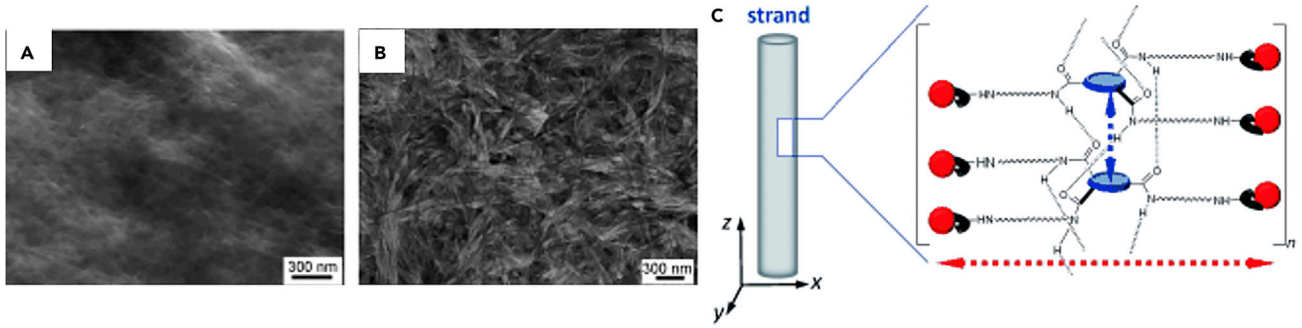

Figure 29. Supramolecular Organo- and Metallogel

(A and B) SEM images of ligand gel **68** (A) and supramolecular gel **$EuCl_3$-68** (B).

(C) Schematic representation of the self-assembly of **68** and Eu(III) ions within $EuCl_3$-**68** gels.

Reprinted with permission from Kotova et al.[91] Copyright 2012 Wiley-VCH Verlag GmbH & Co. KGaA, Weinheim.

drying these gels on quartz slides (Figure 31D) allowed the formation of thin films showing the respective Ln(III) emission. Simple mechanical mixing of equal volumes of these two Ln(III) gels yielded a yellow-orange luminescent Eu(III)/Tb(III) gel (Figure 31D), which showed two main emission bands at 545 and 616 nm for Tb(III) and Eu(III) emissions, respectively (Figures 31E and 31F).

These supramolecular gels showed interesting self-healing behavior, and materials with such features are of particular interests because they have the tendency to mimic naturally occurring biopolymers.[94] When the gel was cut in two and brought together, they reassembled through self-healing without use of any external stimuli (Figure 32). Because both Tb(III) and Eu(III) gels are formed by dynamic processes, the secondary Ln(III) ions added to the **Ln:69_3** complex bind to the terminal carboxylic groups to form a three-dimensional coordination network. As this recognition process occurs at the edge of the cut and not all of the carboxylic groups are coordinated to the Ln(III), it helps in potential self-healing of the cut gels. The SEM images showed that, at first glance, the gels had similar morphology, with fibers of 30–50 nm and intertwined bundles similar to Cotton-like structures. Closer observation revealed that the Tb(III) gels have a more densely packed fibrous network in comparison with the Eu(III) gels. This explains the difference in the gel volume, despite being prepared from the same concentration and volume. Moreover, the Tb(III)/Eu(III) mixed gel morphology was different from its individual component gels in terms of packing

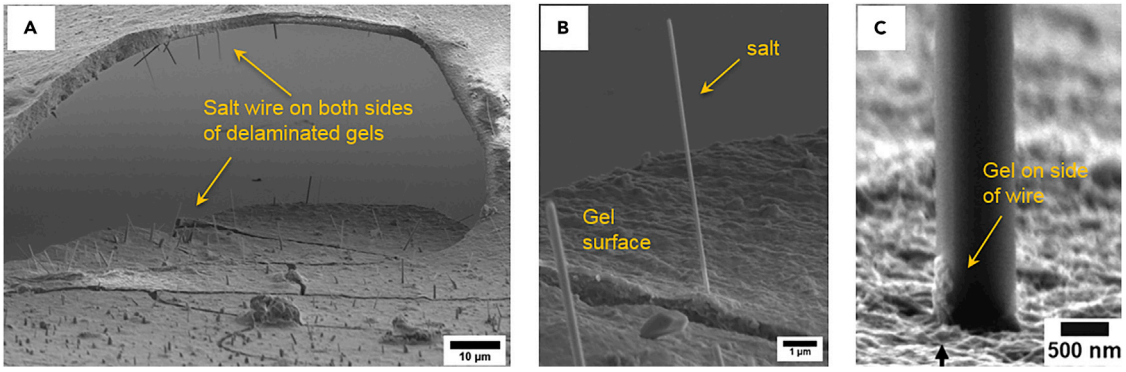

Figure 30. Nanowires of Crystalline Salts Grown on the 68 Gel Surface

Growth of nanowires seen on both sides of delaminated gel film (A), NaCl nanowires grown from a Eu(III) gel (B), and gel observed on the side of nanowires (C). Reprinted with permission from Daly et al.[92] Copyright 2013 American Chemical Society.

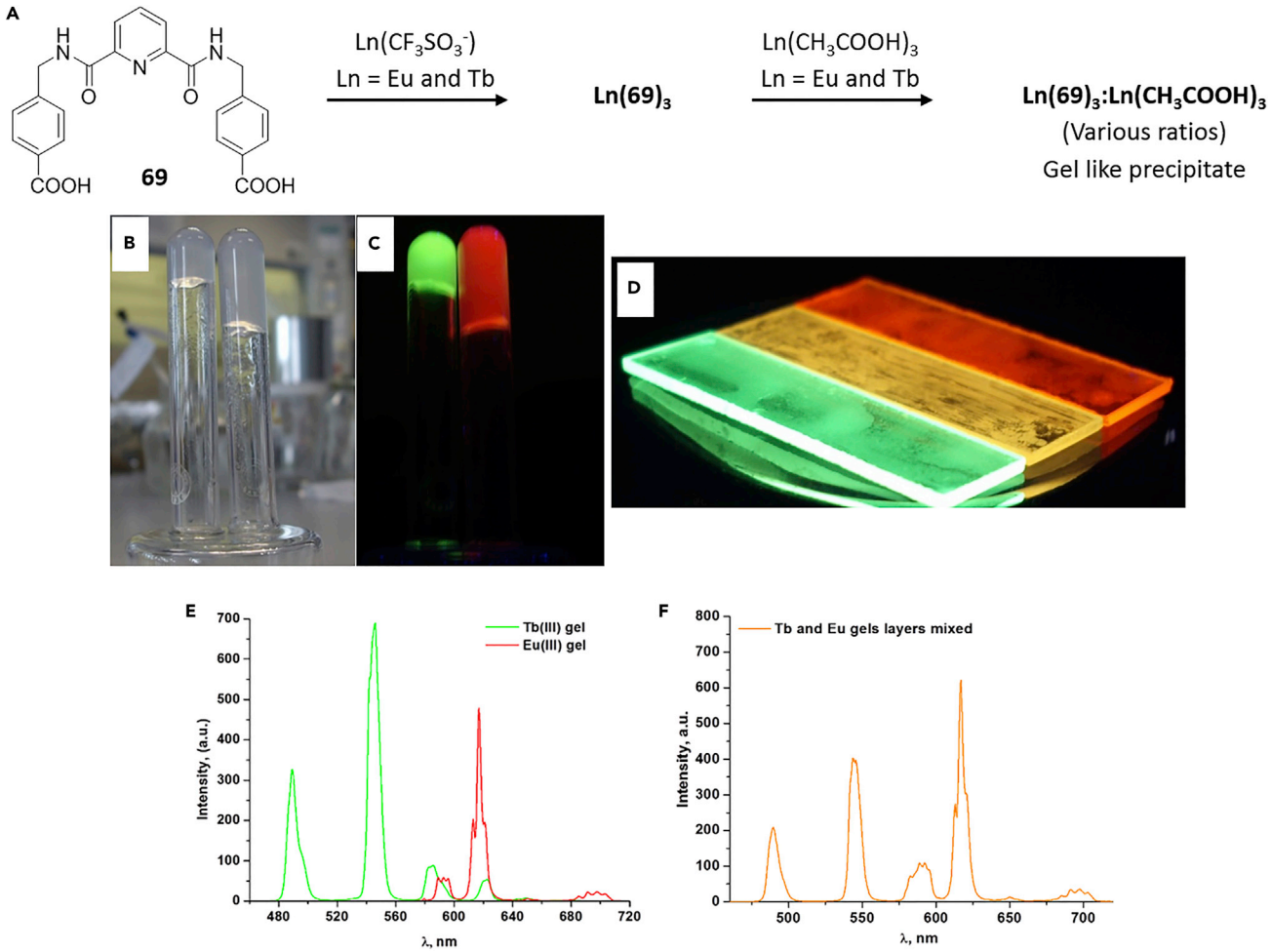

Figure 31. Ln(III)-Based Luminescent Metallogel from 69

(A) Synthesis of Eu(III) and Tb(III) metallogels.

(B–D) Eu(III) and Tb(III) gels in daylight (B) and under UV light (C) and luminescence of Eu(III), Tb(III), and Eu(III)/Tb(III) gels dried on quartz plates (D).

(E and F) Luminescence spectra of Eu(III) and Tb(III) (E) and Eu(III)/Tb(III) mixed gels (F).

Reprinted with permission from Martínez-Calvo et al.[93] Copyright 2015 American Chemical Society.

and porosity. Rheological measurements also confirmed the self-healing nature of individual and Tb(III)/Eu(III) mixed gels, where the recovery of G′ was observed.

In addition, many other Ln(III)-based self-assembled systems, including luminescent metallogels,[95] monometallic and mutimetallic assemblies,[12] thin films,[96] interlocked systems,[17] dual responsive logic mimicking systems,[97] luminescent contrast agents for microdamaged bone,[8] MRI probes,[98] and many more were reported by the Gunnlaugsson group. In this section, various supramolecular interactions and their manipulation leading to the formation of fibers, gels, crystals, nanowires, and aggregates under various conditions and controlling their properties have been discussed. Similar intermolecular interactions leading to the formation of higher aggregates of different morphology are discussed in the following sections.

SELF-ASSEMBLY OF MOLECULES TO HIGHER-ORDERED AGGREGATES

The self-assembly of smaller building units to form higher-ordered aggregates of larger size has become a burgeoning field of study. Micro- and nanometer-sized

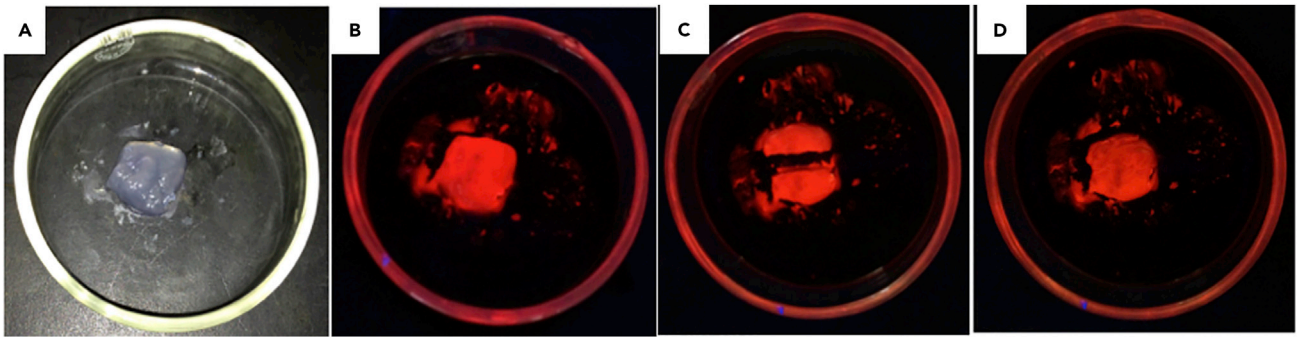

Figure 32. Healing Experiment of Eu(III) Gel from 69

Gel in daylight (A), under UV light (B), cut in half (C), and self-healed (D). Reprinted with permission from Martínez-Calvo et al.[93] Copyright 2015 American Chemical Society.

particles play important roles in many applications, including bio-sensing, catalysis, optics, and more.

Hierarchical Self-Assembly

The concepts of a hierarchically organized self-assembly process were also applied to colloidal systems, where the self-assembly is driven by balancing the amphiphilic properties of building blocks. Manners and co-workers reported the block co-polymer (BCP), which was used to construct amphiphilic cylindrical triblock co-micelle superstructures, where the self-assembly process was controlled by solvent composition.[99] The BCP was formed with a crystallizable poly(ferrocenyldimethylsilane) (PFS) chain possessing either polar (P) **70** or hydrophobic (H) **71** blocks, in which the PFS part acts as the core-forming block, and P/H blocks remains in the co-micelles periphery. Co-polymers **70** and **71** self-assemble to form cylindrical micelles in complementary polar solvents by stacking of the P/H segments. Addition of complementary polar co-polymers to the cylindrical micelles results in the formation of triblock co-micelles (P-H-P or H-P-H), by means of a living crystallization-driven self-assembly (CDSA) approach in hexane/i-PrOH mixture (1:3 v/v) (Figure 33A). The amphiphilic triblock co-micelles possessing P and H segments (P-H-P or H-P-H) are monodisperse in length and were able to self-assemble via side-by-side or end-to-end interactions for the central or terminal segments, respectively, in non-solvents. This enabled them to form cylindrical supermicelles, one- and three-dimensional superstructures that were stable in solution as well as in solid. The advantage of using such approaches with amphiphilic BCPs is that the inverse sequence of P/H segments can be controlled by means of solvent composition.

By appropriately modifying the length of the P/H segment in co-polymers, the resulting P-H-P triblock co-micelles undergo a hierarchical self-assembly process through side-by-side stacking to form well-defined "train-track-like" superstructures in polar media, as observed by TEM and shown in Figure 33B. Significantly tighter packing was observed on increasing the length of the P segment in P-H-P triblock co-micelles. By varying the length of the P segment, an array of well-defined cylindrical superstructures of length 1–10 μm were obtained in a polar solvent medium. This is presumably because of the smaller diameter of the terminal P segment in the co-micelle reducing the steric repulsion between the co-micelles, thus helping the central H segment to pack more tightly (Figure 33C, dark part). In non-polar media, the P-H-P triblock co-micelle with a bigger terminal P segment undergoes end-to-end aggregation, resulting in the formation of linear chain-like superstructures, which were further cross-linked by the addition of Pt nanoparticles via coordination through the pyridyl groups

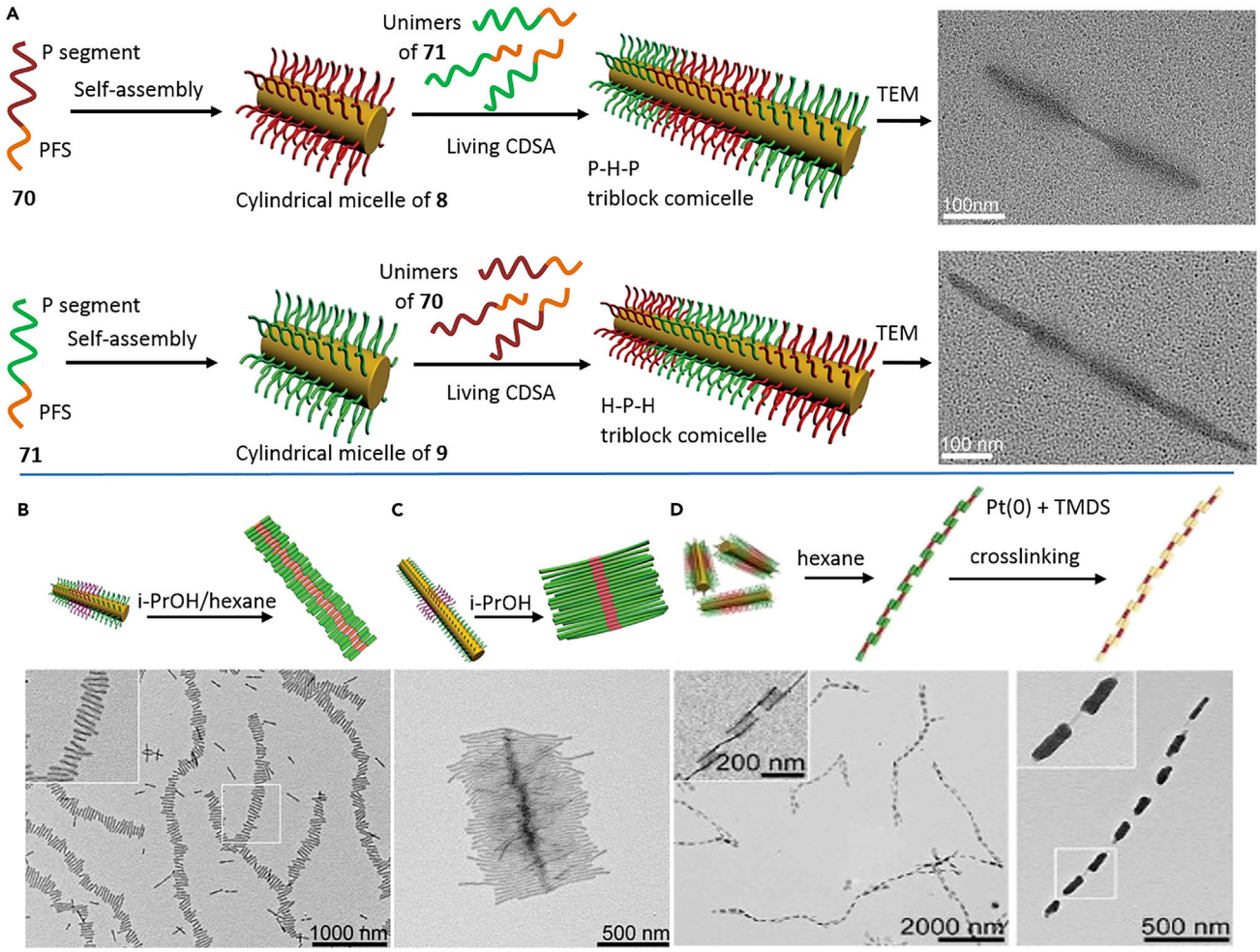

Figure 33. Formation of Cylindrical Co-micelles from Co-polymers

(A) Schematic representation of P-H-P and H-P-H triblock co-micelles and their corresponding TEM images.

(B–D) TEM images of self-assembled P-H-P triblock co-micelles forming different superstructures in various solvent media: (B) iPrOH-hexane, (C) iPrOH, and (D) hexane.

Reprinted with permission from Qui et al.[99] Copyright 2015 American Association for the Advancement of Science.

of the P segments (Figure 33D). Similarly, in other non-polar media, P-H-P aggregates by intermicellar association, forming multi-dimensional superstructures.

Contrary to P-H-P, the H-P-H triblock co-micelle undergoes hierarchical self-assembly in polar medium to form a range of multi-dimensional superlattices on varying the H-segment lengths. Similar triblock co-micelles prepared with different fluorescent dye-tagged co-polymers displayed color-coded blocks in high resolution on imaging under stimulated emission depletion microscopy and single-molecule localization microscopy (SMLM) (Figure 34A).[100] Similarly, spherical supermicelles (size 1–5 μm) were also observed from non-centrosymmetric amphiphilic triblock co-micelles (Figure 34B).[101] Recently, interaction of DNA with triblock co-micelles with positively charged terminal groups was reported, indicating the potential application of hierarchical self-assembly materials in biomedical applications. This "living CDSA" approach was applied to different co-polymers to obtain cylindrical and spherical structures and also in the preparation of BCP nanoparticles.[102] From these observations, it is understood that the hierarchical self-assembly process is

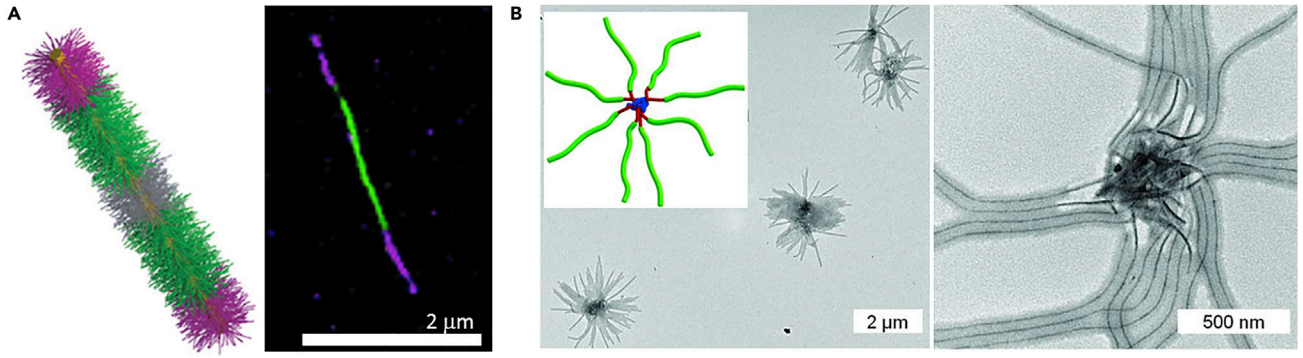

Figure 34. Linear and Spherical Supermicelles Formed from Block Co-micelles

(A) Schematic representation of triblock co-micelles prepared from fluorescent dye-tagged block co-polymer and its SMLM image (640 nm laser). Reprinted from Boott et al.[100]

(B) Schematic representation of spherical supermicelle from non-centrosymmetrical triblock co-micelle (inset) and its TEM images. Reprinted with permission from Rupar et al.[101] Copyright 2012 American Association for the Advancement of Science.

readily controlled by altering the co-micelle architecture and the polarity of the medium.

Aida and co-workers applied this approach of co-assembly for the construction of organic heterojunctions by using two planar molecules, gemini-shaped hexa-*peri*-hexabenzocoronene (HBC) derivatives **72** and **73** with the potential to form nanotubular structures independently.[103] Compound **72** undergoes tubular self-assembly when diffusing CH_3OH vapors into its tetrahydrofuran (THF) solution. The nanotubes formed were stabilized by metal coordination on treating the tubular structures of **72** with Cu^{2+} ions. This makes the surface charged, aiding in homogeneous dispersion as a result of electrostatic repulsion resulting in seed nanotubes ($NT_{1\text{-}Cu}$; Figure 35B). On sequential addition of **73** to a homogeneous solution of seeded nanotubes of **72** ($NT_{1\text{-}Cu}$) at 50°C followed by cooling, **73** undergoes stepwise co-assembly at the ends of $NT_{1\text{-}Cu}$ to form two-component blocked nanotube segments (Figure 35C). This hybrid structure was found to function as a p-n junction, with communication at the interface of the heterojunctions occurring between two electronically dissimilar nanotubes by charge transport and excitation energy transfer. This phenomenon is not observed in two homotropically assembled nanotubes.[103]

Morphology Control by Block Length Ratios

Higher-ordered hollow structures formed from assemblies of mesoscopic amphiphilic systems have also been reported by Mirkin and co-workers.[104] Hollow cylindrical structures were obtained with a rod-shaped mesoscopic metal-polymer amphiphile **74**, the structure of which has a hard hydrophilic metal domain (Au) and a soft hydrophobic domain made of conducting polymer polypyrrole (Ppy). It was hypothesized that the two different block phases segregate and align in a particular way that increases the interactions between similar blocks. In **74**, the diameter of the polymer portion (~360 nm) is smaller than the metal domain (400 nm) (Figure 36A), which helps these building blocks to self-organize into curved cylindrical architectures, such as bundles, tubes, and sheets in aqueous media. Variation of the block length of the Au and Ppy portions in **74** allows control over the morphology of these assembled superstructures.

Compound **74**, with a 1:4 Au/Ppy block length ratio, formed hollow tubular structures when suspended in water. Because of the longer polymer length, the average rod head area (a_h) is smaller, allowing less curved packing of **74** (Figures 36B and

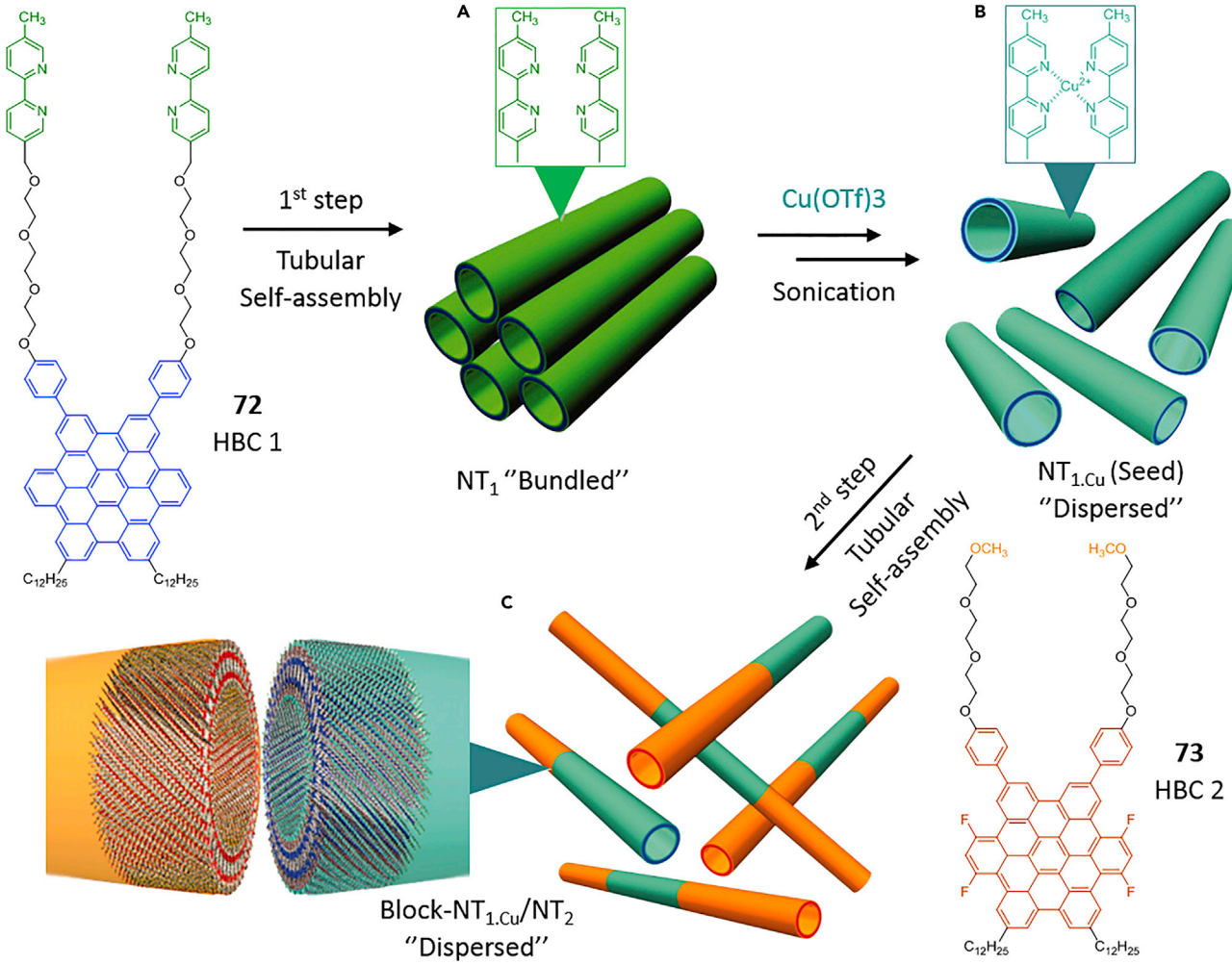

Figure 35. Formation of Nanotubes with Heterojunctions through the Self-Assembly of Two Planar Molecules

(A and B) Schematic illustration of NT_1 nanotubes (A) and $NT_{1.Cu}$ nanotubes (B) from **72**.

(C) Block $NT_{1.Cu}/NT_2$ formed by co-assembly of **73** on seeded $NT_{1.Cu}$, and their cross-section view at the heterojunction.

Reprinted with permission from Zhang et al.[103] Copyright 2011 American Association for the Advancement of Science.

36E). Compound **74** with 3:2 Au/Ppy block length ratio with a shorter polymer chain length also formed tubular structures, and this assembly process continued to complete the closed tubular structure with open ends (Figures 36C and 36F). In the case of **74** with a 4:1 Au/Ppy block length ratio bearing the shortest polymer chain length, an open tubular structure was observed with higher curvature as a result of the larger rod head area (Figures 36D and 36G). In these highly ordered assemblies, a single layer of **74** rods was observed in all cases, in which all the metal domains are on the exterior and the polymer chains are facing inside. This example introduces the concept of using polymer chains of different lengths and the role of metals in hybrid materials for constructing two- and three-dimensional structures with controlled morphology.

Hollow Microcapsules by Host-Guest Self-Assembly

Another elegant application of hierarchical self-assembly is shown by Scherman, Abell, and co-workers in the instantaneous formation of microcapsules through a gold/nanoparticle/co-polymer composite, held together by cucurbit[8]uril (CB[8],

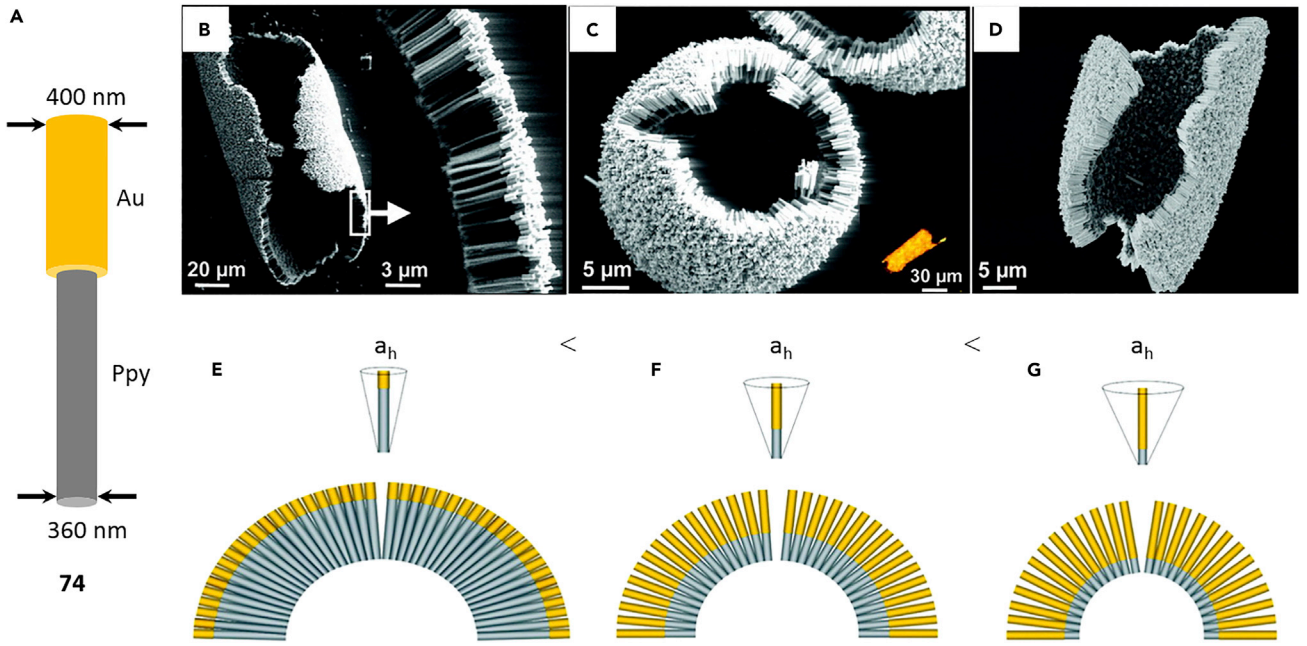

Figure 36. Self-Assembly of Mesoscopic Metal-Polymer Amphiphiles into Hollow Cylindrical Aggregates

(A) Schematic representation of Au/Ppy rod **74**.

(B–D) SEM images of assemblies of **74** with 1:4 Au/Ppy block length ratio (B), 3:2 Au/Ppy block length ratio (C; inset: optical microscopy image of the tubular structure formed from these rods), and 4:1 Au/Ppy block length ratio (D).

(E–G) Representation of packing of **74** forming tubes of different diameters, corresponding to those shown in (B) and (C).

Reprinted with permission from Park et al.[104] Copyright 2004 American Association for the Advancement of Science.

75).[105] Here, **75** (CB[8]) acts as host encapsulating two guest moieties, methyl viologen (MV^{2+}, an electron deficient moiety), functionalized on gold nanoparticles (**76**) (AuNPs), and a naphthol (Np) moiety on a co-polymer (**77**) (Figure 37A). Upon mixing these three components with a simple T-junction geometry in the presence of oil as carrier phase, droplets were formed after thorough mixing (Figures 37B and 37C). Collecting and drying these droplets on glass slides resulted in the formation of microcapsules with high monodispersity and narrow size distribution (Figure 37D). The microcapsules collapsed after dehydration, and upon rehydration, their hollow nature was revealed. Furthermore, on using a Rhodamine-B-tagged co-polymer **78** instead of **77** and fluorescein isothiocyanate-labeled dextran (FITC-dextran) in the medium, the microcapsules formed showed rhodamine fluorescence (red) on the exterior and FITC green fluorescence in the encapsulated medium (Figure 38). The encapsulated cargo was released in a controlled manner in the presence of $Na_2S_2O_4$. Moreover, the encapsulated materials can be analyzed by surface-enhanced Raman spectroscopy. In this case, barrel-shaped CB[8] (**75**) plays a key role by forming a 1:1:1 ternary host-guest complex, in which it holds **76** and **78** moieties in its cavity, acting as a molecular "handcuff." This complex three-component host-guest interaction is helpful in fusing materials with high and selective binding affinity in aqueous medium. With this approach, new stimuli-responsive materials with high mechanical strength displaying fast healing and cargo release were reported.[106]

Recently, Scherman, Abell, and co-workers extended the strategies of hierarchical self-assembly to prepare similar spherical supramolecular microcapsules by using amphiphilic BCP **79**.[107] The BCP **79**, tagged with an electron-donating

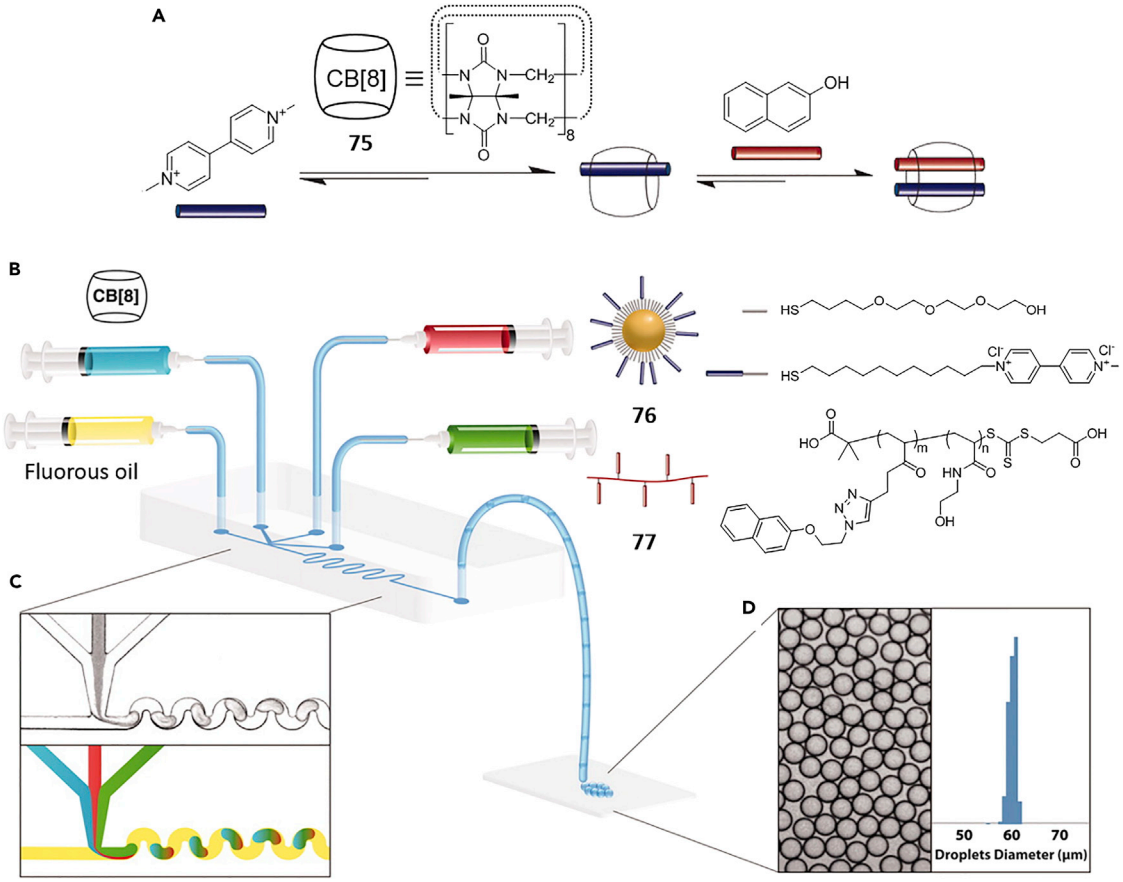

Figure 37. Formation of Microcapsules through the Formation of a Host-Guest Ternary Complex with CB(8) 75

(A) Schematic representation of the formation of the three-component CB(8) **75** ternary complex in H_2O.

(B and C) Microdroplet formation using a T-junction device (B) and the expanded view of the T junction with a wiggled channel for rapid mixing of reagents (C).

(D) Monodispersed microdroplets with narrow size distribution.

Reprinted with permission from Zhang et al.[105] 2012 American Association for the Advancement of Science.

azobenzene moiety, formed spherical micelles at the interface of microdroplet and solvent. This was later cross-linked with another co-polymer (**80**) with the same CB[8] (**75**) to form a microcapsule via the 1:1:1 heteroternary complex. The obtained microcapsules displayed the ability to encapsulate dual cargo (hydrophobic and hydrophilic components) in the compartments (Figure 39), in which the hydrophilic cargo FITC-dextran was loaded in the core (green) and hydrophobic Nile red was trapped in the micelle (red). The encapsulated dual cargo was released in a controlled manner under UV irradiation, whereupon the azobenzene changed conformation, resulting in dissociation of the 1:1:1 heteroternary complex and release of only FITC-dextran while holding Nile red in the micelle (Figure 39A). This kind of approach is highly applicable to the formation of microcapsules through interfacial, colloidal particle, and electrostatic-driven assembly processes, photo-switchable materials, controlled encapsulation and release of guests, hybrid supramolecular-colloidal hydrogels, and many more.[108] Very recently, the Scherman group extended this strategy even further toward developing a hyper-branched polymer by using a benzene-1,3,5-tricarboxamide-based tripodal molecule functionalized with the azobenzene moiety as a guest molecule.[44]

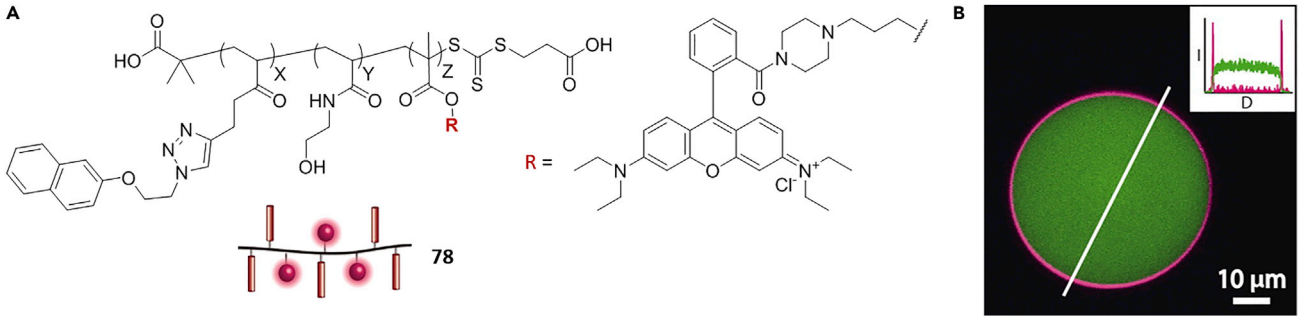

Figure 38. Microcapsules Formation Using Rhodamine-B Tagged Co-polymer 78 with Encapsulated Cargo FITC-Dextran

(A) Chemical structure and schematic representation of Rhodamine-B-containing co-polymer.

(B) LSCM image of microcapsules (red) encapsulating the aqueous solution of FITC-dextran (green). Inset: the corresponding fluorescence intensity profiles.

Reprinted with permission from Zhang et al.[105] 2012 American Association for the Advancement of Science.

Similar functional materials and nanosized self-assembled architectures formed through other supramolecular interactions such as physical aggregation, coordination, and other non-covalent interactions are discussed in the following sections.

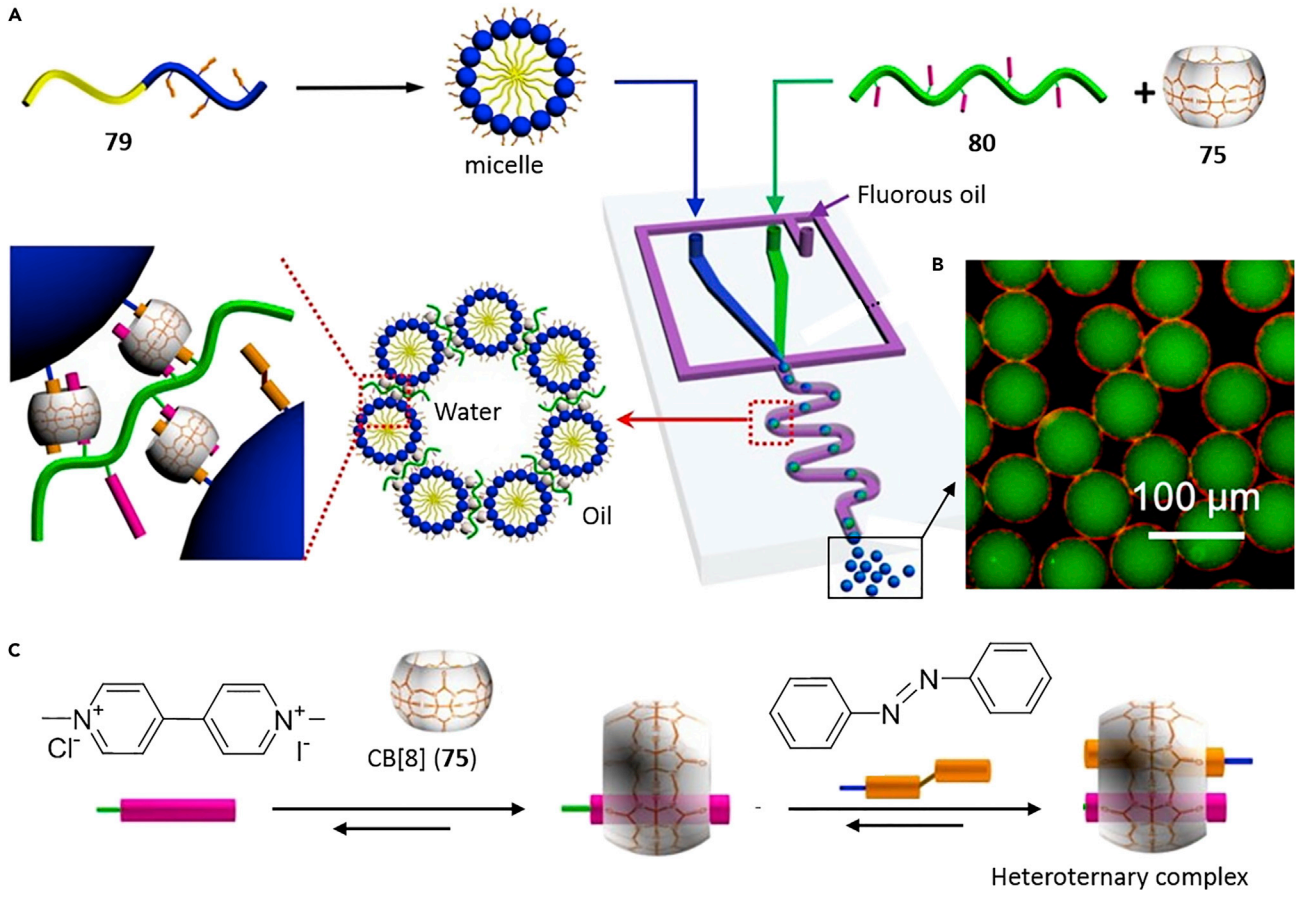

Figure 39. Formation of Microcapsules from an Amphiphilic Co-polymer

(A) Schematic representation of the hierarchical assembly of microcapsules from amphiphilic co-polymer.

(B) Fluorescent microscopy image of microcapsules containing FITC-dextran cargo (green) and Nile red (red).

(C) Stepwise formation of a three-component heteroternary host-guest complex.

Reprinted from Yu et al.[107]

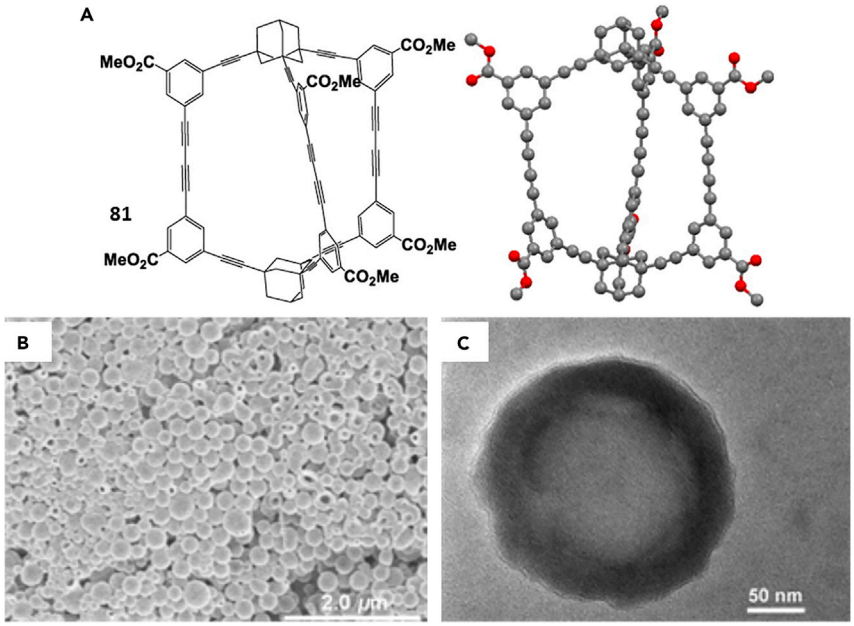

Figure 40. Aggregation of Adamentane-Based Molecule into Spherical Particles

(A) Molecular structure of adamantane-based cage type molecule **81** and its crystal structure.

(B and C) SEM (B) and TEM (C) images of hollow spherical assemblies of **81** formed in CH_3OH/THF (1:2 v/v).

Reprinted with permission from Tominaga et al.[111] Copyright 2014 American Chemical Society.

Organic Spherical Particles Formed through Aggregation

Hollow three-dimensional structures have attracted considerable interest because of their potential in guest inclusion and stabilization of reactive intermediates. In particular, using vesicles and other hollow submicrometer and nanometer scales as transporters has attracted considerable interest in practical applications such as delivery systems.[109] A number of strategies have been designed for the construction of such structures. Azumaya's group reported adamantane-based molecules comprising multiple branches forming networked structures with cavities and one-dimensional channels.[110] One example is an adamantane-based cage-like molecule, **81**, which spontaneously self-assembles to form hollow spherical aggregates in CH_3OH/THF (1:2 v/v) (Figure 40).[111] The aggregates were of narrow size distribution, with a diameter of 230 nm, and were robust and stable even after drying. In more polar CH_3OH/THF (1:1 v/v) solvent mixture, bigger aggregates were observed. However, in CH_3OH/THF (1:4 v/v), spherical aggregates were not present, highlighting the importance of balance between the polar/non-polar ratios of the solvent media. TEM analysis confirms the hollow nature of the particles as clear contrast is seen between the thicker peripheries (darker, as it does not permit the transmission of electrons) and thinner center (Figure 40C).

Morphology Variations Due to Solvent-Dependent Aggregation

Similar spherical nano- and microstructures are also reported from amphiphilic molecules. Liu and co-workers showed two triangular amphiphilic derivatives, **82** and **83**, containing an imine bond and alkyl chains in the periphery, acting as building blocks in the formation of soft colloidal materials.[112] The triangular structure provides more active sites for the interactions, and the alkyl chains make the molecule hydrophobic, enhancing its aggregation property. Despite similar structures, **82** and **83** showed

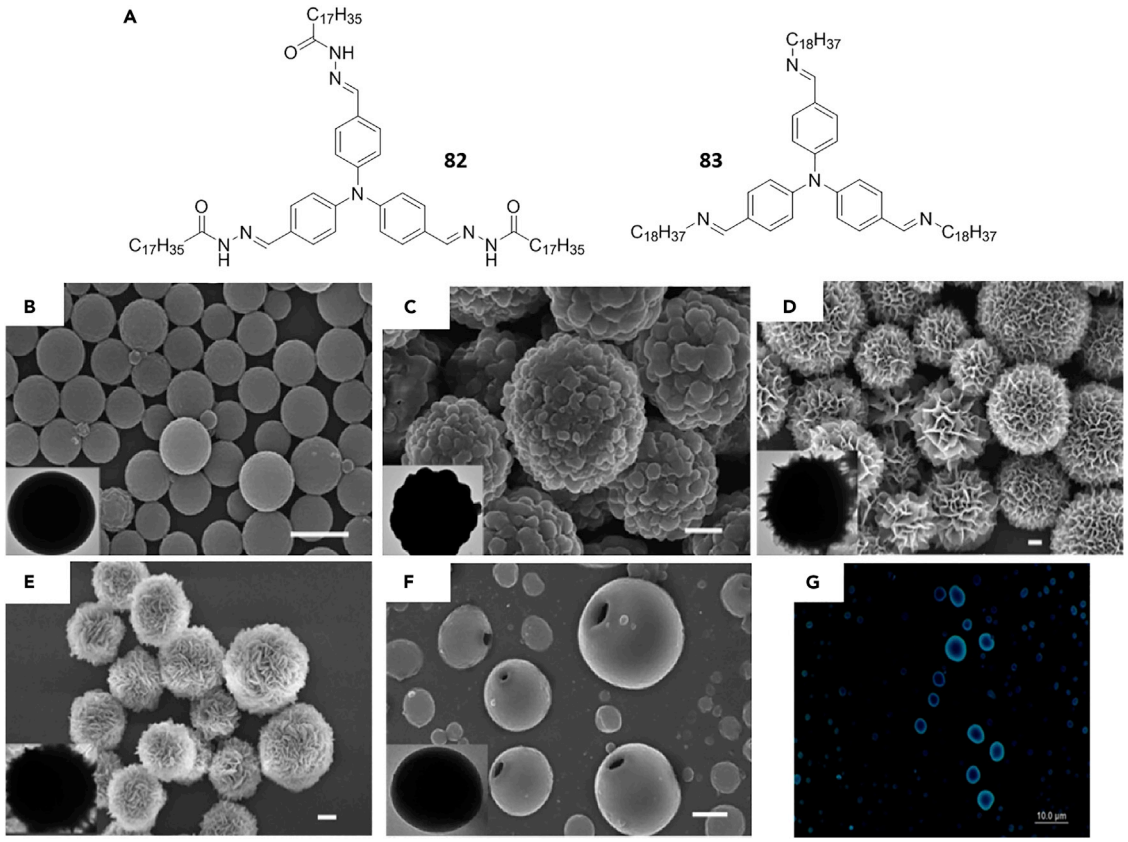

Figure 41. Self-Assembly of Triangular Amphiphiles Displaying Various Morphologies in Different Solvents

(A) Molecular structures of **82** and **83**.

(B–F) SEM images of **82** assemblies formed in DMSO (B), CH_3OH (C), ethyl acetate (D), acetone (E), and THF (F). Scale bar, 2 μm.

(G) LSCM image of **82** hollow spheres. Scale bar, 10 μm.

Reprinted with permission from Lv et al.[112] Copyright 2014 American Chemical Society.

different assembly behavior. Compound **82**, with additional H-bonding sites, self-assembled to furnish microstructures with solvent-regulated morphologies and hollow spheres. Among different organic solvents, compound **82** formed microspheres with different morphologies in polar solvents such as DMSO, CH_3OH, THF, ethyl acetate, etc. In DMSO, solid spherical particles with a smooth surface were formed (Figure 41B), whereas in CH_3OH, spheres with a rough surface morphology were observed (Figure 41C). The assemblies obtained in ethyl acetate and acetone showed regular and uniform flower-like surface morphology (Figures 41D and 41E). The solid nature of these spheres was confirmed by TEM analysis (inset in the respective images). The hollow spheres obtained in THF were further confirmed with laser scanning confocal microscopy showing the large difference in the relative luminescence of the inner and outer ring (Figures 41F and 41G). On decreasing the polarity of the solvent, **82** formed organogels in non-polar organic solvents such as toluene, cyclohexane, and petroleum ether. These drastic changes in the assembly of molecule **82** in different solvent media signifies the influence of solvent polarity on the various non-covalent interactions responsible for the assembly process and fabrication of the morphology of aggregated systems. In addition, the molecule-solvent interactions are greatly influenced by solvent polarity and structural factors. However, **83**, lacking the amide group, did not show any ordered structures in polar solvents and did not form gels in non-polar media. This again highlights the role of

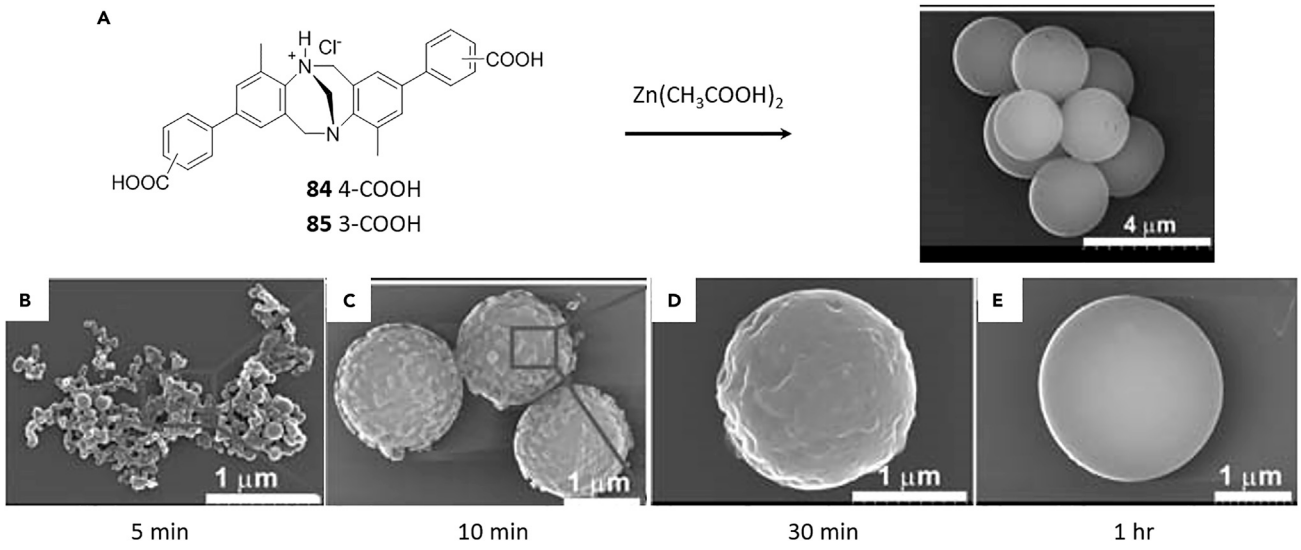

Figure 42. Synthesis of ICP Particles from Modified Tröger's Base Derivatives

Synthesis of ICP particles from **84** and **85** with Zn^{2+} metal ions (A) and SEM images monitoring **84** ICP particle formation at different time intervals (B–E). Reprinted with permission from Jeon et al.[113] Copyright 2009 Wiley-VCH Verlag GmbH & Co. KGaA, Weinheim.

strong H bonding, π-π stacking, and van der Waals interactions in the formation of higher-ordered aggregates.

Infinite Coordination Polymer (ICP) Particles

Another elegant example of such higher-ordered assemblies using metal ions and organic compound was shown by Mirkin and co-workers.[113] Using a modified Tröger's base ligand with terminal aryl-COOH groups **84** and **85**, a coordination polymer was obtained upon reacting with Zn^{2+} (Figure 42A). Upon slow diffusion of ether into a DMF solution of **84** and **85** in the presence of $Zn(CH_3COO)_2$, fluorescent, amorphous, ICP particles were obtained. The average diameter of ICP particles of **84** and **85** were 2.18 ± 1.44 and 2.84 ± 0.62 μm, respectively, and the shape remained spherical in other organic solvents, water, and even after drying. EDX spectroscopy and elemental analysis confirmed the formation of 1:1 (M:L) structures.

The authors analyzed the formation of these particles by following the time-dependent transformation from precursors to particles via SEM. Upon slow diffusion of ether into a solution of mixed **84** (or **85**) and $Zn(CH_3COO)_2$ in DMF with stirring, the precipitates formed at different times were isolated by centrifugation, repeated washing with CH_3OH, and were then imaged by SEM. In the beginning (5 min), nanometer-sized globular seeds were formed (Figure 42B); these were then agglomerated, forming spherical particles with a rough surface in 10 min (Figure 42C). As the reactions proceed, the surface of the particle became smoother after 30 min (Figure 42D). Finally, after 1 hr, smooth-surfaced particles were observed (Figure 42E). These observations suggest a particle-forming mechanism whereby the reaction of **84** and **85** with $Zn(CH_3COO)_2$ forms a linear oligomeric chain that nucleates to form seeds. These further undergo a series of aggregation processes and addition of new layers of seeds, finally forming ICP particles as shown in Figure 43. Thus formed **84** and **85** particles were stable up to ~400°C, as determined by thermogravimetric analysis.

Applying this strategy of using solvent initiation in the preparation of micro- and nanoparticles, Oh and Mirkin reported several other particles composed of a

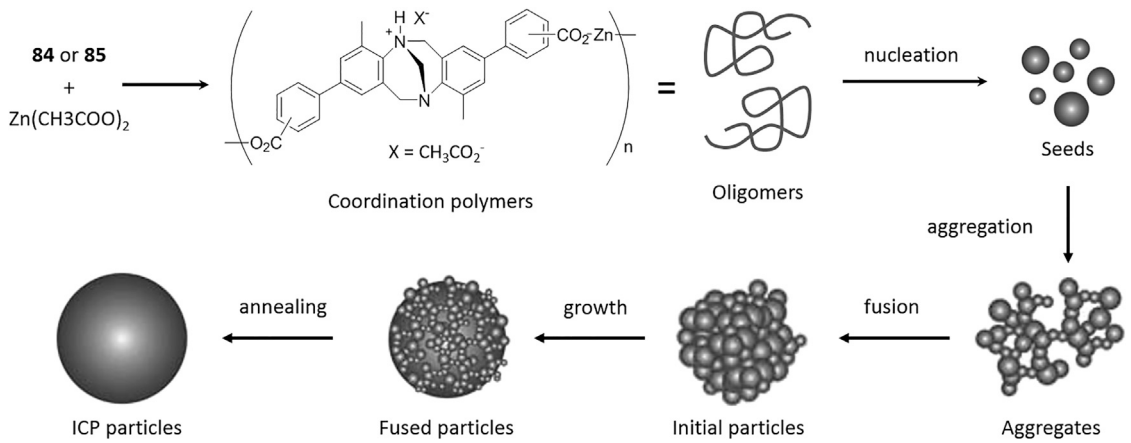

Figure 43. Proposed Mechanism of the ICP Particle Formation
Reprinted with permission from Jeon et al.[113] Copyright 2009 Wiley-VCH Verlag GmbH & Co. KGaA, Weinheim.

polymerized metal-ligand network by using Zn, Cu, and Ni.[114] Aggregation of such metal-based polymeric chains forming spherical particles highlights the role of metal ions and opens up new ways of making nanosized materials.

Recently Gunnlaugsson and co-workers reported a new luminescent nanoscale Zn^{2+} coordination polymer (**86-Zn-CP**) by using a V-shaped 4-amino-1,8-naphthalimide-derived tetracarboxylic acid linker (**86**) comprising Tröger's base functionality (Figure 44A).[115] An aqueous suspension of **86-Zn-CP** showed strong green fluorescence (λ_{max} = 520 nm) characteristics as a result of the internal charge transfer transition

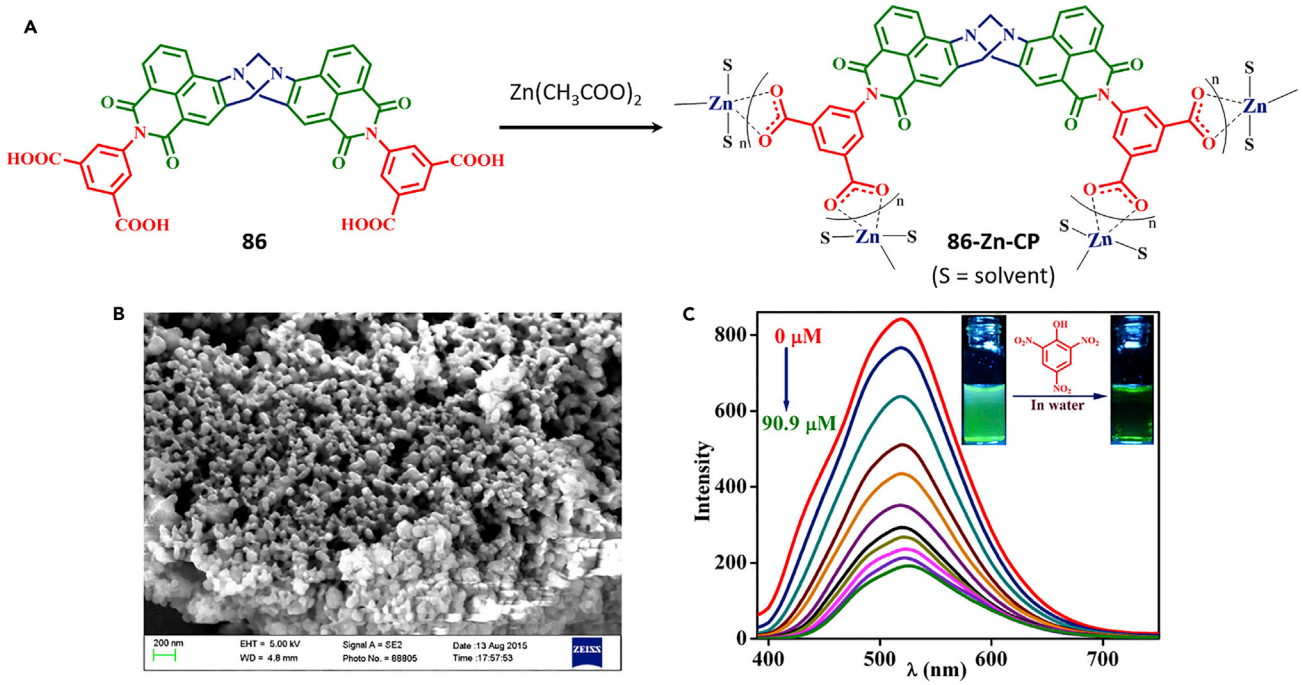

Figure 44. Tröger's-Base-Functionalized Nanoscale Coordination Polymer for Fluorescent Sensing
(A) Synthesis of Zn^{2+} coordination polymeric material derived from teracarboxylic acid (**86**) with Tröger's base functionality.
(B and C) SEM image of TB-Zn-CP shows the porous surface morphology (B) and the fluorescence sensing characteristic of picric acid (C).
Reproduced from Shanmugaraju et al.,[115] published by the Royal Society of Chemistry.

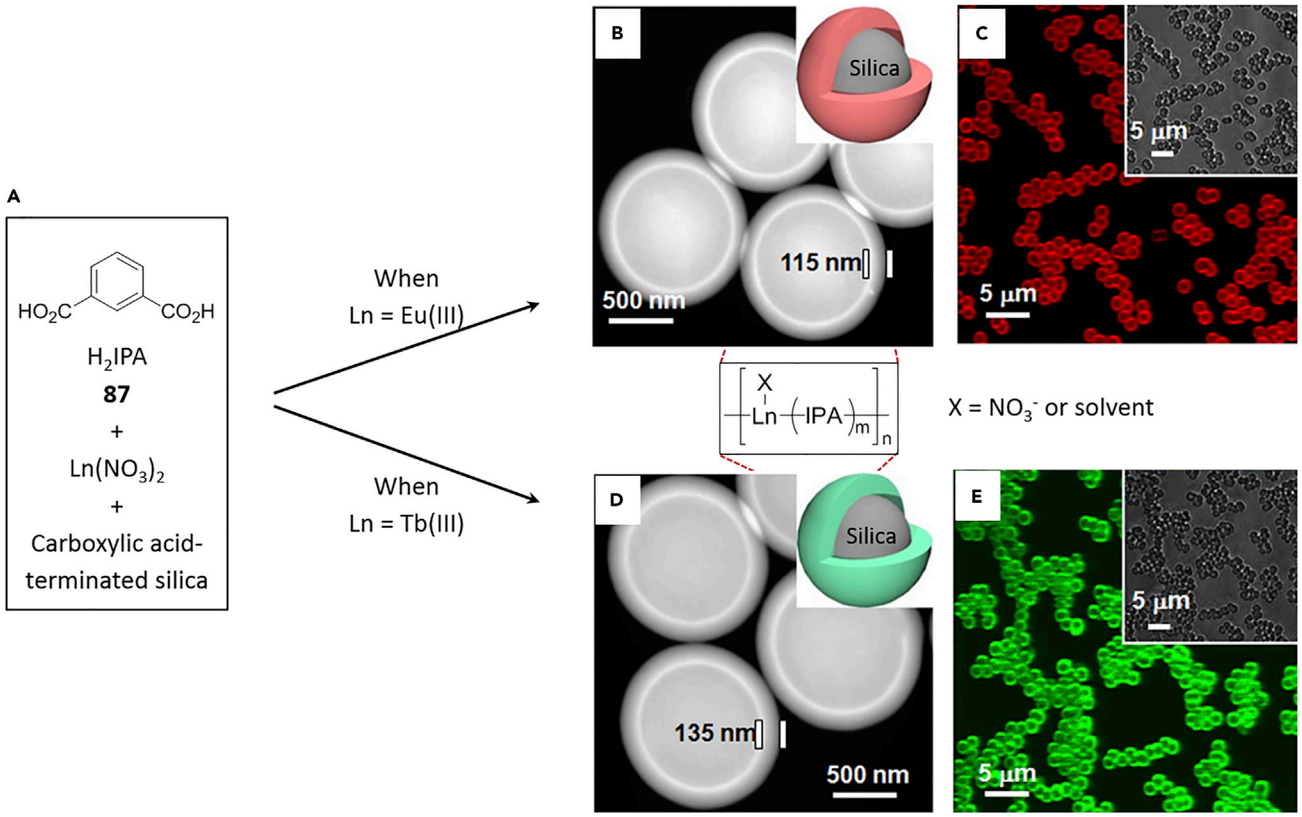

Figure 45. Synthesis of Ln-Based Luminescent Core-Shell Microspheres

(A) Synthesis of Ln-based luminescent core-shell microspheres.

(B and C) STEM images of EuCP microspheres (B) and corresponding confocal microscopy and OM (inset) images (C).

(D and E) STEM images of TbCP microspheres (D) and corresponding confocal microscopy and OM (inset) images (E).

Reprinted with permission from Cho et al.[116] Copyright 2014 Nature Publishing Group.

and was used as a fluorescent sensor for the discriminative sensing of secondary chemical explosives. The aqueous suspension of **86-Zn-CP** showed the largest quenching responses with high selectivity for phenolic nitroaromatics (4-nitrophenol, 2,4-dinitrophenol, and picric acid), even in the concurrent presence of other potentially competing nitroaromatic analytes (Figure 44C), and the limit of detection was found to be 26.3 ppb. The fluorescence sensing ability of **86-Zn-CP** was found to be reversible, demonstrating its long-term in-field applications. The high selectivity, sensitivity, and reversibility make **86-Zn-CP** a promising sensor material for quick and discriminative fluorescent sensing of phenolic nitroaromatic explosives in water.

Luminescent Core-Shell Particles as Sensors

Similarly, luminescent spherical particles with Ln(III)-based coordination polymers in the form of simple microspheres or core-shell species for sensing purposes were reported by Oh and co-workers.[116] Using Eu(III) and Tb(III) metal salts in the presence of isophthalic acid (**87**), they obtained simple luminescent microspheres. However, when the reaction was performed in the presence of carboxylic-acid-terminated silica particles, core-shell-type luminescent particles were formed (Figures 45B and 45D, inset). The isolated particles were ~0.7 μm and ~1.1 mm in size for the simple and core-shell microparticles, respectively (Figures 45B and 45D). The presence of Eu(III) and Tb(III) ions resulted in red and green emission from the particles, respectively, as observed by confocal microscopy (Figures 45C and 45E). The initial

luminescent intensity of the Tb(III)-based microspheres was much stronger than from the Eu(III)-based microsphere analogs. Such luminescent particles were used for selective sensing of metal ions because of their better dispersity in comparison with other heterogeneous solid sensors. The advantage of such sensors is that the turn-off luminescence can be recognized easily by the naked eye and has higher sensitivity than other known sensors, making these superior candidates. Both EuCP and TbCP were selective toward Cu^{2+} detection among various metal ions with TbCP superior to EuCP in this regard.

CONCLUSIONS AND OUTLOOK

Using a select number of examples from the literature, this review summarizes the development of various soft functional materials and organic particles through a range of supramolecular interactions, as well as through their combinations. From the past few decades, the intense research carried out by many research groups has resulted in enormous advancements in the synthesis of new building blocks for the development of materials through non-covalent interactions. The resulting materials have found applications in different areas, such as in the manufacture of elastic materials, bioactive filaments, OLEDs, microcapsules as delivery agents, gels as media for growing nanowires and pharmaceutical crystals, and self-healing materials, etc. The continuous rapid advancements achieved in supramolecular chemistry and materials on the basis of its principles ensures that the field will be at the forefront of the development and economic production of functional materials that will eventually become part of everyday life in the near future to facilitate development and growth. Supramolecular-material-based chemistry thus has a very bright and exciting future.

AUTHOR CONTRIBUTIONS

T.G. proposed the topic of the review and supervised the preparation of the manuscript. A.J.S. wrote the original manuscript, and A.J.S., O.K., and S.S. investigated the literature. All authors, including T.G., S.J.B., and G.M.O., read, revised, and approved the manuscript.

ACKNOWLEDGMENTS

The authors would like to acknowledge Science Foundation Ireland for financial support (SFI PI award 13/IA/1865 to T.G.) and the Trinity College Dublin School of Chemistry for financial support.

REFERENCES AND NOTES

1. Steed, J.W., Turner, D.R., and Wallace, K. (2007). Core Concepts in Supramolecular Chemistry and Nanochemistry (Wiley).

2. Lehn, J.-M. (2002). Toward self-organization and complex matter. Science *295*, 2400.

3. de Silva, A.P., Moody, T.S., and Wright, G.D. (2009). Fluorescent PET (Photoinduced Electron Transfer) sensors as potent analytical tools. Analyst *134*, 2385–2393.

4. Laishram, R., Bhowmik, S., and Maitra, U. (2015). White light emitting soft materials from off-the-shelf ingredients. J. Mater. Chem. C *3*, 5885–5889.

5. Buerkle, L.E., and Rowan, S.J. (2012). Supramolecular gels formed from multi-component low molecular weight species. Chem. Soc. Rev. *41*, 6089–6102.

6. Sutar, P., and Maji, T.K. (2016). Coordination polymer gels: soft metal-organic supramolecular materials and versatile applications. Chem. Commun. *52*, 8055–8074.

7. Bünzli, J.-C.G., Comby, S., Chauvin, A.-S., and Vandevyver, C.D.B. (2007). New opportunities for lanthanide luminescence. J. Rare Earths *25*, 257–274.

8. Surender, E.M., Comby, S., Cavanagh, B.L., Brennan, O., Lee, T.C., and Gunnlaugsson, T. (2016). Two-photon luminescent bone imaging using europium nanoagents. Chem. *1*, 438–455.

9. Bünzli, J.-C.G. (2010). Lanthanide luminescence for biomedical analyses and imaging. Chem. Rev. *110*, 2729–2755.

10. Kitchen, J.A., and Gunnlaugsson, T. (2013). Supramolecular chemistry: from sensors and imaging agents to functional mononuclear and polynuclear self-assembly lanthanide complexes. In The Rare Earth Elements: Fundamentals and Applications, D.A. Atwood, ed. (John Wiley & Sons, Ltd.), pp. 481–494.

11. The Nobel Prize in Chemistry 1987, Nobelprize.org. Nobel Media AB 2014. Web. 23 May 2017. http://www.nobelprize.org/nobel_prizes/chemistry/laureates/1987/.

12. Barry, D.E., Caffrey, D.F., and Gunnlaugsson, T. (2016). Lanthanide-directed synthesis of luminescent self-assembly supramolecular structures and mechanically bonded systems from acyclic coordinating organic ligands. Chem. Soc. Rev. *45*, 3244–3274.

13. Erbas-Cakmak, S., Leigh, D.A., McTernan, C.T., and Nussbaumer, A.L. (2015). Artificial

molecular machines. Chem. Rev. *115*, 10081–10206.

14. Tranchemontagne, D.J., Mendoza-Cortes, J.L., O'Keeffe, M., and Yaghi, O.M. (2009). Secondary building units, nets and bonding in the chemistry of metal-organic frameworks. Chem. Soc. Rev. *38*, 1257–1283.

15. The 2016 Nobel Prize in Chemistry. Press Release. Nobelprize.org. Nobel Media AB 2014. Web. 23 May 2017. http://www.nobelprize.org/nobel_prizes/chemistry/laureates/2016/press.html.

16. Kay, E.R., and Leigh, D.A. (2015). Rise of the molecular machines. Angew. Chem. Int. Ed. *54*, 10080–10088.

17. Byrne, J.P., Blasco, S., Aletti, A.B., Hessman, G., and Gunnlaugsson, T. (2016). Formation of self-templated 2,6-bis(1,2,3-triazol-4-yl) pyridine [2]catenanes by triazolyl hydrogen bonding: selective anion hosts for phosphate. Angew. Chem. Int. Ed. *55*, 8938–8943.

18. De Greef, T.F.A., Smulders, M.M.J., Wolffs, M., Schenning, A.P.H.J., Sijbesma, R.P., and Meijer, E.W. (2009). Supramolecular polymerization. Chem. Rev. *109*, 5687–5754.

19. Fouquey, C., Lehn, J.-M., and Levelut, A.-M. (1990). Molecular recognition directed self-assembly of supramolecular liquid crystalline polymers from complementary chiral components. Adv. Mater. *2*, 254–257.

20. Stupp, S.I., LeBonheur, V., Walker, K., Li, L.S., Huggins, K.E., Keser, M., and Amstutz, A. (1997). Supramolecular materials: self-organized nanostructures. Science *276*, 384.

21. Gulik-Krzywicki, T., Fouquey, C., and Lehn, J. (1993). Electron microscopic study of supramolecular liquid crystalline polymers formed by molecular-recognition-directed self-assembly from complementary chiral components. Proc. Natl. Acad. Sci. USA *90*, 163–167.

22. Stupp, S.I., Son, S., Lin, H.C., and Li, L.S. (1993). Synthesis of two-dimensional polymers. Science *259*, 59.

23. Beijer, F.H., Kooijman, H., Spek, A.L., Sijbesma, R.P., and Meijer, E.W. (1998). Self-complementarity achieved through quadruple hydrogen bonding. Angew. Chem. Int. Ed. *37*, 75–78.

24. Sijbesma, R.P., Beijer, F.H., Brunsveld, L., Folmer, B.J.B., Hirschberg, J.H.K.K., Lange, R.F.M., Lowe, J.K.L., and Meijer, E.W. (1997). Reversible polymers formed from self-complementary monomers using quadruple hydrogen bonding. Science *278*, 1601.

25. Aida, T., Meijer, E.W., and Stupp, S.I. (2012). Functional supramolecular polymers. Science *335*, 813.

26. Folmer, B.J.B., Sijbesma, R.P., Versteegen, R.M., van der Rijt, J.A.J., and Meijer, E.W. (2000). Supramolecular polymer materials: chain extension of telechelic polymers using a reactive hydrogen-bonding synthon. Adv. Mater *12*, 874–878.

27. Brunsveld, L., Folmer, B.J.B., Meijer, E.W., and Sijbesma, R.P. (2001). Supramolecular polymers. Chem. Rev. *101*, 4071–4098.

28. Hartgerink, J.D., Beniash, E., and Stupp, S.I. (2001). Self-assembly and mineralization of peptide-amphiphile nanofibers. Science *294*, 1684.

29. Rożkiewicz, D.I., Myers, B.D., and Stupp, S.I. (2011). Interfacial self-assembly of cell-like filamentous microcapsules. Angew. Chem. Int. Ed. *50*, 6324–6327.

30. Hartgerink, J.D., Beniash, E., and Stupp, S.I. (2002). Peptide-amphiphile nanofibers: a versatile scaffold for the preparation of self-assembling materials. Proc. Natl. Acad. Sci. USA *99*, 5133–5138.

31. Mata, A., Geng, Y., Henrikson, K.J., Aparicio, C., Stock, S.R., Satcher, R.L., and Stupp, S.I. (2010). Bone regeneration mediated by biomimetic mineralization of a nanofiber matrix. Biomaterials *31*, 6004–6012.

32. Rajangam, K., Behanna, H.A., Hui, M.J., Han, X., Hulvat, J.F., Lomasney, J.W., and Stupp, S.I. (2006). Heparin binding nanostructures to promote growth of blood vessels. Nano Lett. *6*, 2086–2090.

33. Capito, R.M., Azevedo, H.S., Velichko, Y.S., Mata, A., and Stupp, S.I. (2008). Self-assembly of large and small molecules into hierarchically ordered sacs and membranes. Science *319*, 1812.

34. Abbel, R., Grenier, C., Pouderoijen, M.J., Stouwdam, J.W., Leclère, P.E.L.G., Sijbesma, R.P., Meijer, E.W., and Schenning, A.P.H.J. (2009). White-light emitting hydrogen-bonded supramolecular copolymers based on π-conjugated oligomers. J. Am. Chem. Soc. *131*, 833–843.

35. Korevaar, P.A., George, S.J., Markvoort, A.J., Smulders, M.M.J., Hilbers, P.A.J., Schenning, A.P.H.J., De Greef, T.F.A., and Meijer, E.W. (2012). Pathway complexity in supramolecular polymerization. Nature *481*, 492–496.

36. Korevaar, P.A., de Greef, T.F.A., and Meijer, E.W. (2014). Pathway complexity in π-conjugated materials. Chem. Mater. *26*, 576–586.

37. Jonkheijm, P., van der Schoot, P., Schenning, A.P.H.J., and Meijer, E.W. (2006). Probing the solvent-assisted nucleation pathway in chemical self-assembly. Science *313*, 80.

38. Cantekin, S., de Greef, T.F.A., and Palmans, A.R.A. (2012). Benzene-1,3,5-tricarboxamide: a versatile ordering moiety for supramolecular chemistry. Chem. Soc. Rev. *41*, 6125–6137.

39. Howe, R.C.T., Smalley, A.P., Guttenplan, A.P.M., Doggett, M.W.R., Eddleston, M.D., Tan, J.C., and Lloyd, G.O. (2013). A family of simple benzene 1,3,5-tricarboxamide (BTA) aromatic carboxylic acid hydrogels. Chem. Commun. *49*, 4268–4270.

40. Paikar, A., Pramanik, A., and Haldar, D. (2015). Influence of side-chain interactions on the self-assembly of discotic tricarboxyamides: a crystallographic insight. RSC Adv. *5*, 31845–31851.

41. Zhong, J.-L., Jia, X.-J., Liu, H.-J., Luo, X.-Z., Hong, S.-G., Zhang, N., and Huang, J.-B. (2016). Self-assembled metallogels formed from N,N′,N″-tris(4-pyridyl)trimesic amide in aqueous solution induced by Fe(III)/Fe(II) ions. Soft Matter *12*, 191–199.

42. Jana, P., Paikar, A., Bera, S., Maity, S.K., and Haldar, D. (2014). Porous organic material from discotic tricarboxyamide: side chain–core interactions. Org. Lett. *16*, 38–41.

43. Desmarchelier, A., Alvarenga, B.G., Caumes, X., Dubreucq, L., Troufflard, C., Tessier, M., Vanthuyne, N., Ide, J., Maistriaux, T., Beljonne, D., et al. (2016). Tuning the nature and stability of self-assemblies formed by ester benzene 1,3,5-tricarboxamides: the crucial role played by the substituents. Soft Matter *12*, 7824–7838.

44. Groombridge, A.S., Palma, A., Parker, R.M., Abell, C., and Scherman, O.A. (2017). Aqueous interfacial gels assembled from small molecule supramolecular polymers. Chem. Sci. *8*, 1350–1355.

45. Besenius, P., Heynens, J.L.M., Straathof, R., Nieuwenhuizen, M.M.L., Bomans, P.H.H., Terreno, E., Aime, S., Strijkers, G.J., Nicolay, K., and Meijer, E.W. (2012). Paramagnetic self-assembled nanoparticles as supramolecular MRI contrast agents. Contrast Media Mol. Imaging *7*, 356–361.

46. Pandurangan, K., Kitchen, J.A., Blasco, S., Boyle, E.M., Fitzpatrick, B., Feeney, M., Kruger, P.E., and Gunnlaugsson, T. (2015). Unexpected self-sorting self-assembly formation of a [4:4] sulfate:ligand cage from a preorganized tripodal urea ligand. Angew. Chem. Int. Ed. *127*, 4649–4653.

47. Bose, P.P., Drew, M.G.B., Das, A.K., and Banerjee, A. (2006). Formation of triple helical nanofibers using self-assembling chiral benzene-1,3,5-tricarboxamides and reversal of the nanostructure's handedness using mirror image building blocks. Chem. Commun. (Camb.), 3196–3198.

48. Brunsveld, L., Schenning, A.P.H.J., Broeren, M.A.C., Janssen, H.M., Vekemans, J.A.J.M., and Meijer, E.W. (2000). Chiral amplification in columns of self-assembled N,N′,N″-tris((S)-3,7-dimethyloctyl)benzene-1,3,5-tricarboxamide in dilute solution. Chem. Lett. *29*, 292–293.

49. Smulders, M.M.J., Schenning, A.P.H.J., and Meijer, E.W. (2008). Insight into the mechanisms of cooperative self-assembly: the "sergeants-and-soldiers" principle of chiral and achiral c3-symmetrical discotic triamides. J. Am. Chem. Soc. *130*, 606–611.

50. Leenders, C.M.A., Albertazzi, L., Mes, T., Koenigs, M.M.E., Palmans, A.R.A., and Meijer, E.W. (2013). Supramolecular polymerization in water harnessing both hydrophobic effects and hydrogen bond formation. Chem. Commun. *49*, 1963–1965.

51. Leenders, C.M.A., Baker, M.B., Pijpers, I.A.B., Lafleur, R.P.M., Albertazzi, L., Palmans, A.R.A., and Meijer, E.W. (2016). Supramolecular polymerisation in water; elucidating the role of hydrophobic and hydrogen-bond interactions. Soft Matter *12*, 2887–2893.

52. Besenius, P., Portale, G., Bomans, P.H.H., Janssen, H.M., Palmans, A.R.A., and Meijer, E.W. (2010). Controlling the growth and shape of chiral supramolecular polymers in water. Proc. Natl. Acad. Sci. USA *107*, 17888–17893.

53. Du, X., Zhou, J., Shi, J., and Xu, B. (2015). Supramolecular hydrogelators and hydrogels: from soft matter to molecular biomaterials. Chem. Rev. *115*, 13165–13307.

54. Bhattacharjee, T., Zehnder, S.M., Rowe, K.G., Jain, S., Nixon, R.M., Sawyer, W.G., and Angelini, T.E. (2015). Writing in the granular gel medium. Sci. Adv. *1*, e1500655.

55. Tam, A.Y.-Y., and Yam, V.W.-W. (2013). Recent advances in metallogels. Chem. Soc. Rev. *42*, 1540–1567.

56. Lovitt, J.I., Hawes, C.S., Lynes, A.D., Haffner, B., Mobius, M.E., and Gunnlaugsson, T. (2017). Coordination chemistry of N-picolyl-1,8-naphthalimides: colourful low molecular weight metallo-gelators and unique chelation behaviours. Inorg. Chem. Front. *4*, 296–308.

57. Lynes, A.D., Hawes, C.S., Ward, E.N., Haffner, B., Mobius, M.E., Byrne, K., Schmitt, W., Pal, R., and Gunnlaugsson, T. (2017). Benzene-1,3,5-tricarboxamide n-alkyl ester and carboxylic acid derivatives: tuneable structural, morphological and thermal properties. CrystEngComm *19*, 1427–1438.

58. Shen, Z., Wang, T., and Liu, M. (2014). Macroscopic chirality of supramolecular gels formed from achiral tris(ethyl cinnamate) benzene-1,3,5-tricarboxamides. Angew. Chem. Int. Ed. *53*, 13424–13428.

59. Huang, X., Li, C., Jiang, S., Wang, X., Zhang, B., and Liu, M. (2004). Self-Assembled spiral nanoarchitecture and supramolecular chirality in Langmuir−Blodgett films of an achiral amphiphilic barbituric acid. J. Am. Chem. Soc. *126*, 1322–1323.

60. Liu, M., Zhang, L., and Wang, T. (2015). Supramolecular chirality in self-assembled systems. Chem. Rev. *115*, 7304–7397.

61. Fitié, C.F.C., Roelofs, W.S.C., Kemerink, M., and Sijbesma, R.P. (2010). Remnant polarization in thin films from a columnar liquid crystal. J. Am. Chem. Soc. *132*, 6892–6893.

62. Fan, E., Yang, J., Geib, S.J., Stoner, T.C., Hopkins, M.D., and Hamilton, A.D. (1995). Hydrogen-bonding control of molecular aggregation: self-complementary subunits lead to rod-shaped structures in the solid state. J. Chem. Soc. Chem. Commun. 1251–1252.

63. van Bommel, K.J.C., van der Pol, C., Muizebelt, I., Friggeri, A., Heeres, A., Meetsma, A., Feringa, B.L., and van Esch, J. (2004). Responsive cyclohexane-based low-molecular-weight hydrogelators with modular architecture. Angew. Chem. Int. Ed. *43*, 1663–1667.

64. Heeres, A., van der Pol, C., Stuart, M., Friggeri, A., Feringa, B.L., and van Esch, J. (2003). Orthogonal self-assembly of low molecular weight hydrogelators and surfactants. J. Am. Chem. Soc. *125*, 14252–14253.

65. Brizard, A., Stuart, M., van Bommel, K., Friggeri, A., de Jong, M., and van Esch, J. (2008). Preparation of nanostructures by orthogonal self-assembly of hydrogelators and surfactants. Angew. Chem. Int. Ed. *47*, 2063–2066.

66. Lightfoot, M.P., Mair, F.S., Pritchard, R.G., and Warren, J.E. (1999). New supramolecular packing motifs: π-stacked rods encased in triply-helical hydrogen bonded amide strands. Chem. Commun. 1945–1946.

67. de Loos, M., van Esch, J.H., Kellogg, R.M., and Feringa, B.L. (2007). C3-Symmetric, amino acid based organogelators and thickeners: a systematic study of structure–property relations. Tetrahedron *63*, 7285–7301.

68. Hirst, A.R., Roy, S., Arora, M., Das, A.K., Hodson, N., Murray, P., Marshall, S., Javid, N., Sefcik, J., Boekhoven, J., et al. (2010). Biocatalytic induction of supramolecular order. Nat. Chem. *2*, 1089–1094.

69. Boekhoven, J., Poolman, J.M., Maity, C., Li, F., van der Mee, L., Minkenberg, C.B., Mendes, E., van EschJan, H., and Eelkema, R. (2013). Catalytic control over supramolecular gel formation. Nat. Chem. *5*, 433–437.

70. Poolman, J.M., Boekhoven, J., Besselink, A., Olive, A.G.L., van Esch, J.H., and Eelkema, R. (2014). Variable gelation time and stiffness of low-molecular-weight hydrogels through catalytic control over self-assembly. Nat. Protoc. *9*, 977–988.

71. Sangeetha, N.M., and Maitra, U. (2005). Supramolecular gels: functions and uses. Chem. Soc. Rev. *34*, 821–836.

72. Hirst, A.R., and Smith, D.K. (2005). Two-component gel-phase materials—highly tunable self-assembling systems. Chem. Eur. J. *11*, 5496–5508.

73. Hirst, A.R., Smith, D.K., Feiters, M.C., and Geurts, H.P.M. (2004). Two-component dendritic gel: effect of spacer chain length on the supramolecular chiral assembly. Langmuir *20*, 7070–7077.

74. Hirst, A.R., Smith, D.K., and Harrington, J.P. (2005). Unique nanoscale morphologies underpinning organic gel-phase materials. Chem. Eur. J. *11*, 6552–6559.

75. Hirst, A.R., Miravet, J.F., Escuder, B., Noirez, L., Castelletto, V., Hamley, I.W., and Smith, D.K. (2009). Self-assembly of two-component gels: stoichiometric control and component selection. Chem. Eur. J. *15*, 372–379.

76. Rao, K.V., Jayaramulu, K., Maji, T.K., and George, S.J. (2010). Supramolecular hydrogels and high-aspect-ratio nanofibers through charge-transfer-induced alternate coassembly. Angew. Chem. Int. Ed. *49*, 4218–4222.

77. Morris, K.L., Chen, L., Raeburn, J., Sellick, O.R., Cotanda, P., Paul, A., Griffiths, P.C., King, S.M., O'Reilly, R.K., Serpell, L.C., and Adams, D.J. (2013). Chemically programmed self-sorting of gelator networks. Nat. Commun. *4*, 1480.

78. Draper, E.R., Eden, E.G.B., McDonald, T.O., and Adams, D.J. (2015). Spatially resolved multicomponent gels. Nat. Chem. *7*, 848–852.

79. Lloyd, G.O., Piepenbrock, M.-O.M., Foster, J.A., Clarke, N., and Steed, J.W. (2012). Anion tuning of chiral bis(urea) low molecular weight gels. Soft Matter *8*, 204–216.

80. Piepenbrock, M.-O.M., Clarke, N., and Steed, J.W. (2010). Shear induced gelation in a copper(ii) metallogel: new aspects of ion-tunable rheology and gel-reformation by external chemical stimuli. Soft Matter *6*, 3541–3547.

81. Meazza, L., Foster, J.A., Fucke, K., Metrangolo, P., Resnati, G., and Steed, J.W. (2013). Halogen-bonding-triggered supramolecular gel formation. Nat. Chem. *5*, 42–47.

82. Priimagi, A., Cavallo, G., Metrangolo, P., and Resnati, G. (2013). The Halogen bond in the design of functional supramolecular materials: recent advances. Acc. Chem. Res. *46*, 2686–2695.

83. Piepenbrock, M.-O.M., Lloyd, G.O., Clarke, N., and Steed, J.W. (2010). Metal- and anion-binding supramolecular gels. Chem. Rev. *110*, 1960–2004.

84. Okesola, B.O., and Smith, D.K. (2016). Applying low-molecular weight supramolecular gelators in an environmental setting - self-assembled gels as smart materials for pollutant removal. Chem. Soc. Rev. *45*, 4226–4251.

85. Foster, J.A., Piepenbrock, M.O., Lloyd, G.O., Clarke, N., Howard, J.A., and Steed, J.W. (2010). Anion-switchable supramolecular gels for controlling pharmaceutical crystal growth. Nat. Chem. *2*, 1037–1043.

86. Foster, J.A., Damodaran, K.K., Maurin, A., Day, G.M., Thompson, H.P.G., Cameron, G.J., Bernal, J.C., and Steed, J.W. (2017). Pharmaceutical polymorph control in a drug-mimetic supramolecular gel. Chem. Sci. *8*, 78–84.

87. Kaufmann, L., Kennedy, S.R., Jones, C.D., and Steed, J.W. (2016). Cavity-containing supramolecular gels as a crystallization tool for hydrophobic pharmaceuticals. Chem. Commun. *52*, 10113–10116.

88. Pandurangan, K., Kitchen, J.A., Blasco, S., Paradisi, F., and Gunnlaugsson, T. (2014). Supramolecular pyridyl urea gels as soft matter with antibacterial properties against MRSA and/or *E. coli*. Chem. Commun. *50*, 10819–10822.

89. Surender, E.M., Bradberry, S.J., Bright, S.A., McCoy, C.P., Williams, D.C., and Gunnlaugsson, T. (2017). Luminescent lanthanide cyclen-based enzymatic assay capable of diagnosing the onset of catheter-associated urinary tract infections both in solution and within polymeric hydrogels. J. Am. Chem. Soc. *139*, 381–388.

90. Bünzli, J.-C.G., and Piguet, C. (2002). Lanthanide-containing molecular and supramolecular polymetallic functional assemblies. Chem. Rev. *102*, 1897–1928.

91. Kotova, O., Daly, R., dos Santos, C.M.G., Boese, M., Kruger, P.E., Boland, J.J., and Gunnlaugsson, T. (2012). Europium-directed self-assembly of a luminescent supramolecular gel from a tripodal terpyridine-based ligand. Angew. Chem. Int. Ed. *51*, 7208–7212.

92. Daly, R., Kotova, O., Boese, M., Gunnlaugsson, T., and Boland, J.J. (2013). Chemical nano-gardens: growth of salt nanowires from supramolecular self-assembly gels. ACS Nano *7*, 4838–4845.

93. Martínez-Calvo, M., Kotova, O., Möbius, M.E., Bell, A.P., McCabe, T., Boland, J.J., and Gunnlaugsson, T. (2015). Healable luminescent self-assembly supramolecular metallogels possessing lanthanide (Eu/Tb) dependent rheological and morphological properties. J. Am. Chem. Soc. *137*, 1983–1992.

94. Fiore, G.L., Rowan, S.J., and Weder, C. (2013). Optically healable polymers. Chem. Soc. Rev. *42*, 7278–7288.

95. McCarney, E.P., Byrne, J.P., Twamley, B., Martinez-Calvo, M., Ryan, G., Mobius, M.E., and Gunnlaugsson, T. (2015). Self-assembly formation of a healable lanthanide luminescent supramolecular metallogel from 2,6-bis(1,2,3-triazol-4-yl)pyridine (btp) ligands. Chem. Commun. *51*, 14123–14126.

96. Galanti, A., Kotova, O., Blasco, S., Johnson, C.J., Peacock, R.D., Mills, S., Boland, J.J., Albrecht, M., and Gunnlaugsson, T. (2016). Exploring the effect of ligand structural isomerism in Langmuir–Blodgett films of chiral luminescent EuIII self-assemblies. Chem. Eur. J. *22*, 9709–9723.

97. Bradberry, S.J., Byrne, J.P., McCoy, C.P., and Gunnlaugsson, T. (2015). Lanthanide luminescent logic gate mimics in soft matter: [H+] and [F-] dual-input device in a polymer gel with potential for selective component release. Chem. Commun. *51*, 16565–16568.

98. Comby, S., Surender, E.M., Kotova, O., Truman, L.K., Molloy, J.K., and Gunnlaugsson, T. (2014). Lanthanide-functionalized nanoparticles as MRI and luminescent probes for sensing and/or imaging applications. Inorg. Chem. *53*, 1867–1879.

99. Qiu, H., Hudson, Z.M., Winnik, M.A., and Manners, I. (2015). Multidimensional hierarchical self-assembly of amphiphilic cylindrical block comicelles. Science *347*, 1329.

100. Boott, C.E., Laine, R.F., Mahou, P., Finnegan, J.R., Leitao, E.M., Webb, S.E.D., Kaminski, C.F., and Manners, I. (2015). In situ visualization of block copolymer self-assembly in organic media by super-resolution fluorescence microscopy. Chem. Eur. J. *21*, 18539–18542.

101. Rupar, P.A., Chabanne, L., Winnik, M.A., and Manners, I. (2012). Non-centrosymmetric cylindrical micelles by unidirectional growth. Science *337*, 559.

102. Gilroy, J.B., Gädt, T., Whittell, G.R., Chabanne, L., Mitchels, J.M., Richardson, R.M., Winnik, M.A., and Manners, I. (2010). Monodisperse cylindrical micelles by crystallization-driven living self-assembly. Nat. Chem. *2*, 566–570.

103. Zhang, W., Jin, W., Fukushima, T., Saeki, A., Seki, S., and Aida, T. (2011). Supramolecular linear heterojunction composed of graphite-like semiconducting nanotubular segments. Science *334*, 340.

104. Park, S., Lim, J.-H., Chung, S.-W., and Mirkin, C.A. (2004). Self-assembly of mesoscopic metal-polymer amphiphiles. Science *303*, 348.

105. Zhang, J., Coulston, R.J., Jones, S.T., Geng, J., Scherman, O.A., and Abell, C. (2012). One-step fabrication of supramolecular microcapsules from microfluidic droplets. Science *335*, 690.

106. Yu, Z., Zhang, J., Coulston, R.J., Parker, R.M., Biedermann, F., Liu, X., Scherman, O.A., and Abell, C. (2015). Supramolecular hydrogel microcapsules via cucurbit[8]uril host-guest interactions with triggered and UV-controlled molecular permeability. Chem. Sci. *6*, 4929–4933.

107. Yu, Z., Zheng, Y., Parker, R.M., Lan, Y., Wu, Y., Coulston, R.J., Zhang, J., Scherman, O.A., and Abell, C. (2016). Microfluidic droplet-facilitated hierarchical assembly for dual cargo loading and synergistic delivery. ACS Appl. Mater. Inter. *8*, 8811–8820.

108. Liu, J., Lan, Y., Yu, Z., Tan, C.S.Y., Parker, R.M., Abell, C., and Scherman, O.A. (2017). Cucurbit [n]uril-based microcapsules self-assembled within microfluidic droplets: a versatile approach for supramolecular architectures and materials. Acc. Chem. Res. *50*, 208–217.

109. Yu, G., Jie, K., and Huang, F. (2015). Supramolecular amphiphiles based on host–guest molecular recognition motifs. Chem. Rev. *115*, 7240–7303.

110. Tominaga, M., Masu, H., and Azumaya, I. (2009). Construction and charge-transfer complexation of adamantane-based macrocycles and a cage with aromatic ring moieties. J. Org. Chem. *74*, 8754–8760.

111. Tominaga, M., Ohara, K., Yamaguchi, K., and Azumaya, I. (2014). Hollow sphere formation from a three-dimensional structure composed of an adamantane-based cage. J. Org. Chem. *79*, 6738–6742.

112. Lv, K., Zhang, L., and Liu, M. (2014). Self-assembly of triangular amphiphiles into diverse nano/microstructures and release behavior of the hollow sphere. Langmuir *30*, 9295–9302.

113. Jeon, Y.-M., Armatas, G.S., Kim, D., Kanatzidis, M.G., and Mirkin, C.A. (2009). Tröger's-base-derived infinite co-ordination polymer microparticles. Small *5*, 46–50.

114. Oh, M., and Mirkin, C.A. (2005). Chemically tailorable colloidal particles from infinite coordination polymers. Nature *438*, 651–654.

115. Shanmugaraju, S., Dabadie, C., Byrne, K., Savyasachi, A.J., Umadevi, D., Schmitt, W., Kitchen, J.A., and Gunnlaugsson, T. (2017). A supramolecular Troger's base derived coordination zinc polymer for fluorescent sensing of phenolic-nitroaromatic explosives in water. Chem. Sci. *8*, 1535–1546.

116. Cho, W., Lee, H.J., Choi, S., Kim, Y., and Oh, M. (2014). Highly effective heterogeneous chemosensors of luminescent silica@coordination polymer core-shell micro-structures for metal ion sensing. Sci. Rep. *4*, 6518.